

**Solution-casting of Disulfonated Poly(arylene ether sulfone) Multiblock  
Copolymer Films for Proton Exchange Membranes**

Myoungbae Lee

Dissertation submitted to the faculty of  
the Virginia Polytechnic Institute and State University  
in partial fulfillment of the requirements for the degree of

Doctor of Philosophy

In

Chemical Engineering

Dr. Donald G. Baird

Dr. Richey M. Davis

Dr. Stephen Martin

Dr. James E. McGrath

April 27, 2009

Blacksburg, VA

Keywords: Proton exchange membrane, block copolymer, phase separation kinetics,  
solvent selectivity, processing temperature

# **Solution-casting of disulfonated poly(arylene ether sulfone) copolymer films for proton exchange membranes**

Myoungbae Lee

## **ABSTRACT**

The overall objective of the project, on which this thesis is based, is to develop a novel hydrocarbon-based proton exchange membrane (PEM) material that can produce a proton conductivity of 0.1 S/cm at the operating conditions of 50 % relative humidity and 120 °C, which is the performance target set by the U.S. DOE for automotive application. As a part of this project, our efforts have been focused on the investigation of the effects of solution-casting conditions on the final morphology and properties of disulfonated poly(arylene ether sulfone) multiblock copolymer films from the viewpoint of phase separation of block copolymers. Of equal importance to this work, is a possibility of utilizing a rheological technique for monitoring the transformation and kinetics of block copolymers during solvent removal process, which was initially examined in order to provide fundamental quantitative understanding and practical information on the solvent removal process.

Our results demonstrated that solvent selectivity and drying temperature as well as the block length had considerable effects on the final morphology and properties. The proton conductivity could be significantly increased by simply utilizing a selective solvent, dimethylacetamide (DMAC), which is good and marginal for the sulfonated and unsulfonated blocks, respectively, rather than N-methyl-2-pyrrolidone (NMP), a neutral solvent for both blocks. The drying temperature was also observed to have considerable

effects on the final properties, being coupled with the effects of solvent selectivity. Also, it was shown that the multiblock copolymer consisting of longer blocks was more sensitive to the processing conditions. From the morphological study using transmission electron microscopy and small-angle X-ray scattering, evidences for the above observations were obtained.

In the second part of this dissertation, the evolution of  $G'$  and  $G''$  of the solutions of a styrene-butadiene-styrene (SBS) triblock copolymer in toluene was obtained as a function of concentration using a modified parallel-plate device and a rheology test scheme developed in this study in an effort to quantify the phase separation kinetics. Then, the information on the phase transformation and kinetics of the SBS block copolymer in the solution was obtained by analyzing the  $G'$  and  $G''$  data with the Avrami equation. The Avrami exponent was found to be approximately 1, which indicates that the phase transformation occurred by a one-dimensional growth mechanism. The rate constant showed a strong concentration-dependence. After the initial increase up to 45 vol %, the rate constant drastically decreased and, finally, converged to 0 at 70 vol %. It is believed that, at the concentration range below 45 vol %, the phase separation became more intense as the polymer molecules had more chances to interact owing to the concentration increase. However, above 45 vol %, the phase transformation became weaker due to the limited mobility of the polymer molecules, which finally led to a “kinetically frozen-in” structure, in which the polymer molecules could not move any longer. Thus, it can be concluded that the solvent removal rate is one of the dominant factors that decide the final microstructures of solution-cast block copolymer films.

## ACKNOWLEDGEMENTS

First of all, I'd like to thank Dr. Donald G. Baird for his support and guidance, which resulted in the completion of this dissertation. His expertise and patience are greatly appreciated. I am considerably indebted to my committee for their guidance: Dr. Richey M. Davis, Dr. Eva Marand, Dr. Stephen Martin, and Dr. James E. McGrath.

Also, I wish to thank the following people:

- My wife, Sunghui Lee, for her love and support, which have driven me to do my best so far.
- My parents, Guang Jung Lee and Kyung Ja Choi, for their unquestionable love and support all through my life.
- My brother, Kyongbae Lee, for his supports and advice, which have enabled me to make right decisions and choices and to focus on my study.
- My mother-in-law, Jin Sook Yu, for her love and prayer.
- Dr. Hae-Seung Lee for many pieces of his valuable advice and discussions about my research. Especially, for his synthesizing the copolymers used in this thesis work. He is also a friend who has shared many of unforgettable memories and experiences in Blacksburg.
- Tyler Shillig and his family for their friendship. In particular, Tyler for his proofreading my proposal and this dissertation. He also helped me to improve my English and taste more facets of American culture.
- Dr. Jumyung Song and Jongkeun Park for their efforts to obtain the SAXS data and for their valuable discussions to analyze the data.

- Stephen McCartney and John McIntosh for their training me in microtoming and TEM.
- Ozma Lane for her proton conductivity measurements.
- Michael Vaught and Riley Chen for their technical supports. Especially, Michael Vaught for his fantastic machining skill which enabled the fulfillment of my ideas on the experiments.
- Diane Cannaday, Mary Jane Smith, and Tammy Ho Hiner for their administrative support.
- My past and present lab mates in Polymer Processing Lab.: Wade DePolo, Nguyen Quang, Matthew Wilding, Brent Cunningham, Christopher Seay, David Litchfield, Aaron Eberle, Desmond VanHouten, Gregorio Velez, Christopher McGrady, Chen Chen, Michael Heinzer, Kevin Ortman, Neeraj Agarwal, and Syed Mazahir.

## Original Contributions

The following are considered to be significant original contribution of this research.

- The effects of solution-casting conditions on the final morphology and properties of partially disulfonated poly(arylene ether sulfone) copolymer films for proton exchange membranes (PEMs) were systematically studied from the viewpoint of the basic principles of microstructure formation of copolymers. It was shown that processing conditions as well as the molecular architecture were crucial for the final morphology and properties.
- A batch convection drying apparatus was designed and constructed to generate drying conditions at a semi-industrial level in the lab. The apparatus also provided well-controlled drying conditions and enabled estimation of the drying rate and total drying time.
- A clearer understanding of the relationship between the structure and properties of hydrocarbon-based PEMs was provided by carrying out the morphological study using both transmission electron microscopy and small angle X-ray scattering.
- A modified parallel-plate device and a measurement scheme of the rheological properties of polymers in the solvent removal process were developed for the study of the phase transformation and kinetics of block copolymers during the solvent removal process.
- Information on the transformation and kinetics of block copolymers in solution-cast films in the solvent removal process was obtained by measuring and analyzing the dynamic mechanical property data of the solution-cast films.

## **Dissertation format**

This dissertation is written in journal format. Chapters 3 and 4 are self contained papers that separately describe the experiments, results, and conclusions relative to each chapter. With the exception of Chapter 2, Literature Review, the figures and tables are inserted after the reference section of each chapter.

# CONTENTS

<b>ABSTRACT</b> .....	<b>ii</b>
<b>ACKNOWLEDGMENTS</b> .....	<b>iv</b>
<b>ORITINAL CONTRIBUTIONS</b> .....	<b>vi</b>
<b>FORMAT OF DISSERTATION</b> .....	<b>vii</b>
<b>LIST OF FIGURES</b> .....	<b>x</b>
<b>LIST OF TABLES</b> .....	<b>xv</b>

## CHAPTERS

### 1. INTRODUCTION / 1

1.1 References / 10

### 2. LITERATURE REVIEW / 12

2.1 Proton exchange membrane / 12

2.1.1 Relevant parameters for evaluation of proton exchange membranes / 14

2.1.2 Disulfonated poly(arylene ether sulfone) random and multi-block copolymer: BPSH<sub>x</sub> and BPSH100-BPS0 / 17

2.2 Production of proton exchange membrane / 28

2.2.1 Previous studies on the production of polymer electrolyte polymer membranes / 29

2.2.2 Thermal characterization and processability of poly(arylene ether sulfone) copolymer / 35

2.3 Morphology of block copolymer systems / 39

2.3.1 Block copolymer melts / 41

2.3.2 Block copolymers in solution / 46

2.3.3 Studies on the phase transformation and kinetics of block copolymer through rheological measurements and scattering techniques / 49

2.4 Drying of polymer films and coatings / 59

2.4.1 Nature of film drying / 61

2.4.1.1 Heat and mass transfer phenomena in film drying / 61

2.4.1.2 Drying regimes and their characteristics / 63

2.4.2 Modeling of film drying / 66

2.5 References / 80

- 3. EFFECTS OF SOLUTION-CASTING CONDITIONS ON THE FINAL MORPHOLOGY AND PROPERTIES OF DISULFOATED POLY(ARYLENE ETHER SULFONE) MULTIBLOCK COPOLYMER FILMS FOR PROTON EXCHANGE MEMBRANES / 87**
  - 3.0 Abstract / 87
  - 3.1 Introduction / 88
  - 3.2 Experimental / 94
  - 3.3 Results and discussion / 98
  - 3.4 Conclusions / 108
  - 3.5 References / 109
  
- 4. STUDY ON THE PHASE TRANSFORMATION AND KINETICS OF BLOCK COPOLYMERS IN SOLUTION-CAST FILMS VIA RHEOLOGICAL PROPERTY MEASUREMENTS / 124**
  - 4.1 Introduction / 124
  - 4.2 Materials and experiments / 129
  - 4.3 Results and discussion / 133
  - 4.4 Summary / 138
  - 4.5 References / 139
  
- 5. RECOMMENDATIONS FOR FUTURE RESEARCH / 152**
  - 5.1 Further study on the effects of solution-casting conditions on the final morphology and properties of proton exchange membranes / 152
  - 5.2 Study on the phase transformation and kinetics of block copolymers in solution-cast films using SAXS and/or POM / 153
  
- APPENDIX A. RHEOLOGICAL DATA AND ANALYSIS FOR SECTION 4.3 / 156**

## List of Figures

- 1-1. (a) Chemical structure of BPSH-x copolymer, and comparison of (b) the proton conductivity and (c) endurance (accelerated membrane degradation test; open-circuit-voltage test) between BPSH-35 and Nafion<sup>®</sup> [McGrath 2006] (Illustrated under “Fair Use” copyright guidelines). / 4
- 2.1-1. Cell used for measurement of proton conductivity: (1) Teflon block, (2) thumbscrew, (3) open area to allow equilibration, (4) membrane sample, (5) blackened Pt foil, and (6) Pt ribbon lead [Zawodzinski 1991] (Illustrated under “Fair Use” copyright guidelines). / 14
- 2.1-2. Chemical structure of poly (arylene ether sulfone)s [Hickner 2004] (Illustrated under “Fair Use” copyright guidelines). / 17
- 2.1-3. Synthesis of sodium sulfonate salt of 3,3'-disulfonated-4,4'-dichlorodiphenyl sulfone (SDCDPS) [Wang 2002] (Illustrated under “Fair Use” copyright guidelines). / 19
- 2.1-4. Synthesis of wholly aromatic, biphenol-based disulfonated poly (arylene ether sulfone) copolymer (BPSH-x) [Wang 2002] (Illustrated under “Fair Use” copyright guidelines). / 19
- 2.1-5. Possible chemical structures of sulfonated poly (arylene ether) copolymers [Hickner 2004] (Illustrated under “Fair Use” copyright guidelines). / 19
- 2.1-6. Different positions of sulfonic acid groups by different sulfonation methods (X = O, S) (Illustrated under “Fair Use” copyright guidelines). / 20
- 2.1-7. Influence of relative humidity on proton conductivity and water uptake of BPSH random copolymer; measurement temperature 80 °C. 1: BPSH-40-Method 2, 2: Nafion 1135-Method 1, 3: BPSH-30-Method 2, 4: BPSH-300-Method 1 [Kim 2003a] (Illustrated under “Fair Use” copyright guidelines). / 22
- 2.1-8. AFM images of BPSH with disulfonation of (a) 20, (b) 40, (c) 50, and (d) 60 % acidified with 2.0 M sulfuric acid aqueous solution at 30 °C [Harrison 2004] (Illustrated under “Fair Use” copyright guidelines). / 23
- 2.1-9. Stress-strain behaviors of BPSH-40 and Nafion 117. The hydrated state of BPSH-40 and Nafion<sup>®</sup> 117 contains water of 22 and 16 %, respectively [Harrison 2004] (Illustrated under “Fair Use” copyright guidelines). / 24
- 2.1-10 Overall synthetic scheme of hydrophilic-hydrophobic multiblock copolymers based on poly(arylene ether sulfone) (BPSH100-BPS0) [Lee 2008]

- (Illustrated under “Fair Use” copyright guidelines). / 26
- 2.2-1. Thermal decomposition of DMF and DMAc [Robertson 2003] (Illustrated under “Fair Use” copyright guidelines). / 30
- 2.2-2. Chemical structure of BisSF-BPSH block copolymer used in Huang et al.’s study [Huang 2007] (Illustrated under “Fair Use” copyright guidelines). / 32
- 2.2-3. Comparison of stress-strain behavior of batch cast and continuous cast BPSH-32 films [Huang 2007] (Illustrated under “Fair Use” copyright guidelines). / 33
- 2.3-1. Block copolymer architectures [Hamley 2004] (Illustrated under “Fair Use” copyright guidelines). / 40
- 2.3-2. Phase diagram for a conformationally symmetric diblock copolymer, calculated using self-consistent mean field theory, along with illustrations of the equilibrium morphologies. In the phase diagram, regions of stability of disordered (dis), lamellar (lam), gyroid (gyr), hexagonal (hex) and body-centered cubic (bcc) phases are indicated [Matsen and Schick 1994, Matsen and Bates 1996] (Illustrated under “Fair Use” copyright guidelines). / 42
- 2.3-3. ABC linear triblock copolymer morphologies [Stadler 1995, Zheng 1995, Bates 1999] (Illustrated under “Fair Use” copyright guidelines). / 44
- 2.3-4. Phase diagram of the polydisperse multiblock copolymer melt [Dobrynin 1997]. Here,  $\langle l \rangle$  represents average block length and  $u$  is the ratio of the two first moments of the distribution, expressed as  $\langle l^2 \rangle / \langle l \rangle^2 - 1$  (Illustrated under “Fair Use” copyright guidelines). / 45
- 2.3-5. (a) Phase diagram for SI as a function of temperature and polymer volume fraction for solution in bis(2-ethylhexyl) phthalate (DOP), Di-n-butyl phthalate (DBP), diethyl phthalate (DEP), and tetradecane (C14). Filled and open circles identify ODTs and OOTs, respectively. The dilute solution critical micelle temperature is indicated by a filled square. (b) Phase trajectories of SI in DOP, DBP, DEP, and C14 [Chastek 2004] (Illustrated under “Fair Use” copyright guidelines). / 47
- 2.3-6. Variations of  $G'$  with temperature obtained at  $\omega = 0.5$  rad/s ( $\circ$ ) and at  $\omega = 0.5$  rad/s ( $\blacktriangle$ ) (a) for SI diblock copolymer with  $f_{PS} = 0.461$ .  $T_{ODT} = 115$  °C determined by an abrupt drop in  $G'$ . (b) for SI diblock copolymer with  $f_{PS} = 0.372$ .  $T_{ODT} = 82$  °C determined by a large change of the slope of the plot. (c) for SI diblock copolymer with  $f_{PS} = 0.186$ . No discernable evidence of  $T_{ODT}$  observed [Han 1995] (Illustrated under “Fair Use” copyright guidelines). / 50

- 2.3-7. (1) Time evolution of  $G'$  and  $G''$  for a symmetric poly(styrene-*b*-isoprene) diblock copolymer following quenches from the disordered state to different final temperatures in the ordered phase: rhombus: 359, circles: 358, X: 356.5, +: 356, squares: 355, triangles: 353, and inverted triangles: 347.6 K.  
 (2) a. Time evolution of  $G'$  and  $G''$  at 356.5 K following a quench from 363 K and b. time-dependence of the volume fraction of  $\phi$  of the ordered phase calculated using the 'parallel' (squares) and 'series' (circles) models. Solid lines are fits to the Avrami equation [Floudas 1994] (Illustrated under "Fair Use" copyright guidelines). / 52
- 2.3-8. Evolution of the peak scattering intensity  $I(q^*)(t)$  following a temperature jump from the disordered to the ordered state of a SI graft copolymer. The line is a fit to the Avrami equation [Fluodas 1994] (Illustrated under "Fair Use" copyright guidelines). / 55
- 2.4-1. A schematic of industrial coating and drying apparatus [Kim, S. 2001] (Illustrated under "Fair Use" copyright guidelines). / 59
- 2.4-2. Elemental heat and mass transfer phenomena of the drying process of coated films. / 61
- 2.4-3. Characteristic drying curves of the coated polymer solution films: changes of film temperature and drying rate as a function of the drying time [Kim, S. 2001] (Illustrated under "Fair Use" copyright guidelines). / 63
- 2.4-4. Binary diffusion coefficient of toluene in the polystyrene-toluene solution as a function of concentration and temperature by Vrentas et al [1982] (Illustrated under "Fair Use" copyright guidelines). / 65
- 2.4-5. A schematic of the drying geometry and the model equations by Vrentas et al [1994] . / 72
- 3.1-1. Chemical structures of BPSH35 random (top) and BPSH100-BPS0 multi-block (bottom) copolymer. / 111
- 3.2-2. Schematic of batch convection drying apparatus. / 113
- 3.3-1. Characteristic drying curves of the BPSH100-BPS0 (15k-15k) multiblock copolymer films dried by convection air at 0.2 m/s. / 114
- 3.2-2. Effects of block length and solvent type on proton conductivity of the BPSH100-BPS0 multiblock copolymer films (measured at 30 °C and fully hydrated conditions). / 116
- 3.3-3. Effects of block length and casting conditions on water uptake of the BPSH100-BPS0 multiblock copolymer films (measured at 20 °C). /117

- 3.3-4. Swelling behavior of the BPSH100-BPS0 (15k-15k) copolymer films cast with DMAC as a function of drying temperature. / 118
- 3.3-5. Estimated volume-based IEC values of the multiblock copolymer films in a wet state. / 119
- 3.3-6. TEM micrographs of the copolymer films. (block length, solvent type, drying temp. [ $^{\circ}\text{C}$ ]). Length of scale bar = 100 nm. / 120
- 3.3-7. TEM micrographs of the BPSH100-BPS0 (15k-15k) multiblock copolymer films (solvent type, drying temp. [ $^{\circ}\text{C}$ ]). Length of scale bar = 100 nm. / 121
- 3.3-8. SAXS profiles of the BPSH100-BPS0 multiblock copolymer films cast with NMP and dried at 20  $^{\circ}\text{C}$ . / 122
- 3.3-9. Comparison of the distance between the ionic domains estimated from the SAXS profiles and TEM images of the BPSH100-BPS0 multiblock copolymer films cast with NMP and dried at 20  $^{\circ}\text{C}$ . / 123
- 4.1-1. (a) Time evolution of  $G'$  and  $G''$  for a symmetric poly(styrene-*b*-isoprene) diblock copolymer following quenches from the disordered state to different final temperatures in the ordered phase: rhombus: 359, circles: 358, X: 356.5, +: 356, squares: 355, triangles: 353, and inverted triangles: 347.6 K. (b) a. Time evolution of  $G'$  and  $G''$  at 356.5 K following a quench from 363 K and b. time-dependence of the volume fraction of  $\phi$  of the ordered phase calculated using the ‘parallel’ (squares) and ‘series’ (circles) models. Solid lines are fits to the Avrami equation [Floudas 1994]. / 140
- 4.2-1. Modified parallel-plate rheometer plates: (a) design of the parts, dimensions in mm (in scale); (b) the cross-sectional view; and (c) picture of the plates installed onto the RMS-800. / 143
- 4.2-2. Drawings of **test station** and **gap indicator** (Figure 6-25 and –26 in the user manual of the RMS-800 [Manual]). / 144
- 4.2-3. Pictures of gap indicator at each step for gap-zeroing procedure. / 145
- 4.3-1. Evaluation of the viscosity measurement accuracy of the modified parallel plate rheometry fixtures adapted to the RMS-800 by comparing viscosity values of PDMS and Brookfield Viscosity Standard Solution measured at  $22 \pm 1$   $^{\circ}\text{C}$  with the manufacturer’s quoted value (300 and 92 Pa•sec). / 146
- 4.3-2. Evaluation of the  $G'$ ,  $G''$ , and  $\eta^*$  measurement accuracy of the modified parallel plate rheometry fixtures adapted to the RMS-800 by comparing  $G'$ ,  $G''$ , and  $\eta^*$  values of PDMS measured with the modified parallel plate rheometry fixtures at  $22 \pm 1$   $^{\circ}\text{C}$  with those measured with standard 25 mm

parallel plates. / 147

- 4.3-3. Test of the ability of prevent solvent evaporation of the modified parallel plate rheometry fixtures adapted to the RMS-800 by comparing the steady shear viscosity values of a 36 vol % polystyrene/toluene solution measured with the modified parallel plates at  $22 \pm 1$  °C with those measured with standard 25 mm parallel plates. / 148
- 4.3-4. Time evolution of  $G'$  and  $G''$  of the SBS/toluene films obtained at 6 difference concentrations at  $22 \pm 0.5$  °C. / 149
- 4.3-5. (a)  $G'$  and  $G''$  measured at 40 vol %. (b) Corresponding complex modulus. (c) Time dependence of the volume fraction,  $\phi$ , of the final phase calculated from the complex modulus using the parallel and series model. (d) Estimation of Avrami parameters by fitting the volume fraction vs. time data into the Avrami equation. / 150
- 4.3-6. Avrami parameters estimated by fitting the volume fraction vs. time data to the Avrami equation. / 151

## List of Tables

- 1-1. Comparison of proton conductivities of sulfonated poly(ether ether ketone) membranes reported in the literature. / 7
- 2.1-1. Dependence of proton conductivity and water uptake on degree of sulfonation, hydrothermal treatment, and temperature [Kim 2003a] (Illustrated under “Fair Use” copyright guidelines). / 21
- 2.2-1. Effects of solvent-casting conditions on the proton conductivity of BisSF/BPSH block copolymers [Huang 2007] (Illustrated under “Fair Use” copyright guidelines). / 34
- 2.2-2. Effect of the degree of sulfonation on the thermal properties of BPSH copolymer [Wang 2002] (Illustrated under “Fair Use” copyright guidelines). / 35
- 2.4-1. Model parameters of free volume theory by Vrentas-Duda’s. / 66
- 2.4-2. Summary of previous modeling works of drying of non-reactive polymer-solvent system on an impermeable substrate. / 69
- 2.4-3. Summary of model parameters used in the modeling of film drying by Alsoy et al [1998 & 1999]. / 73
- 3.2-1. Copolymer characteristics. / 112
- 3.3-1 Total drying time of the BPSH100-BPS0 (15k-15k) multiblock copolymer films. / 115
- 4.2-1. Characterization of the SBS triblock copolymers used in this study [Certificate]. / 141
- 4.2-2. Physical properties of toluene [Smallwood 1996]. / 142

# CHAPTER 1

## INTRODUCTION

A fuel cell is an electrochemical device that converts fuel to electricity without the utilization of a combustion process [Johnstone 2001]. It uses hydrogen as a fuel, which has numerous sources on the earth such as natural gas, methane, propane, etc. The overall chemical reaction in fuel cells is the combination of hydrogen with oxygen to produce electricity, heat and water. So, its essential features are extremely low emissions as well as high fuel efficiency [Larminie 2003]. Even though the basic principle of the fuel cell was first reported by a British amateur physicist, William Grove, in the 1830s, the first modern application of the fuel cell as a power generation system appeared in the 1960s for the spaceship Gemini [Dönitz 1998]. At that time, however, fuel cells were extremely expensive and had a short lifetime for practical applications such as a personal transport vehicle. In the 1990s, fuel cells began to gain more interest as an advanced power system for widespread terrestrial applications such as automobiles, stationary power plants, and portable power devices. Currently, impending fossil fuel depletion, international laws on green house gas control, and the U.S. national renewable energy policy attribute more importance to fuel cells, which are essentially sustainable, clean, and environment-friendly [Vishnayakov 2006].

In spite of the aforementioned advantages of the fuel cell, its high cost and some technological problems are delaying commercial production [Alberti 2006]. Especially, technical barriers related to proton exchange membranes (PEMs) are the key issues. The current leading PEM material, Nafion<sup>®</sup>, is well known for its excellent proton conductivity owing to its highly acidic nature, and its poly(perfluorosulfonic acid) structure imparts outstanding oxidative and chemical stability and, ultimately, an unsurpassed lifetime in a fuel cell environment [Alberti 2001]. However, the widespread usage of Nafion<sup>®</sup> membranes is limited by its high cost and degradation while operating at temperature above 80 °C [Rozière 2003]. It is expected that the development of a non-perfluorinated PEM can result in substantial reduction of fuel cell cost and achieve the operation of fuel cells at elevated temperature. Thus, much research effort is being put forth to develop a hydrocarbon-based material for PEMs that show better performances than the Nafion<sup>®</sup> membrane [Sopian 2006]. Furthermore, Nafion<sup>®</sup> and all other current membranes, in order to produce a proton conductivity sufficient for commercialization (~0.1 S/cm), need a fully hydrated condition that induces serious degradation of the membranes. So, it is additionally required for an alternative PEM material to produce a satisfactory proton conductivity at a lower humidity.

Therefore, the general objective of the project entitled ***High Temperature, Low Relative Humidity, Polymer-type Membranes Based on Disulfonated Poly(arylene ether) Block and Random Copolymers Optionally Incorporating Protonic Conducting Layered Water Insoluble Zirconium Fillers*** and granted by the U.S. Department of Energy (DOE) (Grant NO. DE-FG36-06G016038) is to develop a novel hydrocarbon-based PEM material and a production method in order to manufacture a fuel cell PEM

that has a proton conductivity of 0.1 S/cm at the operating conditions of 120 °C and 50 % RH (relative humidity), the performance target set by the U.S. DOE for automotive application [DOE]. As a part of this project, the primary goal of this thesis work is to develop a production method of disulfonated poly(arylene ether sulfone) copolymer films for proton exchange membranes in fuel cells and, ultimately, to optimize the processing conditions.

Wholly aromatic polymers are expected to be the most promising alternative PEM materials for high temperature operation of fuel cells because of their availability, processability, wide variety of chemical compositions, and anticipated endurance in the fuel cell environment [Wang 2003]. Particularly, poly(arylene ether) polymers such as poly(arylene ether ether ketone), poly(arylene ether sulfone), and their derivatives have received much attention because of their attractive features as a PEM material such as oxidative and hydrolytic stability and many possible different chemical structures, even with partially fluorinated materials [Hickner 2004]. The introduction of active proton exchange sites (sulfonic acid groups in most cases) has been achieved by both post-sulfonation of the polymers and direct copolymerization of sulfonated monomers [Zaidi 2000, Johnson 1984]. However, post-sulfonated polymers are known to have disadvantages due to the lack of precise and reproducible control over the degree and location of sulfonation and the possibility of side reactions or degradation. In order to overcome these drawbacks of post-sulfonated polymers, Prof. McGrath's group in the Department of Chemistry at Virginia Tech synthesized a disulfonated poly(arylene ether sulfone) copolymer via direct copolymerization under reaction conditions which were very similar to those used for the synthesis of unsulfonated poly(arylene ethers) [Wang

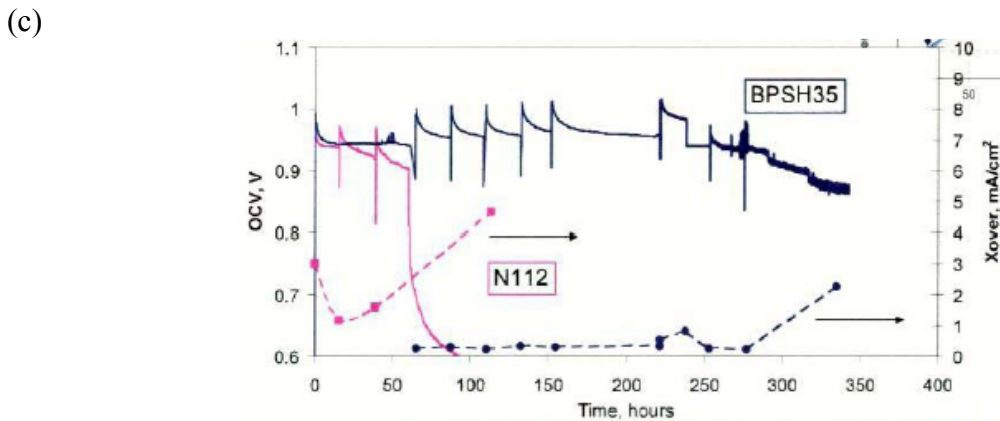
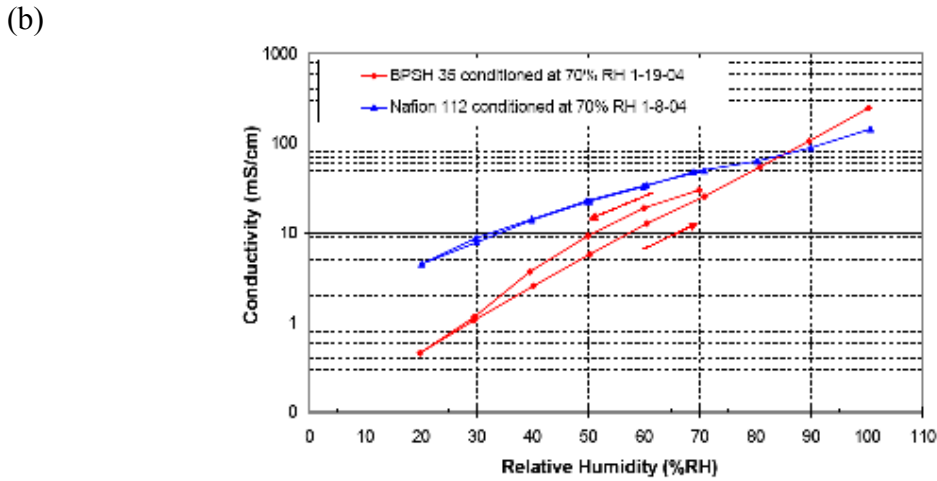
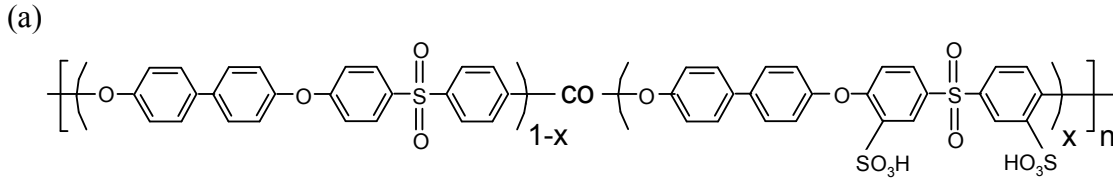


Figure 1-1. (a) Chemical structure of BPSH-x copolymer, and comparison of (b) the proton conductivity and (c) endurance (accelerated membrane degradation test; open-circuit-voltage test) between BPSH-35 and Nafion<sup>®</sup> [McGrath 2006] (Illustrated under “Fair Use” copyright guidelines).

2001]. They named this disulfonated poly(arylene ether sulfone) copolymer as **BPSH-x**, which stands for biphenol (BP), sulfone (S), acid form (H), with the mole % (x) of the sulfonated repeat unit appended to the end. In Figure 1-1 is shown the chemical structure

of the BPSH-x copolymer, and is also given the comparison of the proton conductivity and accelerated membrane degradation test results between the BPSH-35 copolymer and Nafion<sup>®</sup>. At and near fully hydrated conditions, the proton conductivity of BPSH-35 is comparable with and even superior to that of Nafion<sup>®</sup>. The proton conductivity for both BPSH-35 and Nafion<sup>®</sup> decreases exponentially as the relative humidity decreases. The humidity-dependency of the proton conductivity of BPSH-35 is larger than that of Nafion<sup>®</sup> and, at 50 % relative humidity, the conductivity of BPSH-35 is somewhat lower than that of Nafion<sup>®</sup>. However, as expected, the results of the accelerated membrane degradation test show that the endurance of BPSH-35 is much better than Nafion<sup>®</sup>. While serious gas crossover through the Nafion<sup>®</sup> membrane begins just after 40 hours and the open-circuit-voltage of Nafion<sup>®</sup> membrane drastically drops at around 60 hours, the BPSH-35 membrane endures the open-circuit-voltage test for more than 250 hours. Consequently, the BPSH copolymer is expected to be practically feasible and has potential for fuel cell applications at elevated temperatures (above 100 °C). In order to improve the proton conductivity of the BPSH copolymer at lower humidity by modifying its chemical structure and/or composition, research on its synthesis is underway in the Department of Chemistry at Virginia Tech. In this thesis work, the production of membranes of the disulfonated directly copolymerized poly(arylene ether sulfone) random and multiblock copolymer systems will be investigated.

PEMs are typically prepared in the laboratory by a batch solution casting process for a preliminary evaluation of their performance. However, commercial production-scale manufacture of the membranes cannot be achieved by the same batch process because the production rate is too low, and the requirements for the physical shape of the membranes

such as thickness and uniformity cannot be easily satisfied, especially for fuel cell PEM application. So, it is vital to develop and optimize a continuous process for the manufacture of poly(arylene ether sulfone) copolymer films for PEMs in fuel cells.

Generally, thin polymer membrane films can be continuously manufactured using solvent-casting and melt-extrusion casting techniques [Tadmor 2006]. While non-sulfonated poly(arylene ethers) can simply be melt-extruded due to their wide processing window (gap between melting temperature and thermal degradation temperature) usually larger than 200 °C, the introduction of sulfonic acid groups, to a great extent, increases the melting temperature of the BPSH copolymer and decreases the thermal degradation temperature and, consequently, a small processing window of the BPSH copolymer prohibits the melt-extrusion. For example, the processing window for BPSH-35 is less than 50 °C, whereas a processing window of at least 100 °C is required for industrial melt-extrusion [Rosato 1998]. So, solvent casting is the only technically available production method for manufacturing the BPSH films. Also, the solvent-casting technique is known to be more advantageous for the production of thinner films with fewer physical defects and to induce larger microphase separation of block copolymers, which may lead to higher proton conductivity [Banerjee 2004, Lodge 2003]. Therefore, it can be safely concluded that solvent-casting is a more appropriate production method for the manufacture of BPSH films.

Huang et al. [2007] found that the final performance of the sulfonated poly(arylene ether sulfone) block copolymer significantly depended on film drying conditions, possibly such as drying temperature, initial solution concentration, and rate of solvent removal, while they were exploring the possibility of manufacturing the PEM

Table 1-1. Comparison of proton conductivities of sulfonated poly(ether ether ketone) membranes reported in the literature.

Degree of sulfonation [%]	Casting solvent <sup>b)</sup>	Conductivity [S/cm]	Reference
0.65	DMF	$1 \times 10^{-5}$	Kobayashi 1998
N/A <sup>a)</sup>	DMF	$7 \times 10^{-4}$	Rikukawa 2000
0.60	NMP	$6.4 \times 10^{-2}$	Cui 1998
0.60	NMP, DMAc	$2 \times 10^{-2}$	Bonnet 2000
0.73	N/A	$6.6 \times 10^{-2}$	Ise 1999

a) Not reported in the literature

b) DMF: dimethylformamide, NMP: n-methylpyrrolidone, DMAc: dimethylacetamide

films by solvent-casting using reverse-roll coating. However, their morphological study with the AFM (atomic force microscopy) images of the films provided no conclusive explanation. Generally, in the final stage of PEM preparation, thin uniform films are typically prepared by casting the polymer solutions at low concentrations on a flat surface and drying them under an infra-red lamp or in a heating oven in an uncontrolled manner. Based on the scarcity of any discussion of the issue in relevant literature, the significance of solvent-casting conditions has not attracted much attention. In Table 1-1 is given a comparison of the proton conductivities of sulfonated poly(ether ether ketone) membranes reported in the literature. Probable effects of solvent-casting conditions used in their preparation may explain the noticeable variation in their conductivity data in spite of the similarity in their compositions.

Another important factor that has not gained much attention, in the opinion of the author, is that the morphology of PEM films, like other common copolymer systems, may develop through the self-assembly process in which separate or linked components spontaneously demix and form ordered aggregates due to the incompatibility between the

components [Whitesides 2002]. It is generally known that the preparation method, morphology formation, and final properties of copolymers are quite interrelated. Even though it is fully recognized that partially sulfonated polymer systems for PEMs are also typical copolymers, the effects of solvent-casting conditions on their morphology formation have not been addressed at all in terms of self-assembly of copolymers, and it is unclear as to why previous studies have neglected the mechanism of self-assembly of copolymers in their preparation of PEMs. Also, there is a relative lack of understanding about the phase transformation and kinetics of copolymers in solution during processing, while many previous studies have been dedicated to the monitoring of the phase transformation and kinetics of block copolymers as melts and in solutions at equilibrium using rheology and scattering techniques, and reported their successful results. The ability to monitor the phase transformation of copolymers in solution in processing will be definitely beneficial for the optimization of the film drying process of copolymer systems.

The primary goal of this research is to optimize the performance of disulfonated poly(arylene ether sulfone) copolymer films for proton exchange membranes by controlling the solvent removal during film casting. With regard to this goal, the first objective of this thesis is to determine the effects of solvent selectivity, film drying temperature, and solvent removal rate on the final morphology and properties of the disulfonated copolymer films from a viewpoint of the phase separation of block copolymers. Additionally, the cause and mechanism of the effects are to be investigated through chemical analysis, spectroscopy, and so on. The second objective of this thesis is to develop a method to assess rheological properties ( $G'$  and  $G''$ ) of the block copolymer

during phase separation and to determine whether the rheological measurements can be used to monitor the phase separation and kinetics of block copolymers in solutions during solvent removal.

## 1.1 References

1. Alberti, G., Casciola, M., Constantino, R., Narducci, M., and Pca, M. Sganappa, Proton Conducting Membranes for Medium Temperature Fuel Cells: Recent Advances and New Strategies, *Desalination*, 199, 4-5, 2006.
2. Alberti, G., Costantino, U., Casciola, M., Ferroni, S., Massinelli, L., and Staiti, P., Preparation, Characterization and Proton Conductivity of Titanium Phosphate Sulfophenylphosphonate, *Solid State Ionics*, 145, 249-255, 2001.
3. Banerjee, S., and Curtin, D. E., Nafion<sup>®</sup> perfluorinated membranes in fuel cells, *Journal of Fluorine Chemistry*, 125, 1211-1216, 2004.
4. Bonnet, B., Jones, D. J., Roziere, J., Tchicaya, L., Alberti, G., Casciola, M., Massinelli, L., Bauer, B., Peraio, A., and Ramunni, E., Hybrid Organic-inorganic Membranes for a Medium Temperature Fuel Cell, *Journal of New Materials for Electrochemical Systems*, 3, 87-92, 2000.
5. Cui, W., Kerres, J., and Eigenberger, G., Development and Characterization of Ion-exchange Polymer Blend Membranes, *Separation and Purification Technology*, 14, 145-154, 1998
6. Dönitz, W., Fuel Cells for Mobile Applications, Status, Requirements and Future Application Potential, *International Journal of Hydrogen Energy*, 23, 611-615, 1998.
7. Johnson, B., Yilgor, I., Tran, C., Iqbal, M., Wightman, J. P., Lloyd, D. R., and McGrath, J. E., Synthesis and Characterization of Sulfonated Poly(Arylene Ether Sulfones), *Journal of Polymer Science: Polymer Chemistry*, 22, 721-737, 1984.
8. Johnstone, H., A Membrane's Role in Fuel Cells, *Filtration & Separation*, 38, 22-24, 2001.
9. Hickner, M. A., Ghassemi, H., Kim, Y. S., Einsla, B. R., and McGrath, J. E., Alternative Polymer Systems for Proton Exchange Membranes (PEMs), *Chemical Reviews*, 104, 4587-4612, 2004.
10. Huang, J., Baird, D. G., Fan, G., Zhang, Z., Badami, A., Takamuku, S., and McGrath, J. E., Continuous film casting and evaluation of polymer membranes for fuel cells, 2007 Society of Plastics Engineers Annual Conference, Cincinnati, OH, 2007.
11. Ise, M., Kreuer, K. D., and Maier, J., Electroosmotic Drag in Polymer Electrolyte Membranes: an Electrophoretic NMR Study, *Solid State Ionics*, 125, 213-223, 1999.
12. Kobayashi, T., Rikukawa, M., Sanui, K., and Ogata, N., Proton conducting Polymers Derived from Poly(ether ether ketone) and poly(4-phenoxybenzoyl-1,4-phenylene), *Solid State Ionics*, 106, 219-225, 1998
13. Larminie, J., and Dicks, A., *Fuel Cell Systems Explained*, 2<sup>nd</sup> Ed., John Wiley & Sons, New York, 2003.
14. Lodge, T. P., Block Copolymers: Past Successes and Future Challenges, *Macromolecular Chemistry and Physics*, 204, 265-273, 2003.
15. McGrath, J. E., Disulfonated Directly Copolymerized Poly(arylene ether) random and block systems: Synthesis, Characterization, and Applications to Fuel Cells and Chlorine Resistant Reverse Osmosis Membranes, Technical Conference and Review of the Macromolecules and Interfaces Institute, Blacksburg, VA, April 9-11, 2006.

16. Qiao, J., Saito, M., Hayamizu, K., and Okada, T., Degradation of Perfluorinated Ionomer Membranes for PEM Fuel Cells during Processing with H<sub>2</sub>O<sub>2</sub>, *Journal of The Electrochemical Society*, 153, A967-A974, 2006.
17. Rikukawa, M., and Sanui, K., Proton Conducting Polymer Electrolyte Membranes Based on Hydrocarbon Polymers, *Progress in Polymer Science*, 25, 1463-1502, 2000.
18. Robertson, G. P., Mikhailenko, S. D., Wang, K., Xing, P., Guiver, M. D., and Kaliaguine, S., Casting solvent interactions with sulfonated poly(ether ether ketone) during proton exchange membrane fabrication, *Journal of Membrane Science*, 219, 113-121, 2003.
19. Rosato, D. V., *Extruding plastics: A practical processing handbook*, Chapman & Hall, London, 1998.
20. Rozière, J., and Jone, D. J., Non-Fluorinated Polymer Materials for Proton Exchange Membrane Fuel Cells, *Annual Review of Materials Research*, 33, 503-555, 2003.
21. Sopian, K., and Daud, W. R. W., Challenges and future developments in proton exchange membrane fuel cells, *Renewable Energy*, 31, 719-727, 2006.
22. Tadmor, Z., and Gogos, C. G., *Principles of Polymer Processing*, Wiley-Interscience, New York, 2006.
23. Vishnyakov, V. M., Proton Exchange Membrane Fuel Cells, *Vaccum*, 80, 1053-1065, 2006.
24. Wang, S., and McGrath, J. E., Synthesis of Poly(Arylene Ether)s, in *Synthetic Methods in Step-Growth Polymers*, Martin, E. R., and Long, T. E. Eds. Wiley, New York, 2003.
25. Wang, F., Hickner, M., Ji, Q., Harrison, W., Mecham, J., Zawodzinski, T. A., and McGrath, J. E., Synthesis of Highly Sulfonated Poly(arylene ether sulfone) Random (Statistical) Copolymers via Direct Polymerization., *Macromol. Symp.* 175, 387-395, 2001.
26. Wang, F., Hickner, M., Kim, Y. S., Zawodzinski, T. A., and McGrath, J. E., Direct Polymerization of Sulfonated Poly (arylene ether sulfone) Random (statistical) Copolymers: Candidates for New Proton Exchange Membranes, *Journal of Membrane Science*, 197, 231-242, 2002.
27. Whitesides, G. M., and Boncheva, M., Beyond Molecules: Self-assembly of mesoscopic and macroscopic components, *Proceedings of the National Academy of Sciences*, 99, 4769-4774, 2002.
28. Zaidi, S. M. J., Mikhailenko, S. D., Robertson, G. P., Guiver, M. D., and Kaliaguine, G., Proton Conducting Composite Membranes from Polyether Ether Ketone and Heteropolyacids for Fuel Cell Applications, *Journal of Membrane Science*, 173, 17-34, 2000.

## CHAPTER 2

### LITERATURE REVIEW

#### 2.1 Proton exchange membrane

The proton exchange membrane (PEM), also referred to as the polymer electrolyte membrane, is one of the most fundamental components in the operation of PEM fuel cells (FCs). Its essential function is to conduct protons while separating the fuel from the oxidant [Larminie 2003]. Three main applications of PEM FCs are automotive, stationary, and portable power, and each application requires its own materials and operating conditions. However, high proton conductivity, low electron conductivity, low permeability to gases, low water transport through diffusion and electro-osmosis, good chemical stability, good mechanical properties, and reasonable cost are commonly required for PEMs [Hickner 2004]. It was recently reported that reduced swelling-and-deswelling behavior of PEMs was also required for improved endurance and easy control of FC systems [McGrath 2006].

The current high cost of fuel cells, approximated at \$ 200/kW, is one of the main barriers for widespread commercialization, and must be reduced in order for fuel cells to be more competitive than any other energy conversion technology [Bar-On 2002]. The performance of essential components such as PEMs, electrodes, and bipolar plates should also be improved [Haile 2003]. Sopian et al. [2006] itemized the major technical barriers in the order of priority as follows: membrane cost reduction, electrodes with low Pt

content, CO tolerant anode electro-catalysts, bipolar plate material, stack and bipolar plate design, and PEM FC system design. The development and improvement of a hydrocarbon PEM has the highest priority for widespread commercialization of PEM FCs because of the following two reasons: (1) huge cost reduction can be attained by replacing perfluorinated Nafion<sup>®</sup> with non-fluorinated polymer electrolytes that employ a cheaper sulfonated polymer backbone, and (2) the type and operating conditions of PEMs decide the design, operation, and control of other major components.

In order to produce satisfactory proton conductivity, all of the current PEMs need a fully hydrated condition, which results in a complicated water management system [Sopian 2006], and causes serious deterioration of the mechanical properties of PEMs, especially at elevated temperature [Kim 2003]. Thus, the development of ‘water-free’ electrolytes is believed to be the most ideal alternative [Kreuer 1998]. However, because the current performance of non-hydrated membranes is much less effective than that of the state-of-the-art PEM, Nafion<sup>®</sup>, many efforts are being focused on the development of a PEM with improved proton conductivity and endurance. Specifically, the U.S. Department of Energy has currently established a goal of 0.1 S/cm for the proton conductivity of a membrane at 120 °C and 50 % relative humidity, the target operating conditions for automotive application [DOE].

The first section of this chapter discusses parameters relevant to the evaluation of PEMs, and the following section introduces some promising polymer systems for PEMs that will be investigated in this study, particularly wholly aromatic bisphenol-based poly(arylene ether sulfone) random copolymer (BPSH) with a focus on its potential for proton exchange membranes in fuel cells as well as its synthesis and characterization.

### 2.1.1 Relevant parameters for evaluation of proton exchange membranes

Before a detailed discussion of potential PEM systems, it is necessary to define some terminologies relevant to the evaluation of PEMs in order to compare different PEM systems, and to present their measurement methods. In this section, the definitions and measurement methods of proton conductivity, water uptake, and ion exchange capacity (IEC) will be presented.

Proton conductivity is the primary property that demonstrates the performance of proton exchange membranes, and can be measured with a simple method devised by Zawodzinski et al. [1991], “by using electrochemical impedance spectroscopy and a simple cell that allows equilibration in a variety of environments.” A typical cell for the measurement of the in-plane proton conductivity is shown in Figure 2.1-1. This cell was designed to minimize the resistance of the cell so that the determined value of resistance was mostly due to the membrane [Wang 2002]. This method only enables the

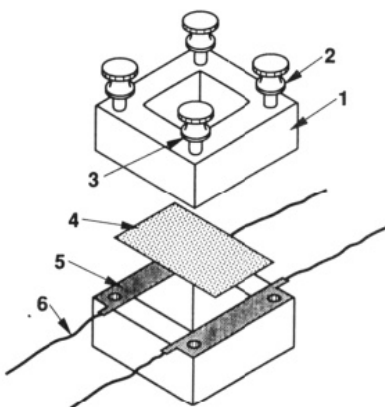


Figure 2.1-1. Cell used for measurement of proton conductivity: (1) Teflon block, (2) thumbscrew, (3) open area to allow equilibration, (4) membrane sample, (5) blackened Pt foil, and (6) Pt ribbon lead [Zawodzinski 1991] (Illustrated under “Fair Use” copyright guidelines).

determination of the in-plane proton conductivity of the membranes as opposed to the through-plane proton conductivity that is more similar to actual proton conduction in the operation of fuel cells. However, it has wide usage as a preliminary screening test because the measurement of through-plane conductivity is more intricate due to the relatively small magnitude of measured membrane resistances and relatively large interfacial resistances [Alberti 2000 & 2001, Pivovar 1999]. The conductivity of PEMs can be calculated from the measured resistance and the geometry of the cell using the following equation:

$$\text{Proton conductivity, } \sigma = \frac{l}{A \cdot Z'} \quad (\text{Eq. 2.1-1})$$

where  $l$ ,  $A$ , and  $Z'$  represent the distance between the electrodes, the cross sectional area of the membrane, and the real contribution of the impedance response, respectively.

Water uptake is also a significant index for the assessment of final performance of PEMs because all current potential PEM materials need water as the mobile phase to facilitate proton conduction [Kim 2003]. However, absorbed water also has an adverse effect on the mechanical properties of membranes by acting as a plasticizer and lowering the  $T_g$  of the membranes. Water uptake of PEMs is usually represented as the weight ratio of the absorbed water to the membrane, as established by Zawodzinski et al. [1993]:

$$\text{Water uptake (\%)} = \frac{W_{wet} - W_{dry}}{W_{dry}} \times 100 \quad (\text{Eq. 2.1-2})$$

where  $W_{wet}$  and  $W_{dry}$  mean the weight of fully hydrated and dry membranes. Water uptake is also represented by  $\lambda$ , which is the number of water molecules absorbed by an acid site:

$$\lambda = \frac{(W_{wet} - W_{dry}) / MW_{H_2O}}{IEC \times W_{dry}} \quad (\text{Eq. 2.1-3})$$

where IEC is the ion exchange capacity of the dry membrane in equivalents per gram.

Both proton conductivity and water uptake are substantially dependent on the concentration of ion-conducting moieties (most commonly sulfonic acid) in the polymer electrolyte membrane. The amount of ion-conducting moieties is expressed as an ion exchange capacity (IEC) with units of milliequivalents per gram of polymer (mequiv/g or mmol/g) or as an equivalent weight (EW) with units of grams of polymer per equivalent (g/equiv or g/mol). That is, IEC and EW are inversely proportional to each other. Proton conductivity and water uptake can be improved by simply increasing the number of ion-conducting moieties. However, the amount of ion-conducting moieties must be controlled with respect to other physical properties, because an excessive amount of ion-conducting moieties causes excessive swelling of the membrane, which leads to serious deterioration of mechanical properties and durability. The IEC values of the BPSH copolymer and its variations can be determined by titration and  $^1\text{H}$  NMR spectroscopy.

### 2.1.2 Disulfonated poly(arylene ether sulfone) random and multi-block copolymer: BPSHx and BPSH100-BPSO

Poly(arylene ether sulfone) copolymer, of which chemical structure is shown in Figure 2.1-2, is a class of amorphous thermoplastic polymers characterized by high glass transition temperatures, good mechanical strength and stiffness, and superior thermal and oxidative resistance, especially when they consist of wholly aromatic units. Because of these attractive properties as well as its availability, its practical applications are diverse [Cotter 1995]. These polymers are commercially synthesized by nucleophilic aromatic substitution, which is widely used for industrial scale manufacturing because of its simplicity and cost-effectiveness [El-Hibri 2003]. Wang et al. [2002] accomplished a sophisticated sulfonation of poly(arylene ether sulfone) copolymers by slightly modifying the nucleophilic aromatic substitution as described below, with the aim of developing a polyelectrolyte material for proton exchange membranes in fuel cells without sacrificing the aforementioned excellent physical and other properties.

Unlike the post-sulfonated poly(arylene ether sulfone) copolymers, the sulfonation of disulfonated poly (arylene ether sulfone) copolymers is achieved at the stage of monomer preparation, and the degree of sulfonation is controlled by altering the

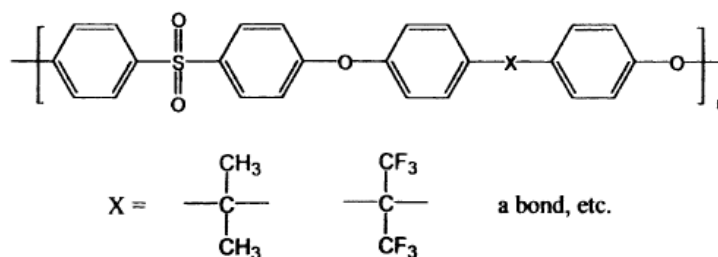


Figure 2.1-2. Chemical structure of poly (arylene ether sulfone)s [Hickner 2004] (Illustrated under “Fair Use” copyright guidelines).

stoichiometry of the sulfonated and non-sulfonated monomer feeds [Wang 2002]. Robeson et al. [1983] first reported the disulfonation of 4,4'-dichlorodiphenyl sulfone (DCDPS) into 3,3'-disulfonated-4,4'-dichlorodiphenyl sulfone (SDCDPS), and utilized it as a flame retarding additive. Recently, Ueda et al. [1993] also reported the sulfonation of DCDPS and revealed the general procedure for its purification and characterization, and the key procedure for the polymerization of disulfonated DCDPS into bisphenol A-based poly(arylene ethers). The synthetic schematics of the monomer and wholly aromatic bisphenol-based disulfonated poly(arylene ether sulfone) copolymer are presented in Figure 2.1-3 and -4. SDCDPS is attained via a plain electrophilic aromatic substitution reaction between DCDPS and excess oleum (a solution of trioxide in sulfuric acid) with 3.3 to 1 mole equivalent  $\text{SO}_3$  ratio [Sankir 2003]. Disulfonated poly(arylene ether sulfone) copolymers are then synthesized via common direct aromatic nucleophilic substitution polycondensation. The only differentiating feature of the reaction is the reaction temperature: somewhat higher reaction temperature (around 190 °C) must be provided in order to effectively facilitate the nucleophilic substitution reaction on the sterically hindered SDCDPS, and consequently obtain copolymers with high molecular weight, whereas the commercial nucleophilic aromatic substitution polymerization is usually carried out at 130 ~ 160 °C and results in copolymer with low molecular weight [Harrison 2005]. It is widely known that high molecular weight can develop the entanglement of molecular chains, accordingly enabling the final product to have improved mechanical properties. As shown in Figure 2.1-5, a variety of sulfonated poly(arylene ethers) may be synthesized by simply employing commercially available bisphenols

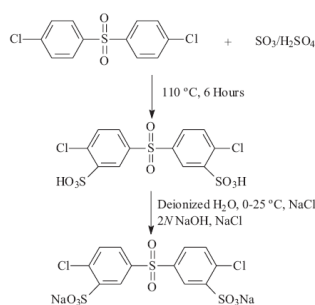


Figure 2.1-3. Synthesis of sodium sulfonate salt of 3,3'-disulfonated-4,4'-dichlorodiphenyl sulfone (SDCDPS) [Wang 2002] (Illustrated under “Fair Use” copyright guidelines).

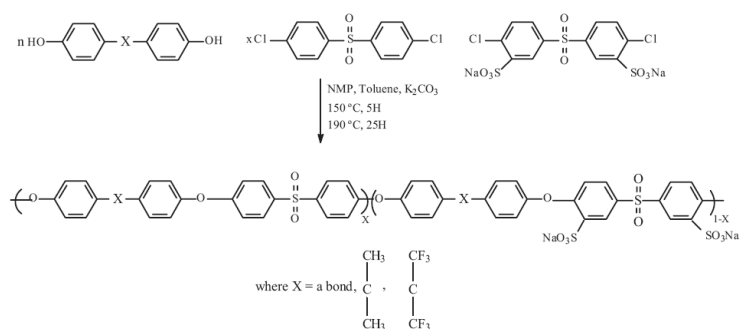


Figure 2.1-4. Synthesis of wholly aromatic, biphenol-based disulfonated poly(arylene ether sulfone) copolymer (BPSH-x) [Wang 2002] (Illustrated under “Fair Use” copyright guidelines).

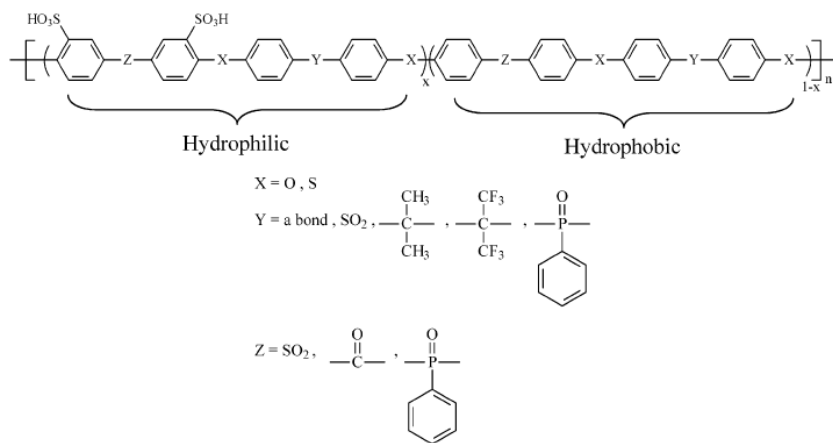


Figure 2.1-5. Possible chemical structures of sulfonated poly(arylene ether) copolymers [Hickner 2004] (Illustrated under “Fair Use” copyright guidelines).

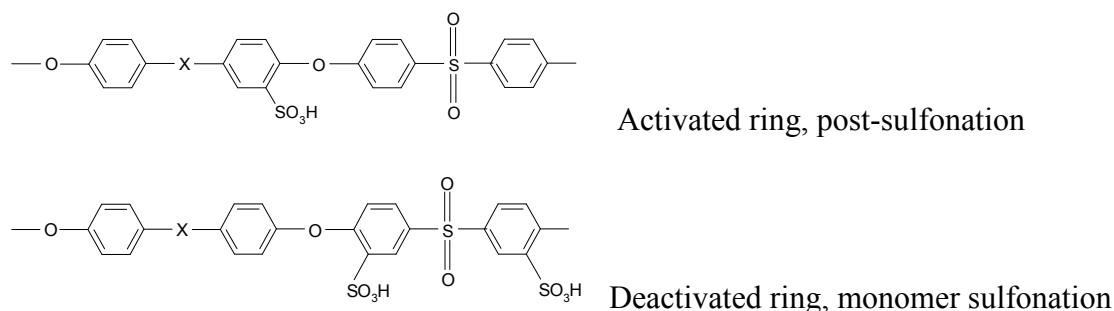


Figure 2.1-6. Different positions of sulfonic acid groups by different sulfonation methods (X = O, S) (Illustrated under “Fair Use” copyright guidelines).

such as bisphenol A, hydroquinone, biphenol, hexafluoroisopropylidene, etc [Harrison 2003]. Hereinafter, the scope of this literature review will be limited to ***biphenol-based wholly aromatic disulfonated poly (arylene ether sulfone) copolymers*** named as ***BPSH-x***, which denotes biphenol (BP), sulfone (S), acid form (H), and mole % (x) of the sulfonated repeat unit, respectively.

The BPSH copolymer synthesized by the direct copolymerization route described above has several advantages, especially over the post-sulfonated polymers. A comparison between the chemical structures of post-sulfonated poly(arylene ethers) and the BPSH copolymer is given in Figure 2.1-6. First, the sulfonation of the monomer (DCDPS) enables the attachment of the proton-conducting sulfonic acid group to a deactivated phenyl ring, which thus enhances stability against desulfonation because “the anticipated intermediate carbocation required for desulfonation is more difficult to stabilize on such a sulfone deactivated ring.” [Wang 2002] This may also induce higher acidity of the attached sulfonic acid groups, which is favorable for proton conductivity. Furthermore, a more precise and reproducible degree of sulfonation can be achieved by varying the stoichiometry of the monomer feeds. In addition, BPSH is a polymer system

Table 2.1-1. Dependence of proton conductivity and water uptake on degree of sulfonation, hydrothermal treatment, and temperature [Kim 2003a] (Illustrated under “Fair Use” copyright guidelines).

Specimen	Proton conductivity (S/cm)				Water uptake (%) at 30 °C	
	30 °C in liquid water		70 °C in saturated water vapor		Method 1	Method 2
	Method 1 a	Method 2 b	Method 1	Method 2		
BPSH-20	0.01	0.02	-	-	12	17
BPSH-30	0.03	0.04	0.02	0.06	24	31
BPSH-35	0.07	0.08	0.05	0.09	32	38
BPSH-40	0.08	0.10	0.07	0.12	39	58
BPSH-60	0.16	0.31	-	-	148	> 1000
Nafion <sup>®</sup> 1135	0.11	0.11	0.12	0.12	19	19

<sup>a</sup> Acidified in 2.0 M sulfuric acid aqueous solution at 30 °C.

<sup>b</sup> Acidified in 0.5 M sulfuric acid aqueous solution at 100 °C.

based on commercially readily available and reasonably priced materials, and therefore is advantageous for widespread commercialization.

The proton conductivity and water uptake of the BPSH copolymers strongly depend on degree of sulfonation, relative humidity, temperature, and hydrothermal treatment [Kim 2003]. Table 2.1-1 demonstrates the effect that the degree of disulfonation has on the proton conductivity and water uptake. It is not surprising that the proton conductivity and water uptake of the BPSH copolymers increase with degree of disulfonation [Kim 2003]. Table 2.1-1 and Figure 2.1-7 also show the influence of temperature and relative humidity on the proton conductivity and water uptake; both proton conductivity and water uptake increase with temperature and humidity. Like the other hydrocarbon aromatic proton exchange membranes studied by Kreuer [2001] and by Alberti et al. [2001], the temperature and humidity dependences of the BPSH copolymer are generally larger than those of Nafion<sup>®</sup> probably because the acidity of the

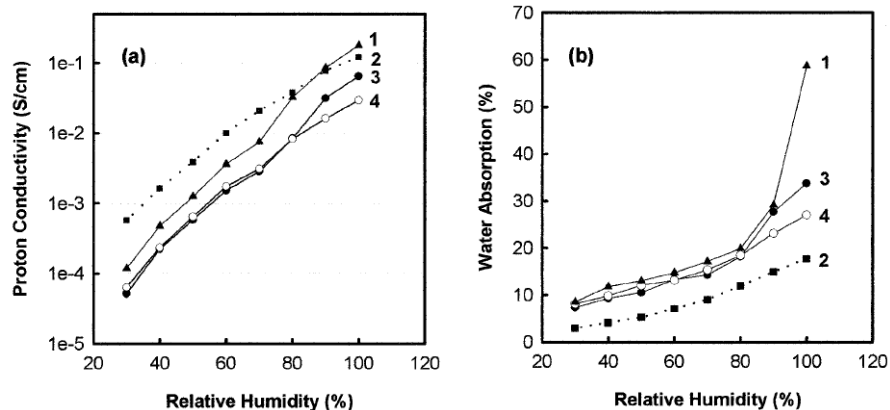


Figure 2.1-7. Influence of relative humidity on proton conductivity and water uptake of BPSH random copolymer; measurement temperature 80 °C. 1: BPSH-40-Method 2, 2: Nafion 1135-Method 1, 3: BPSH-30-Method 2, 4: BPSH-300-Method 1 [Kim 2003a] (Illustrated under “Fair Use” copyright guidelines).

aryl sulfonic acid groups is lower than that of the sulfonic acid groups in perfluorinated Nafion<sup>®</sup>. Kim et al. [2003] also reported that high temperature acidification of the BPSH copolymer, i.e. immersion in a sulfuric acid solution around 100 °C, induced higher water uptake, and subsequently higher proton conductivity, as presented in Table 2.1-1. They showed via analytical chemistry analysis and AFM image analysis that the increase in the proton conductivity resulted entirely from morphological changes that will be mentioned below in detail.

Morphological studies of BPSH have elucidated that the microphase-separated morphology of the PEM plays a key role in determining the performance [Kim 2003a, b, Hickner 2001]. The morphology of the BPSH copolymer strongly depends on the degree of disulfonation as shown in Figure 2.1-8 [Harrison 2005]. The degree of continuousness of hydrophilic domains increases with degree of disulfonation; the hydrophilic domains of the BPSH copolymers with a lower degree of disulfonation are surrounded by a hydrophobic matrix, while the BPSH copolymer with a higher degree of disulfonation

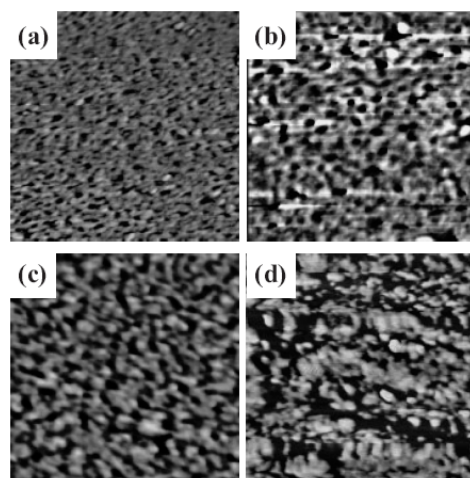


Figure 2.1-8. AFM images of BPSH with disulfonation of (a) 20, (b) 40, (c) 50, and (d) 60 % acidified with 2.0 M sulfuric acid aqueous solution at 30 °C [Harrison 2004] (Illustrated under “Fair Use” copyright guidelines).

has a more open and continuous hydrophilic domain structure. Hydrothermal treatment also has a serious effect on the morphology of the BPSH copolymers [Kim 2003a]. High temperature acidification induced more aggregations of hydrophilic domains, whereas room temperature acidification yielded a more closed hydrophilic domain structure. This morphological difference resulted in a noticeable difference in the water uptake and proton conductivity of the BPSH polymers in spite of the same degree of disulfonation.

One of the distinct differences between the wholly aromatic BPSH copolymer and the perfluorinated sulfonic acid copolymer is their mechanical properties [Kim 2002, Hickner 2001]. In Figure 2.1-9 is given the comparison of the stress-strain behavior of BPSH-40 with Nafion<sup>®</sup> 117 in dry and hydrated states. The BPSH copolymer in its dry state showed the typical stress-strain behavior of a tough and ductile thermoplastic, whereas Nafion<sup>®</sup> 117 in dry states had considerably lower strength but much larger

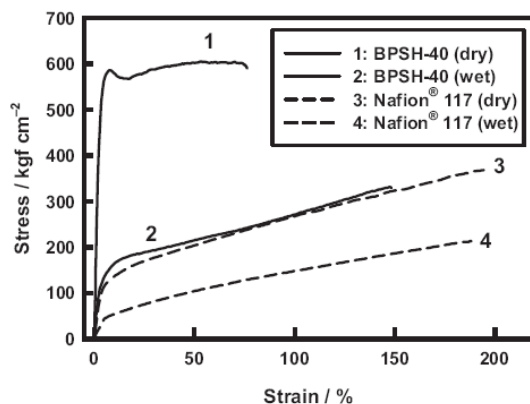


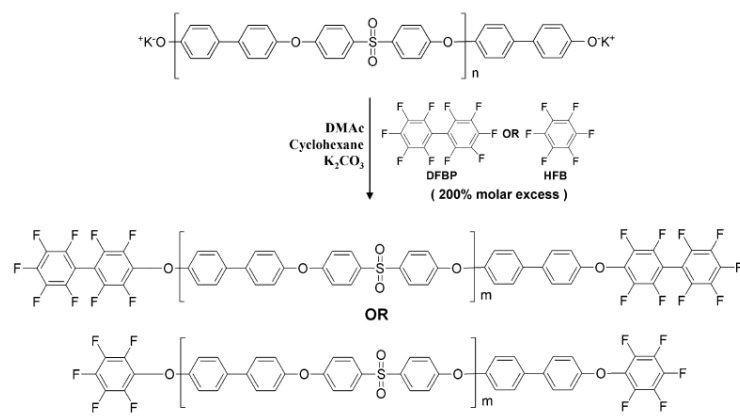
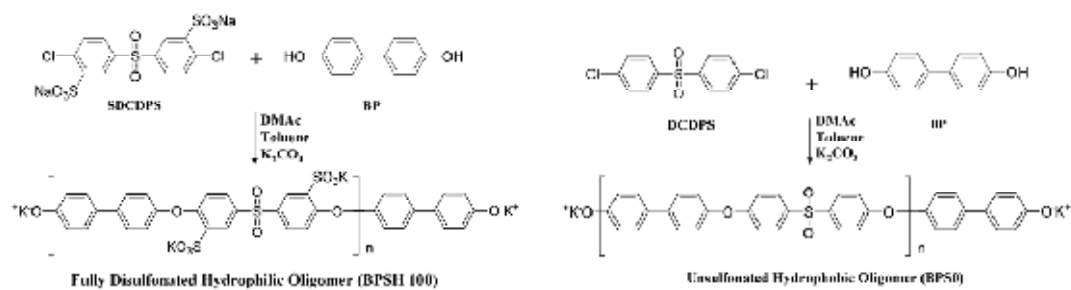
Figure 2.1-9. Stress-strain behaviors of BPSH-40 and Nafion 117. The hydrated state of BPSH-40 and Nafion<sup>®</sup> 117 contains water of 22 and 16 %, respectively [Harrison 2004] (Illustrated under “Fair Use” copyright guidelines).

elongation, which is the characteristic behavior of elastomeric materials. The hydrated BPSH copolymer still had the same magnitude of modulus as dry Nafion<sup>®</sup> 117, although the modulus noticeably decreased in comparison with the dry state. In contrast, the modulus decrease of hydrated Nafion<sup>®</sup> 117 was much smaller than that of the BPSH copolymer, and the stress-strain behavior showed a similar qualitative trend, probably owing to the maintained crystallinity. That is, the great decrease in the mechanical properties of hydrated copolymers may be attributable to their amorphousness and the greater degree of phase mixing between the hydrophilic and hydrophobic domains of the BPSH copolymer. From the comparison of the mechanical properties, it is worthy to note that the toughness of both dry and hydrated BPSH copolymer was superior to Nafion<sup>®</sup>.

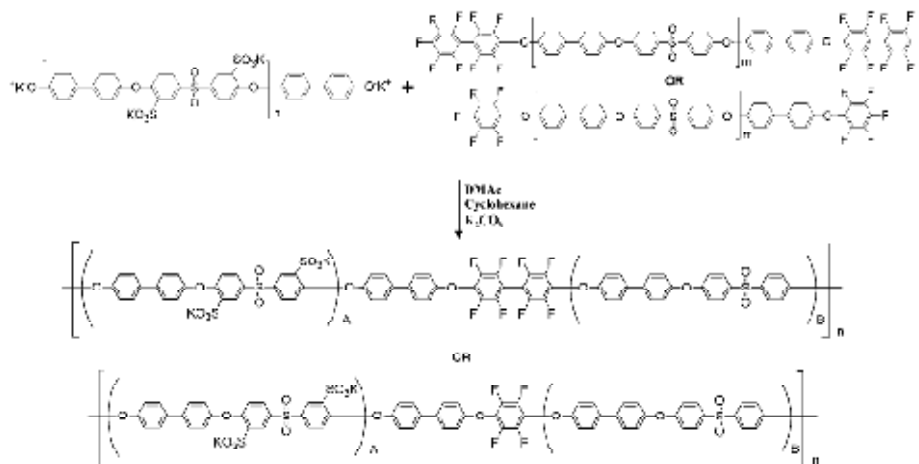
Thermal properties of the BPSH random copolymer both in its salt form (BPS-x) and in its acid form (BPSH-x) are also important parameters that decide the processing method and conditions as well as the operating conditions of PEM FCs. As such, they will be discussed with the processing of polymer electrolyte membranes in Section 4.2.

A more advanced version of the BPSH random copolymer is multiblock copolymers consisting of sulfonated and non-sulfonated poly(arylene ether sulfone) blocks (BPSH100-BPS0) [Lee 2008]. Instead of consisting of the same monomers as the random copolymer, the sequence lengths of the multiblock copolymers are longer than that of the random copolymer, which hypothetically leads to more ordered and continuous structure of sulfonated regions and, accordingly, higher proton conductivity.

The overall synthetic scheme of the multiblock copolymer is shown in Figure 2.1-10. A series of phenoxide terminated wholly disulfonated poly(arylene ether sulfone) hydrophilic oligomers (BPSH100) and a series of non-sulfonated poly(arylene ether sulfone) hydrophobic oligomers (BPS0) with different molecular weights (3, 5, 10, 15, and 20 kg/mol) were first prepared by a common direct aromatic nucleophilic substitution polycondensation. Then, the phenoxide terminated BPS0 oligomers were end-capped with decafluorobiphenyl (DFBP) or hexafluorobenzene (HFB) using a nucleophilic aromatic substitution reaction. Finally, multiblock copolymers were obtained by a coupling reaction between the DFBP or HFB end-capped BPS0 oligomers and the phenoxide terminated BPSH100 oligomers. Owing to the highly reactive nature of DFBP and HFB, the coupling reaction could be carried out at mild conditions, e.g., below 105 °C, which enabled prevention of possible ether-ether exchange reactions. Or else, the ether-ether exchange reaction may induce randomization of the well-defined hydrophilic-hydrophobic sequences. It is worthy to note that the block length of the copolymers had strong effects on their proton conductivity and water uptake [Lee 2008]. The proton conductivity increased with the block length in spite of comparable degree of sulfonation values of the copolymers. The multiblock copolymers with longer sequences developed



End-capping of BPS0 hydrophobic oligomer with DFBP or HFB.



Synthesis of segmented sulfonated multiblock copolymers (BPSH-BPS) with different linkage groups.

Figure 2.1-10. Overall synthetic scheme of hydrophilic-hydrophobic multiblock copolymers based on poly(arylene ether sulfone) (BPSH100-BPS0) [Lee 2008] (Illustrated under “Fair Use” copyright guidelines).

well-defined sulfonated regions, which resulted in enhanced proton conductivity, especially, at low relative humidity. This structure-property relationship has been confirmed via measurement of self-diffusion coefficient of water in the membranes and states of water analysis as well as morphological studies using atomic force microscopy and transmission electron microscopy [Roy 2008, Anand 2009].

As presented thus far, the random and multiblock copolymers (BPSH and BPSH100-BPS0) are competitive in terms of proton conduction and mechanical and thermal properties, in addition to being easier to synthesize. This indicates that the copolymers are practically viable and have potential for fuel cell application at elevated temperatures (above 100 °C). In order to improve the performance by modifying their chemical structure and/or composition, research on their synthesis is underway in the Department of Chemistry at Virginia Tech.

## 2.2 Production of proton exchange membranes

Since proton exchange membrane (PEM) fuel cell (FC) technology began to regain interest and support as an alternative energy source in the early 1990s [Banerjee and Curtin 2004], scientists and engineers have introduced and tested numerous candidate materials and their variations in order to develop a PEM with satisfactory performance and availability. However, in general, almost all the membranes generated in the laboratory, to the knowledge of the author, were prepared using a batch system: a polymer solution with a very low concentration is hand-cast onto glass plates, with the solvent then being removed by means of evaporation in the presence of a heat lamp or in an oven. This batch casting approach cannot lead to the manufacture of the membranes at the rate required for commercialization mainly because of its low production rate. Thus, it is essential to utilize an appropriate film casting technique in order to improve the production rate up to a commercially viable level.

On a commercial basis PEM films are manufactured by means of melt extrusion casting or solvent casting. Melt extrusion casting consists of melt extrusion and die casting, while solvent casting is composed of three main steps: polymer solution preparation, solution deposition onto a substrate, and solvent evaporation [Kim and Hyun 2001]. Several previous studies [Kim et al. 2003 JPS, Zawodzinski et al. 1991, Bauer et al. 2000, Robertson et al. 2003, Bébin and Galiano 2006 a and b, Banerjee and Curtin 2004] investigated the effects of processing conditions of melt extrusion casting and solvent casting on the final properties of PEMs. For example, Bébin and Galiano [2006 a, b] reported that solvent casting and extrusion casting induced different final properties of sulfonated poly (ether ether ketone) (SPEEK) membranes. Zawodzinski et al. [1991] also

showed that drying temperature of a perfluoro sulfonic acid PEM, Nafion<sup>®</sup>, is crucial for the final properties and performance. Even though the aforementioned previous studies strongly imply that processing conditions may have substantial effects on the final properties of PEMs, the significance of material processing seems to have been underestimated. Therefore, this section will cover the details of previous studies on the processing of polymer systems for the PEMs in order to examine the significance of the production methods of PEMs and then explore the processability of biphenol-based wholly aromatic disulfonated poly (arylene ether sulfone) random copolymer (BPSH-35) based on its thermal characterization.

#### 2.2.1 Previous studies on the production of polymer electrolyte polymer membranes

First, the effects of the drying temperature of PEM films on their final performance have been reported in several previous studies [Zawodzinski et al. 1991, Robertson et al. 2003]. Zawodzinski et al. [1991] investigated the effects of the drying temperature of Nafion<sup>®</sup> films. Their results showed that drying of a Nafion dispersion (10 ~ 15 wt %) at around 100 °C induced lower water uptake and subsequently lower proton conductivity of the resultant Nafion<sup>®</sup> membranes. They ascribed this reduction to the high-temperature conditions unfavorable for the aggregation of the hydrophilic ionic clusters. Robertson et al. [2003] observed the effects of solvent type (dimethylformamide (DMF) and dimethylacetamide (DMAc)) and drying temperature (up to solvent boiling temperature) on the proton conductivity of sulfonated poly (ether ether ketone) (SPEEK) membranes. They reported through <sup>1</sup>H NMR spectroscopy that the amide functional groups of DMF and DMAc were subjected to partial thermal decomposition during



with the synthesis, characterization, and performance of the BPSH random copolymer. However, an adverse effect of hydrothermal treatment was also reported. Li et al. [2003] found that a SPEEK membrane cured by a sulfuric acid solution at its boiling temperature was more susceptible to methanol permeation, which lead to inferior performance as a direct methanol fuel cell (DMFC) membrane.

Recently, Bébin and Galiano [2006 a, b] explored the possibility of manufacturing films of sulfonated poly (ether ether ketone) (SPEEK) by a continuous extrusion process. Their plasticization and thermal studies revealed that grafting sulfonic acid groups onto the chemical structure of the PEEK remarkably reduced its range of processing temperature. Hence, it was required to introduce high amounts of plasticizer (about 30 wt % of polyethyleneglycol (PEG)) in order to enable the melt-phase processing of the SPEEK in its acid form. The removal of PEG made the resultant SPEEK film highly porous, which is unquestionably problematic for the operation of fuel cells. Because more plasticizer is necessary for an industrial production, they concluded that the melt-phase processing of the SPEEK in its acid form is not practically viable. Bébin and Galiano [2006 b] also examined the melt-processability of SPEEK in its salt form. The lower reactivity and better chemical stability of the salt form enabled the melt-phase processing of SPEEK with even less plasticizer (about 10 % of PEG). They reported that the usage of a removable plasticizer increased the surface area of the films so that more sulfonic acid groups were readily accessible, which consequently improved the proton conductivity. However, they did not clearly reveal whether or not the residual porosity of the membrane has any undesirable effects such as weakened mechanical properties and/or increased vulnerability to fuel crossover in a long-term application, which are, to a

great extent, suspected to occur in the operation of PEM FC. They also compared the performance of solvent-cast and extrusion-cast SPEEK films: extrusion-cast ones had better durability than solvent-cast ones.

Recently it was reported that solvent casting improves the overall quality of the current leading polymer electrolyte membrane, Nafion<sup>®</sup>, that has been manufactured by extrusion-casting for more than 35 years. Especially, thinner membranes with a superior uniformity of their thickness can be obtained [Banerjee and Curtin 2004]. However, no details of the extrusion-cast and solvent-cast processing conditions have been disclosed yet.

More recently Huang and coworkers [2007] reported that solvent-casting conditions of the BPSH random and block copolymer systems (Figure 2.2-2) had substantial effects on membrane properties and performances. In particular, they investigated membranes generated by means of continuous solvent-casting using a reverse roll coating technique. In Figure 2.2-3 is shown the mechanical anisotropic behavior of the continuous-cast BPSH-32 films. The elongation of the continuous-cast films in the machine direction was more than twice that in the transverse direction, in spite of no discernible difference in their strength. The average of their elongations ( $\approx 55\%$ ) was almost the same as that of the batch-cast films. They attributed this anisotropic

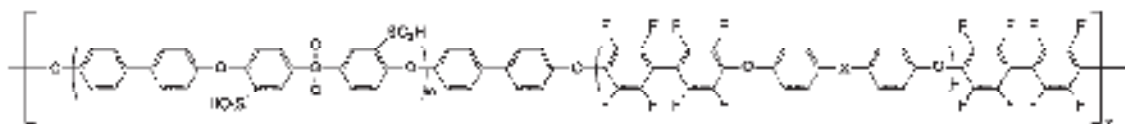


Figure 2.2-2. Chemical structure of BisSF-BPSH block copolymer used in Huang et al.'s study [Huang 2007] (Illustrated under "Fair Use" copyright guidelines).

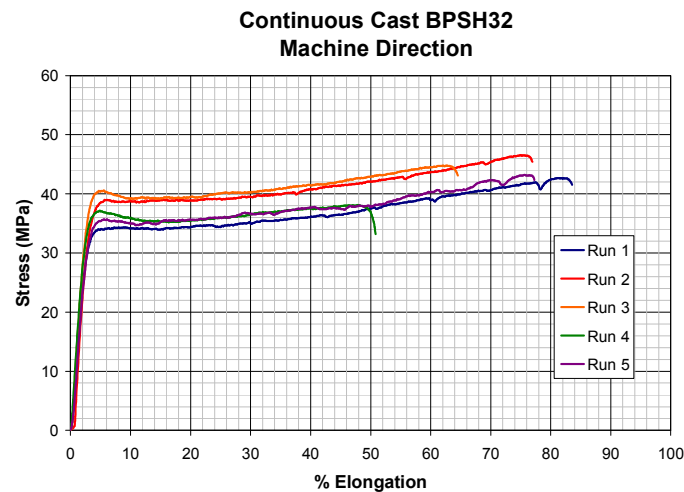
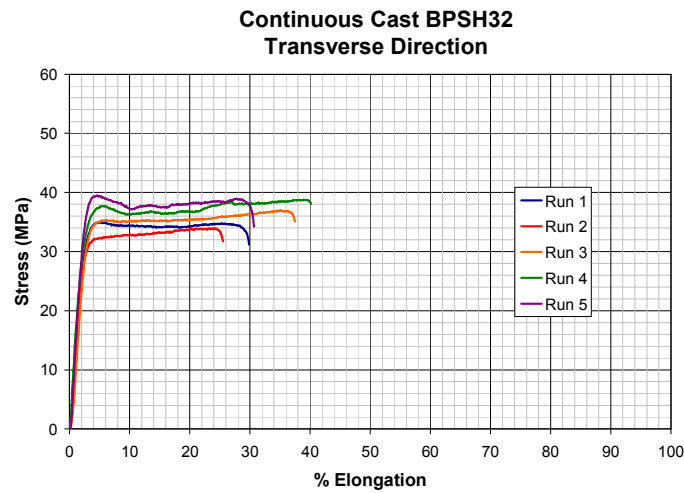


Figure 2.2-3. Comparison of stress-strain behavior of batch cast and continuous cast BPSH-32 films [Huang 2007] (Illustrated under “Fair Use” copyright guidelines)

Table 2.2-1. Effects of solvent-casting conditions on the proton conductivity of BisSF/BPSH block copolymers [Huang 2007] (Illustrated under “Fair Use” copyright guidelines).

Polymer	Casting method	Solution initial concentration w/v %	Drying temperature [°C]	Proton conductivity <sup>a</sup> [S/cm]
BisSF 17k/12k	Continuous	12.5	50	0.065
BisSF 17k/12k	Batch	5	~ 30	0.13
BisSF 17k/12k	Batch recast	5	~ 30	0.12
BisSF 18k/13k	Continuous	8	30, then 50	0.10
BisSF 18k/13k	Batch	5	~ 30	0.10
BisSF 22k/14k	Continuous	10	30, then 50	0.090
BisSF 22k/14k	Batch	5	~ 30	0.095

<sup>a</sup> Measured in liquid water at 30 °C ( $\pm 5$  %)

mechanical property of the continuous-cast films to the alignment of polymer molecules caused by extremely high shearing at the coating region. Another important feature is the effect of solvent-casting conditions on the proton conductivity of the block copolymer system. As presented in Table 2.2-1, it was very clear that the processing conditions such as the coating method, drying temperature, and initial polymer concentration had profound impacts on the proton conductivity. However, the origin of these differences could not be determined from the casting conditions, and their explanation of the relationship with the AFM images of the films was not conclusive.

As discussed so far, previous studies strongly suggest that altering processing methods and conditions can significantly vary the final morphology and properties of PEMs. Therefore, both the membrane material and its method of production have to be considered in the development stage in order to successfully manufacture new polymer electrolyte membranes.

## 2.2.2 Thermal characterization and processability of poly (arylene ether sulfone) copolymer

A wide range of processing temperature (usually larger than 200 °C) of poly sulfone polymers enables their melt-phase processing [El-Hibri and Weinberg 2003]. The processing temperature range is bounded by the glass transition temperature ( $T_g$ ) and the thermal decomposition temperature ( $T_d$ ) of the polymer material.  $T_g$  and  $T_d$  of non-sulfonated poly (arylene ether sulfone) copolymer, commercialized as RADEL<sup>®</sup> R by Solvay Advanced Polymers, are 221 and 516 °C, respectively [Wang et al. 2002, Solvay Advanced Polymers 2002]. However, the sulfonation of poly (arylene ether sulfone) copolymer complicates the thermal properties. The thermal characterization of BPSH copolymers is summarized in Table 2.2-2. The  $T_g$  of the dry BPSH copolymers increased with degree of sulfonation, ranging from 230 to 280 °C [Wang et al. 2002], because the molecular motion is restricted by the increased amount of intermolecular interaction and

Table 2.2-2. Effect of the degree of sulfonation on the thermal properties of BPSH copolymer [Wang 2002] (Illustrated under “Fair Use” copyright guidelines).

Degree of sulfonation	$T_g$ [°C] <sup>a</sup>		$T_d$ [°C] <sup>b</sup>		Processing temp. range [°C] <sup>c</sup>
	Acid form	Sodium form	Acid form	Acid form	Acid form
BPSH-00	221	516	516		119
BPSH-10	232	507	452		108
BPSH-20	246	506	395		94
BPSH-30	260	506	372		80
BPSH-40	271	501	361		69
BPSH-50	277, 303	498	356		-
BPSH-60	283, 314	495	351		-

<sup>a</sup> Determined by differential scanning calorimetry.

<sup>b</sup> 5 % weight loss temperatures determined by dynamic thermal gravimetric analysis.

<sup>c</sup> Processing temperature range =  $T_d$  of sulfonic acid group (340 °C) -  $T_g$

molecular bulkiness caused by the introduction of sulfonate groups. In contrast, the  $T_g$  of the hydrated BPSH copolymers decreased due to the plasticization effect of absorbed water strongly bound to the sulfonic acid groups [Kim et al. 2003 Macromolecule]. Thus the  $T_g$  of the hydrated BPSH copolymers decreased with degree of sulfonation. The  $T_g$  of hydrated BPSH-40 turned out to be lower than that of Nafion<sup>®</sup> [Kim et al. 2003 JPS], indicating that BPSH-40 is not suitable for use as a PEM in an automotive application because of its extensive morphological relaxation and consequent deterioration. Therefore, it was suggested that a lower degree of disulfonation (30 or 35 %) would be the trade-off between the proton conductivity and morphological stability of the BPSH copolymer for elevated temperature applications ( $\sim 120$  °C).

Wang et al. [Wang et al. 2002] reported that the acidified, disulfonated BPSH copolymer had a two-step degradation. The first thermal degradation occurred around 340 °C, and was attributed to the loss of sulfonic acid groups, while the higher temperature degradation happened around 500 °C in the air, and was attributed to the degradation of polymer backbone. The first thermal degradation temperature of Nafion<sup>®</sup> (313 °C) is slightly lower than that of BPSH [Kopitzke 2000]. However, both are well above the intended operation temperature of fuel cells ( $\sim 120$  °C). It is also noteworthy as observed in Table 2.2-2 that  $T_d$ , the temperature at which there is a 5 % weight loss as determined by dynamic thermal gravimetric analysis at the heating rate of 10 °C/min in nitrogen, of the sodium form is higher than that of the equivalent acid form, indicating that BPSH in its sodium form is more thermally stable than BPSH in its acid form.

Table 2.2-2 also presents the processing temperature range of the BPSH copolymer in its acid form as a function of degree of sulfonation. Because the lower

boundary, the  $T_g$  of the BPSH copolymer, increases with the degree of sulfonation while the  $T_d$  of the sulfonic acid group fixes the upper boundary at 340 °C as described above, the processing temperature range diminishes with the degree of sulfonation. This indicates that in consideration of the fact that the minimum processing temperature range for an industrial melt-phase extrusion is about 100 °C due to current technical limitations of thermal control and analysis in extruders [Rauwendaal 2001], the BPSH copolymer in its acid form with a degree of sulfonation higher than approximately 15 % needs a certain amount of plasticizer in order to widen its processing temperature range and, thus, enable its melt-phase processing. Also, the required amount of plasticizer increases with degree of sulfonation. The  $T_g$  of the BPSH copolymer in its sodium sulfate salt form has not been reported yet, but it is easily figured out that the BPSH copolymer in its salt form needs more plasticizer for melt-phase processing than the equivalent acid form because the  $T_g$  of the sodium sulfate salt form of ion-containing polymers is higher than that of the corresponding acid form [Eisenberg and Kim 1998]. However, it is not desirable to introduce plasticizer for practical reasons. The existence of even a small amount of plasticizer in PEMs certainly decays the mechanical integrity of PEMs during the operation of fuel cells at even slightly elevated temperatures due to its low  $T_g$ , and the removal of the plasticizer from PEMs after their processing make PEMs porous, which will potentially cause a serious drop in the efficiency of PEM FCs.

Therefore, it can be safely concluded that solvent casting is more practically viable compared to melt extrusion-casting, even though high cost for the installation and operation of solvent-casting apparatus is still a drawback. Furthermore, as already pointed out by Banerjee and Curtin [2004], solvent-casting can produce thinner films

with even better uniformity, which is critical for the performance of PEMs in fuel cells [Nissan]. Another advantage could be that the higher mobility of polymeric molecules in the solution may enable the tailoring of the morphology of PEM polymer systems in a wider range through the rearrangement of the polymeric molecules [Krausch 2002].

### 2.3 Morphology of block copolymer systems

The nano-structure formation of materials through molecular self-assembly has gained growing interest during the last decade because of its inherent scientific value and numerous potential technological applications [Bockstaller 2001]. Block copolymers are an outstanding example of this class of material because they develop a great variety of microstructures of molecular dimensions [Bates and Fredrickson 1990].

Block copolymers are long-chain molecules consisting of two or more types of monomers that are grouped together in blocks. The different component blocks are usually incompatible with each other, and thus demix into domains in which a single component block is dominant. The size of the domains cannot exceed a typical block length because the blocks are covalently linked to each other at their ends. Due to this limitation of the domain size, the demixing process and separated region are called *microphase separation* and *microdomain*, respectively [Krausch 2002]. For example, thermoplastic elastomers are block copolymers that contain a rubbery matrix (often polybutadiene or polyisoprene) and glassy hard domains (usually polystyrene). This block copolymer can be molded at high temperatures owing to the presence of the glassy domains, whereas the rubbery matrix provides elasticity at ambient conditions.

Block copolymers consist of two or more chemically distinct covalent bonded polymer blocks. In Figure 2.3-1 are given common architectures of block copolymers [Hamley 2004]. Linear block copolymers contain two or more polymer chains in series, whereas a starblock copolymer comprises multiple linear block copolymers connected at a common branch point. Polymers containing more than two polymer chains connected at a common branching point are referred to as mixed arm block copolymers.

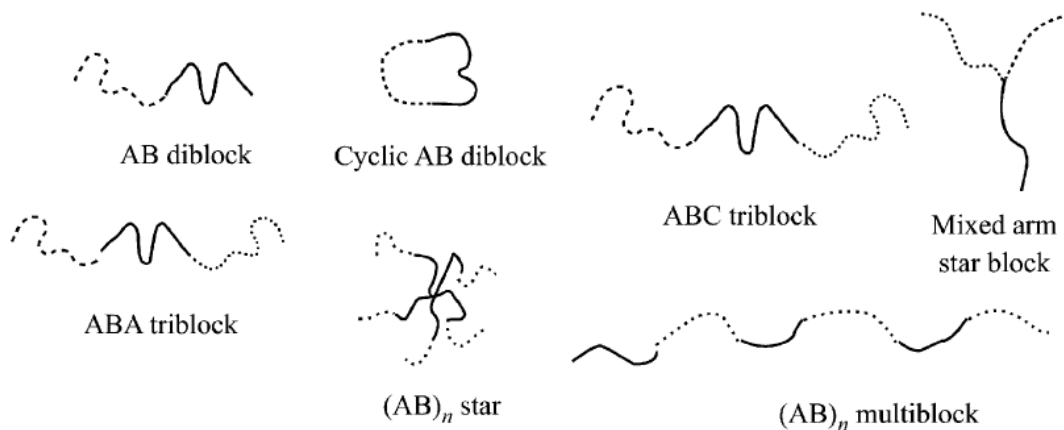


Figure 2.3-1 Block copolymer architectures [Hamley 2004] (Illustrated under “Fair Use” copyright guidelines).

The kinetics of phase transformation of block copolymers is one of the challenging topics in polymer physics [Hadjichristidis 2003]. In contrast to spinodal decomposition such as a demixing process in alloys or binary liquids caused by an abrupt change in temperature below the stability line, the kinetics of phase transformation of block copolymers have richer and more interesting phenomena because of the softness of interactions and long relaxation times. Because the phase transformation of block copolymers has many current and potential applications, it is of practical importance to understand its kinetics and to design a processing method for obtaining suitable structures for nanotechnology applications.

Recently, microphase separation of block copolymer systems in the field of production of proton exchange membrane (PEM) production for fuel cells (FCs) has also gained growing interest [Yang 2005]. FC PEMs are also copolymer systems that consist of sulfonated components for proton conduction and non-sulfonated components for mechanical integrity. Even though the morphological model is still a subject of debate, the proton conductivity of sulfonated copolymers is related to extensive nano-scale phase

separation, which leads to more co-continuous connectivity of the sulfonated ionic domains. Therefore, understanding the physics behind the phase transformations of PEM copolymers during processing may be helpful in the design and operation of processes that produce an appropriate microstructure for optimum PEM performance.

Therefore, in this section the general background of block copolymer melts and block copolymers in solution will be covered first with a focus on the previous morphological studies. Then, the following section will cover previous studies on the phase transformation of block copolymers and its kinetics, and the experimental techniques for the detection of the phase transformation.

### 2.3.1 Block copolymer melts

The variety of morphologies of block copolymers induced by microphase separation makes the phase behavior of block copolymers very interesting. The phase behavior of block copolymer melts can be approximately represented in a morphology diagram in terms of two parameters,  $\chi N$  and  $f$  [Hamley 1999]. Here,  $f$  is the volume fraction of one component block, and  $\chi$  is the Flory-Huggins interaction parameter, which indicates the interaction energy between different component blocks.  $\chi$  is known to be inversely proportional to temperature, i.e.,  $\chi = A + B/T$ . The configurational entropy contribution is also proportional to  $N$ , the degree of polymerization, which is the number of statistical segments per chain and is proportional to molecular weight. If the product is larger than a critical value,  $(\chi N)_{\text{ODT}}$  (order-disorder transition value of  $\chi N$ ), the block copolymer separates into a periodically ordered structure with a dimension of

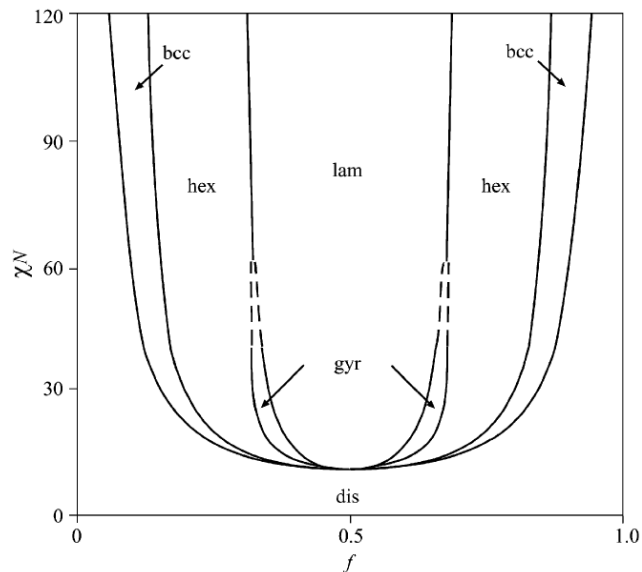
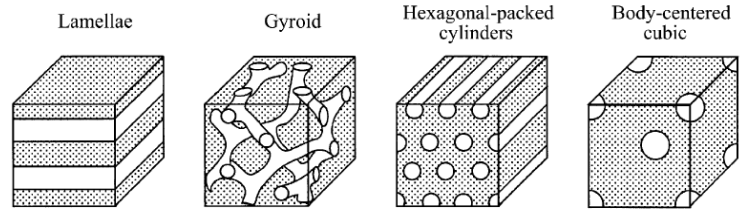


Figure 2.3-2. Phase diagram for a conformationally symmetric diblock copolymer, calculated using self-consistent mean field theory, along with illustrations of the equilibrium morphologies. In the phase diagram, regions of stability of disordered (dis), lamellar (lam), gyroid (gyr), hexagonal (hex) and body-centered cubic (bcc) phases are indicated [Matsen and Schick 1994, Matsen and Bates 1996] (Illustrated under “Fair Use” copyright guidelines)

approximately 5 ~ 500 nm. The microphase-separated structure depends on the architecture and composition of block copolymer molecules [Hamley 1999]. In Figure 2.3-2 is presented the phase diagram of a conformationally symmetric diblock copolymer. A lamellar phase is observed for a conformationally symmetric diblock copolymer ( $f = 0.5$ ), while asymmetric diblock copolymers develop hexagonal-packed cylinder or body-centered cubic spherical structures. The existence of a rather complex bicontinuous cubic gyroid phase and a hexagonal-perforated layer phase of diblock

copolymers between the lamellar and hexagonal-packed cylinder phases has also been reported by Hajduk et al. [1994] and Förster et al [1994]. However, the hexagonal-perforated layer phase has been found to be metastable in this region [Hamley 1993, Hajduk 1997, Vigild 1998]. The extent of segregation of block copolymers has been known to depend on the magnitude of  $\chi N$  [Fredrickson 1987, 1989]. Up to around the order-disorder transition, the composition profile fluctuates in an approximately sinusoidal way. For example, the density of both components of symmetric diblock copolymers varies sinusoidally up to  $\chi N = 12$ , whereas  $(\chi N)_{\text{ODT}}$  is 10.495. This is designated as weak-segregation limit (WSL). At much higher values of  $\chi N$  ( $> \sim 100$ ), the component blocks strongly segregate and the domain of each component is nearly pure, with a narrow interphase between them. This is the strong segregation limit (SSL).

Helfand et al. [1975, 1976] introduced the first theories for block copolymers at the SSL, and established the basic principles of the phase behavior of block copolymers. They developed the self-consistent field (SCF) theory, which allowed the calculation of free energies and composition profiles using modified diffusion equations for the description of macromolecular conformations. Leibler [1980] theoretically investigated the phase behavior of noncrystalline block copolymers of type AB in the WSL by employing the Landau-Ginzburg approach to analyze the free energy and composition profiles. Matsen et al. [1994, 1996] developed a powerful new method to solve the SCF theory equations for block copolymers. This enabled the analysis of the ordering of many types of block copolymer even in the intermediate region, as well as in the SSL and WSL. Finally, the phase diagram shown in Figure 2.3-2 was established. This phase diagram shows the generic sequence of phases generated below the order-disorder

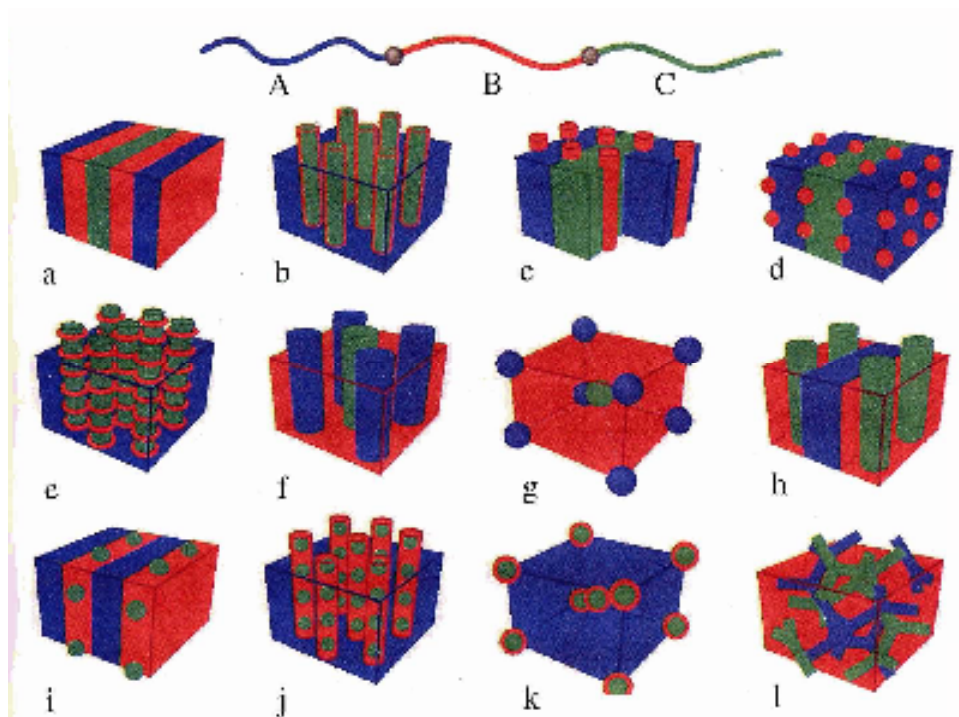


Figure 2.3-3. ABC linear triblock copolymer morphologies [Stadler 1995, Zheng 1995, Bates 1999] (Illustrated under “Fair Use” copyright guidelines).

transition temperature for diblock copolymers of different compositions. The detailed features of phase diagrams for particular systems are different, but their qualitative trends are very similar [Hamley 2004].

The phase behavior of ABC triblock copolymers is much more complex than diblock copolymers or two-component triblock copolymers of type ABA [Bates 1999]. A portion of identified morphologies of ABC linear triblock copolymer are shown in Figure 2.3-3 [Stadler 1995, Zheng 1995, Bates 1999]. ABC triblock copolymers have a large number of possible morphologies, and multiple interaction parameters ( $\chi_{AB}$ ,  $\chi_{AC}$ ,  $\chi_{BC}$ ) resulting from the introduction of a distinct third component complicate the

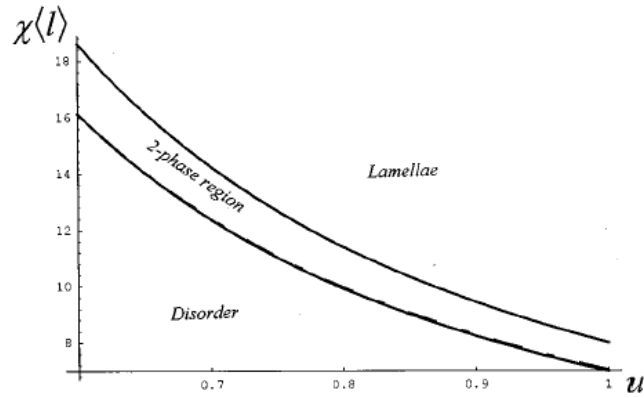


Figure 2.3-4. Phase diagram of the polydisperse multiblock copolymer melt [Dobrynin 1997]. Here,  $\langle l \rangle$  represents average block length and  $u$  is the ratio of the two first moments of the distribution, expressed as  $\langle l^2 \rangle / \langle l \rangle^2 - 1$  (Illustrated under “Fair Use” copyright guidelines).

theoretical prediction of the phase behavior. So far, more than 30 morphologies have been identified with no obvious limit in the number of its morphologies.

A theory for the prediction of microdomain structures of random copolymers and of highly polydisperse multiblock copolymers has been introduced by Fredrickson et al. [1991], Sfatos et al. [1995], and Dobrynin [1997]. In order to illustrate the phase behavior of the random copolymers, they calculated the phase diagram of a polydisperse AB multiblock copolymer melt. This theoretical work suggested that in the case of random copolymers, lamellar and liquid-like disordered phases exist, and these two phases are separated by a two-phase region in which both structures coexist (Figure 2.3-4). However, no experimental study that confirms their theory has been reported [Dobrynin 1997].

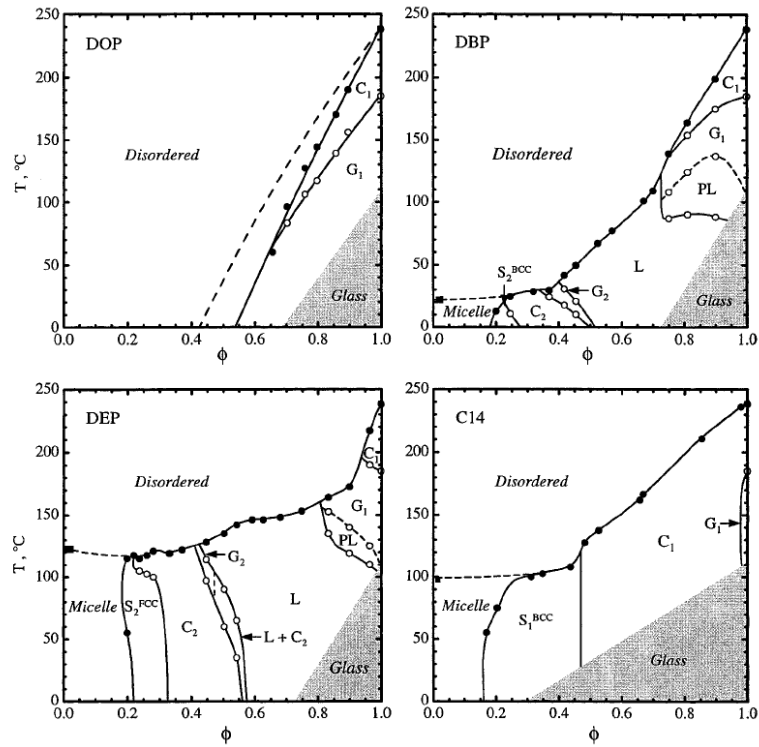
The useful techniques for the investigation of solid block copolymer microstructures are transmission electron microscopy (TEM) and small-angle X-ray/neutron scattering [Hamley 2004]. TEM presents direct images of the microstructure.

Typically, samples need staining in order to increase the contrast for electrons between domains. The vapors from a solution of a heavy metal acid ( $\text{OsO}_4$  or  $\text{RuO}_4$ ) are usually used for staining [Kato 1965]. While TEM provides the information over a small area of the sample, small-angle scattering probes the microstructure over the whole sample and gives a diffraction pattern, which can be utilized to identify the symmetry of the phase by examining the positions of the reflections [Hamley 2004].

### 2.3.2 Block copolymers in solution

The phase behavior of block copolymers in a solvent is governed by the interactions between the polymer segments and the solvent molecules, as well as the interactions between the two segments of the block copolymers. If the solvent is selective for one of the blocks, block copolymers in the dilute solution form micelles. The insoluble block forms the core, while the soluble block forms the corona [Tuzar 1996]. The phase behavior of concentrated solutions was investigated in previous experimental studies by Wanka et al [1994]., and Hanley et al [2000]. It has been observed that lamellar, hexagonal-packed cylinder, micellar cubic and bicontinuous cubic structures exist. Hanley et al. [2000] investigated the effect of the thermodynamic selectivity of a solvent on the self-assembly of a styrene-isoprene (SI) diblock copolymer. They also examined its phase behavior in solvents with different selectivity from the dilute solution to the melt state. In Figure 2.3-5 are given the phase diagrams for the SI diblock copolymer in various solutions as a function of temperature and polymer volume fraction, and as its melt state. Order-order transitions (OOT) and order-disorder transitions (ODT) were located and identified using small-angle X-ray scattering and static birefringence

(a)



(b)

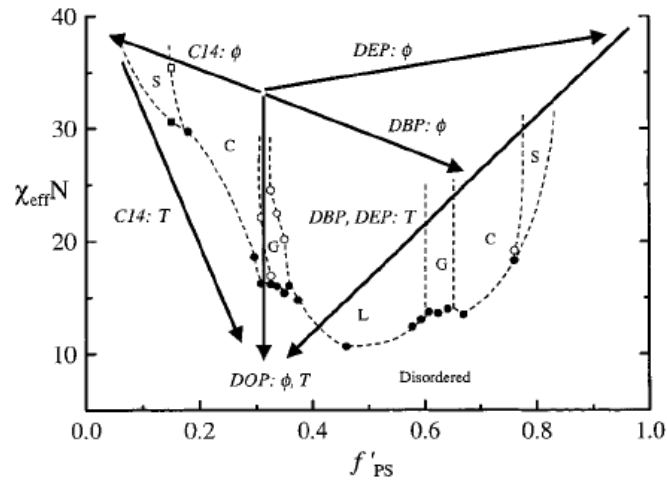


Figure 2.3-5. (a) Phase diagram for SI as a function of temperature and polymer volume fraction for solution in bis(2-ethylhexyl) phthalate (DOP), Di-n-butyl phthalate (DBP), diethyl phthalate (DEP), and tetradecane (C14). Filled and open circles identify ODTs and OOTs, respectively. The dilute solution critical micelle temperature is indicated by a filled square. (b) Phase trajectories of SI in DOP, DBP, DEP, and C14 [Chastek 2004] (Illustrated under “Fair Use” copyright guidelines).

techniques. Dynamic and static light scattering were utilized to examine the micellization and micellar behavior of the dilute solutions. Hanley et al. [2000] also discussed that the routes of phase transition in the solvents could be superimposed onto the melt phase map of the degree of segregation ( $\chi N_{eff}$ ) vs. effective volume fraction ( $f^*$ ).

Other block copolymer systems extensively examined in solution are polyoxyethylene-based block copolymers commercialized as Pluronic or Synperonic. These block copolymers are widely used as surfactants in detergents and personal care products and even in pharmaceutical applications [Edens 1996]. Wanka et al. [1994] studied the micellization, micellar behavior, and phase behavior of poly(oxyethylene)-poly(xoypropylene)-poly(oxyethylene) [(EO)<sub>x</sub>(PO)<sub>y</sub>(EO)<sub>x</sub>] triblock copolymers. They found out that the critical micelle concentration (cmc), above which the surface tension is independent of concentration, decreased exponentially with  $y$ , and also decreased strongly with increasing temperature. They also reported that the shape of the micelles of the copolymer systems with a ratio of  $x$  to  $y$  larger than 0.5 is spherical at concentrations higher than the cmc, and that the size of the micelles was independent of both concentration and temperature at temperatures above the micellization temperature,  $T_m$ , which was about 20 °C for [(EO)<sub>x</sub>(PO)<sub>y</sub>(EO)<sub>x</sub>] copolymers. However, in the transition region around  $T_m$ , the micellar size increases considerably with temperature. They also observed that at higher concentrations and temperatures the copolymers had a variety of mesophases such as lamellar, hexagonal, cubic, and mixed structures, depending on the composition of the copolymers.

Theory for the prediction of the phase behavior of semidilute or concentrated block copolymer solutions is less developed due to the complexity of interactions

between the polymer segments and the solvent molecules, as compared to those for melts and dilute solutions [Hamley 2004]. Linse's research group [Noolandi 1996, Svensson 1999], by introducing SCF theory, generated phase diagrams for specific Pluronic copolymers in aqueous solution that were in excellent agreement with the aforementioned experimental results of Wanka et al [1994].

### 2.3.3 Studies on the phase transformation and kinetics of block copolymer through rheological measurements and scattering techniques

Rheology is a very effective method to investigate the order-to-disorder transition of block copolymers, because of the distinct differences in the viscoelastic properties of block copolymers in their ordered and disordered states [Winey 1994]. Han et al. [1995] determined the order-disorder transition temperature ( $T_{ODT}$ ) of low molecular weight SI diblock copolymers using two different rheological methods: (1) the temperature sweep of  $G'$  at low angular frequencies, and (2) plots of  $\log G'$  vs.  $\log \omega$ . First they found  $T_{ODT}$  by conducting temperature sweep experiments at low angular frequencies for SI diblock copolymers with different compositional symmetry ( $f_{PS}$ , volume fraction of polystyrene = 0.186 ~ 0.811). Before the study of Han et al. [1995]'s, it had already been reported in several previous studies [Gehlsen 1993, Winey 1994] that  $G'$  decreased precipitously at or near a certain critical temperature. Accordingly, the precipitous change in  $G'$  indicated that such temperature be considered as the  $T_{ODT}$  of a block copolymer. Han et al. [1995] also reported the limitations of this  $T_{ODT}$  detection method. In Figure 2.3-6 are shown the results of the temperature sweep experiments in oscillatory shear flow mode of the SI diblock copolymers with different  $f_{PS}$ . For a SI diblock copolymer with  $f_{PS} = 0.461$  (Figure 2.3-6 (a)), an abrupt drop in  $G'$  was observed at around 115 °C, at which the SI

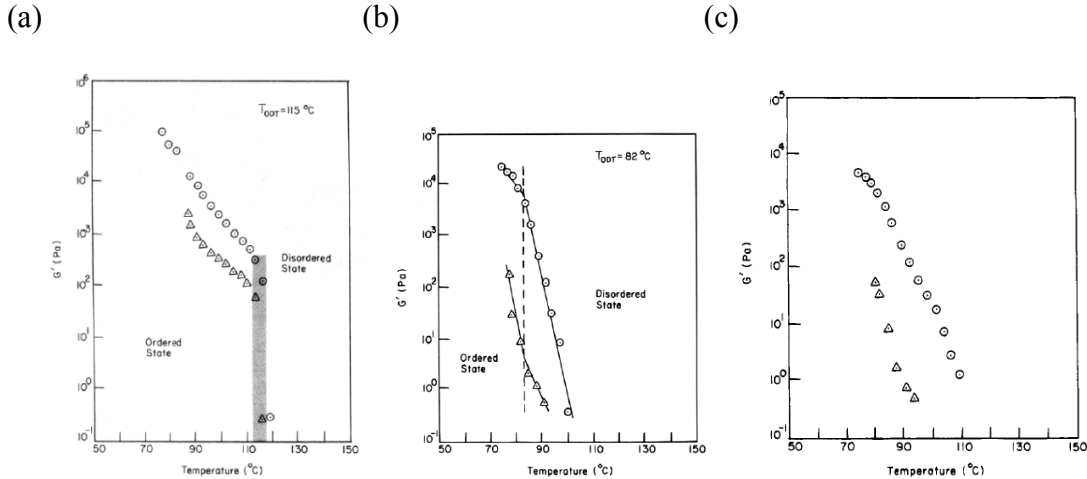


Figure 2.3-6. Variations of  $G'$  with temperature obtained at  $\omega = 0.5$  rad/s ( $\circ$ ) and at  $\omega = 0.5$  rad/s ( $\blacktriangle$ ) (a) for SI diblock copolymer with  $f_{PS} = 0.461$ .  $T_{ODT} = 115$  °C determined by an abrupt drop in  $G'$ . (b) for SI diblock copolymer with  $f_{PS} = 0.372$ .  $T_{ODT} = 82$  °C determined by a large change of the slope of the plot. (c) for SI diblock copolymer with  $f_{PS} = 0.186$ . No discernable evidence of  $T_{ODT}$  observed [Han 1995] (Illustrated under “Fair Use” copyright guidelines).

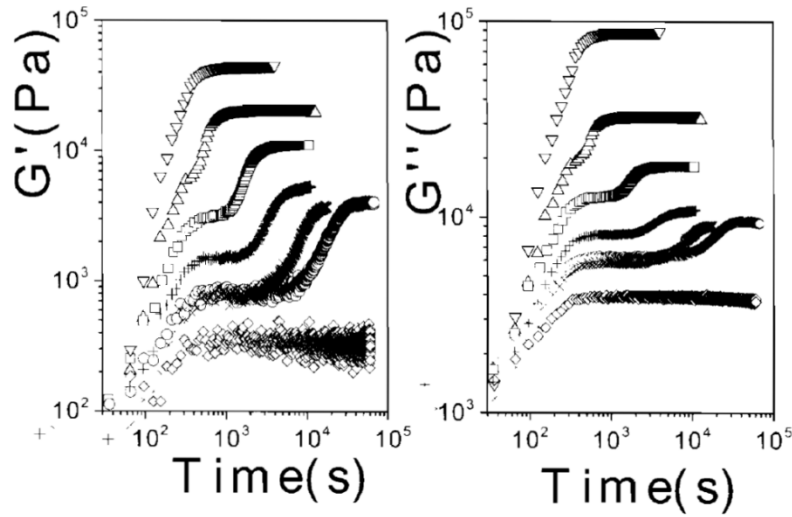
diblock copolymer exhibited lamellar microdomains. On the other hand, it was not easy to find a critical temperature at which the value of  $G'$  dropped discontinuously for a SI diblock copolymer with  $f_{PS} = 0.372$  (Figure 2.3-6 (b)). Instead, a large and abrupt change in the slope of the plot was observed at around 82 °C. However, for the SI diblock copolymer with the highest compositional asymmetry ( $f_{PS} = 0.186$ ), neither an abrupt drop nor sudden change in the slope of  $G'$  was observed around the  $T_{ODT}$ . Thus, they concluded that temperature sweep experiments in oscillatory shear flow mode were not effective in determining  $T_{ODT}$  of the SI diblock copolymers with high compositional asymmetry. In plots of  $\log G'$  vs.  $\log \omega$ , a very similar trend was also observed. For somewhat compositionally symmetric SI diblock copolymers, the slope of  $\log G''$  vs.  $\log \omega$  at and below  $T_{ODT}$  was about 0.5, while the slope of  $\log G''$  vs.  $\log \omega$  above  $T_{ODT}$  was about 2, which is typical for flexible homopolymers or random copolymers. However, as

the compositional asymmetry increased, no noticeable changes in the plots of  $\log G''$  vs.  $\log \omega$  at or near a certain critical temperature were reported.

A variety of different experimental techniques that have been used to observe the crystallization process, i.e., dilatometry, X-ray diffraction, rheology, etc. can also be used to monitor the ordering process of block copolymers because of its similarities with the crystallization process of semicrystalline materials [Hadjichristidis 2003]. Dilatometry, which enables the detection of the discontinuous change in specific volume and isothermal compressibility of the materials around the critical point, is considered to be the most effective method [Kasten 1995, Floudas 1993]. However, earlier studies found that dilatometry might not be an appropriate method for block copolymers because the change of the density and compressibility of diblock copolymers at the ODT was very small. In contrast, small angle X-ray scattering (SAXS) and rheology are very responsive to the structure evolution and viscoelastic properties of the block copolymer during the ordering process. Therefore, most experimental studies on the ODT in block copolymers involved scattering and rheological techniques [Hadjichristidis 2003].

The success of rheology in detecting the ordering kinetics of block copolymers is also based on the large viscoelastic contrast between the disordered and ordered phases [Hadjichristidis 2003]. The storage ( $G'$ ) and loss ( $G''$ ) moduli of block copolymers jump up considerably during the structural evolution from the disordered to the ordered phase. The evolution shape of  $G'$  and  $G''$  can be used to analyze the kinetics of structure ordering [Floudas 1994a]. In Figure 2.3-7 are presented some typical evolutions of  $G'$  and  $G''$  for a symmetric styrene-isoprene (SI) diblock copolymer. Both  $G'$  and  $G''$  showed a sigmoidal shape with apparent plateaus before and after the upward change. The plateaus of  $G'$  and

(1)



(2)

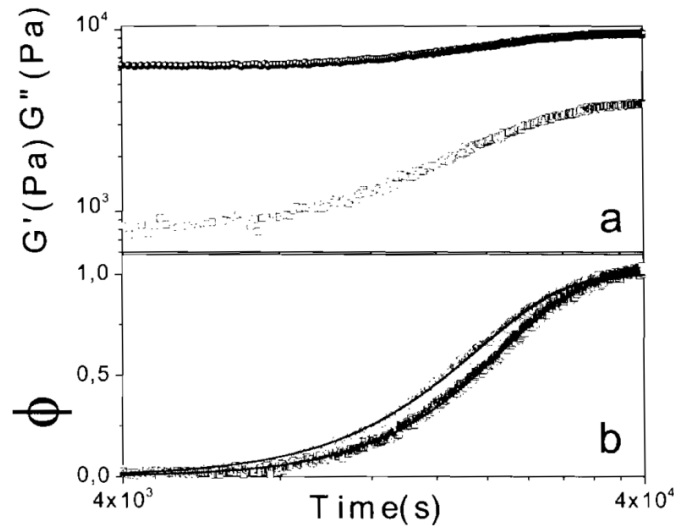


Figure 2.3-7. (1) Time evolution of  $G'$  and  $G''$  for a symmetric poly(styrene-*b*-isoprene) diblock copolymer following quenches from the disordered state to different final temperatures in the ordered phase: rhombus: 359, circles: 358, X: 356.5, +: 356, squares: 355, triangles: 353, and inverted triangles: 347.6 K.

(2) a. Time evolution of  $G'$  and  $G''$  at 356.5 K following a quench from 363 K and b. time-dependence of the volume fraction of  $\phi$  of the ordered phase calculated using the 'parallel' (squares) and 'series' (circles) models. Solid lines are fits to the Avrami equation [Floudas 1994] (Illustrated under "Fair Use" copyright guidelines).

$G''$  before the change are the viscoelastic properties of the disordered phase at the quenched temperature, while the plateaus after the change describe the properties of the final ordered state. During the course of ordering, the block copolymer is considered to be a composite material consisting of disordered and ordered phases. The proportion of the two phases also changes, inducing the observed changes in the mechanical properties.

Floudas et al. [1994a] used the simplest ‘series’ and ‘parallel’ mechanical models, which provide the limits for the mechanical response of a two-phase system as a function of the properties of the constituent components and the composition, in order to investigate the time-dependence of the volume fractions of the constituent phases, and finally to analyze the ordering kinetics based on a nucleation and growth mechanism. The ‘series’ model allows the modulus of the two-phase system to be expressed as a linear combination of the compliances:

$$\frac{1}{G(t)} = \frac{1-\phi(t)}{G_0} + \frac{\phi(t)}{G_\infty} \quad (\text{Eq. 2.3-1})$$

and the ‘parallel’ model as a linear combination of the moduli of the constituent phases:

$$G(t) = (1-\phi(t))G_0 + \phi(t)G_\infty \quad (\text{Eq. 2.3-2})$$

where  $G(t) (= \sqrt{G'^2(t) + G''^2(t)})$  is the absolute value of the complex modulus,  $\phi(t)$  is the fraction of the ordered phase, and  $G_0$  and  $G_\infty$  are the moduli of the completely disordered and ordered phases at the initial and final stages, respectively. The time-dependences of  $\phi$  obtained from the two models are analyzed by applying the Avrami equation [Avrami 1939, 1940, 1941]. The Avrami equation describes how materials

transform from one phase to another, specifically, the kinetics of crystallization, which consists of two major steps, nucleation and crystal growth. Nucleation is the first process, where the solute molecules in the solvent gather and develop clusters, which finally form nuclei. Crystal growth is the following growth process of these nuclei. The Avrami equation is as follows:

$$\phi(t) = 1 - \exp(-zt^n) \quad (\text{Eq. 2.3-3})$$

where  $n$  is the Avrami exponent, which is a combined function of the growth dimensionality and the time-dependence of the nucleation process. This exponent presents qualitative information on the nature of the nucleation and growth process. In Eq. 2.3-3, the rate constant,  $z$ , gives quantitative information on the course of crystallization, and the half-time equation,

$$t_{1/2} = \left( \frac{\ln 2}{z} \right)^{1/n} \quad (\text{Eq. 2.3-4})$$

is usually used to describe the ordering time. These Avrami parameters can be determined from a plot of  $\log(-\log(1-\phi))$  versus  $\log t$ :

$$\log(-\log(1-\phi(t))) = n \log t + \log z \quad (\text{Eq. 2.3-3'})$$

where the Avrami exponent,  $n$ , and the logarithm of the rate constant,  $z$ , are the slope and y-intercept, respectively. In Figure 2.3-7 are also given the evolution of the viscoelastic properties during the phase transformation of the symmetric SI diblock copolymer and the equivalent volume fraction of the ordered phase obtained using the two extreme ‘series’ and ‘parallel’ models. Based on this analysis method, the Avrami exponent was

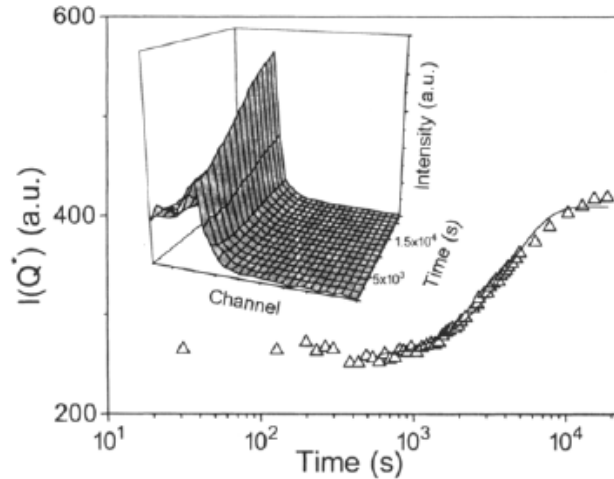


Figure 2.3-8. Evolution of the peak scattering intensity  $I(q^*)(t)$  following a temperature jump from the disordered to the ordered state of a SI graft copolymer. The line is a fit to the Avrami equation [Floudas 1994] (Illustrated under “Fair Use” copyright guidelines).

found to be about 3 for shallow quenches, indicating that the ordering process proceeds by heterogeneous nucleation and growth of three-dimensional objects. The kinetics curves for the SI block copolymer that were cooled more had a higher value of  $n$  ( $\approx 4$ ), suggesting spinodal decomposition as a possible mechanism of phase transformation [Floudas 1994a].

SAXS is known to be a good tool for following the microstructural change in block copolymers during the self-assembly process [Hadjichristidis 2003]. Changes in the scattering intensity over the relevant range of the length scale ( $q^*$ ), which is responsive to the structural changes during the phase transformation, give information about the evolution of the structure factor. In Figure 2.3-8 is given an example SAXS profile for an SI graft copolymer under isothermal conditions following a temperature jump from the disordered phase [Floudas 1994b]. The SAXS profile changes from a relatively broad

liquid-like peak to a narrow solid-like peak, suggesting an ordered microdomain structure, and the shape of  $I(q^*, t)$  can be fitted to the Avrami equation.

For a comparison with the rheological data, the volume fraction of the ordered phase can be quantified by measuring the total scattering power of the medium:

$$P = \frac{1}{2\pi^2} \int_0^{\infty} q^2 I(q) dq \quad (\text{Eq. 2.3-5})$$

which is determined from the integration of the scattering intensity over all  $q$ . The volume fraction extracted from the SAXS data can then be compared with rheological results. One of the advantages of using rheology for the studies on the kinetics of phase transformation is that one can increase the step size in  $G^*(t)$  by a factor of one order of magnitude just by choosing a low frequency, whereas the change of  $I(q^*, t)$  can be at most a factor of three [Hadjichristidis 2003].

Recently, the ordering kinetics of block copolymers in solutions was also characterized by Lodge group [Hanley 2000, Chastek 2004]. Hanley et al. [2000] empirically showed that the phase behavior of a styrene-isoprene (SI) diblock copolymer strongly depended on temperature, solvent selectivity, and solution concentration by generating the phase diagrams of the SI diblock copolymer in four different solvents with different degree of selectivity for each block using small-angle X-ray scattering (SAXS), static birefringence, and dynamic light scattering. They also reported that the SI diblock copolymer had a more tendency to form ordered structures in a more selective solvent. Then, the ordering kinetics of the cylinder phase of the SI diblock copolymer in di-n-butyl phthalate induced by thermal quenching was investigated using polarizing optical microscopy (POM) [Chastek 2004]. Not only dimensional and kinetics information in

such a way as Floudas and coworkers [1994a] but also detailed information such as grain growth velocity were obtained.

As presented in this section, self-assembly of block copolymers is a promising strategy for the production of nano-structured materials. Also, it has been shown that multiple morphologies may be obtained from a single type of copolymer by inducing the variations in the interactions between the two segments of block copolymers. This self-assembly of block copolymers may be enhanced through the introduction of solvents selective for one of the polymer segments, and accordingly different morphologies of block copolymers more favorable for proton conduction may be obtained. However, so far most copolymer films for FC PEMs were prepared for their evaluation usually by spreading of dilute polymer solution onto a flat plate followed by the evaporation of the solvent at an uncontrolled manner under infra-red radiation or in heating ovens. No previous studies reported multiple morphologies of copolymers for PEMs. This strongly indicates that the previous studies overlooked the significance of self-assembly of block copolymers at the preparation stage of PEM films. Therefore, the investigation on the effects of solvent-casting conditions on the morphology formation is to be performed in a systematic way in terms of self-assembly of copolymers.

It has also been presented that the phase transformation and kinetics of block copolymer melts and block copolymers in solutions have been steadily investigated using a variety of techniques such as rheology, scattering, POM, etc. On the other hand, to the knowledge of the author, studies on the phase transformation and kinetics of block copolymers in solution in processing such as film drying are very rare. Most of the previous studies on block copolymer in solution have been focused on the equilibrium

states at certain concentrations and temperatures. However, because the number of practical applications of block copolymer products manufactured by solvent-casting has considerably increased, the study of the phase transformation and kinetics of block copolymers in solution in processing is in practical demand for the design and operation of solvent removal process. It is expected that rheology will be better at probing phase transformations of block copolymers in solution than scattering techniques because the change in the viscoelasticity of block copolymers during phase transformation is usually more noticeable than that of the intensity peak in scattering profiles [Hadjichristidis 2003].

## 2.4 Drying of polymer films and coatings

Thin film coating and drying are crucial unit operations in the production of many functional polymeric films such as photographic films, adhesives, magnetic media, protective coatings, and recently, lithium battery coatings [Kim, S. 2003]. A schematic of an industrial coating and drying apparatus is given in Figure 2.4-1. A typical formulation of a coating solution is composed of polymer resins, solvents, and additives such as pigments, hardener, coating aids, and so on. The solvents are used to solubilize the coating formulation by dissolving the polymers and suspending other additives. This solubilization finally gives the coating solution an appropriate rheological processability. One or more layers of the coating solutions are deposited on a substrate at a coating station and are dried by passing through a drying oven. The drying oven consists of a series of separate zones in which conditions such as air velocity, temperature, and humidity are independently controlled. Air is impinged through nozzles usually in the direction parallel with the substrate from the side of the drying duct or perpendicular to

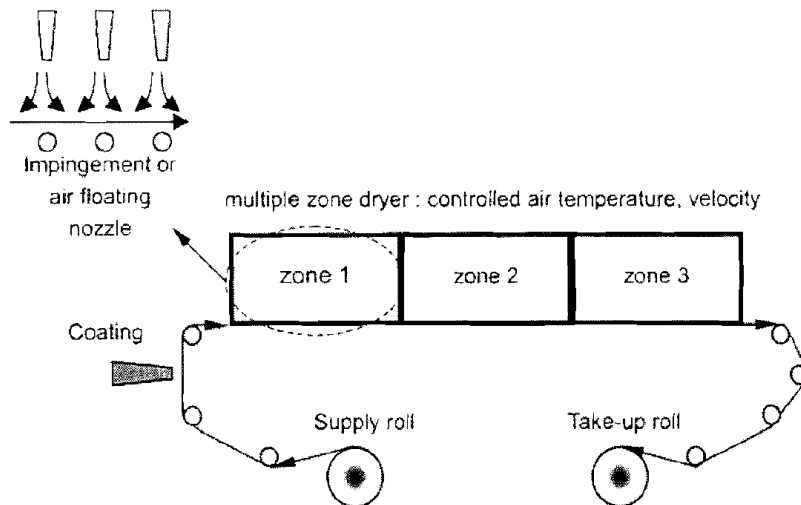


Figure 2.4-1. A schematic of industrial coating and drying apparatus [Kim, S. 2001] (Illustrated under “Fair Use” copyright guidelines).

the substrate from the top of the drying duct. The impinged air supplies the heat necessary for the evaporation of the solvents and sweeps away the solvent vapor from the surface of the coated solution. Finally, all the solvents are evaporated, and only the desired thin film remains on the substrate. Essentially, film drying can be defined as a unit operation for removing solvents used to solubilize the coating formulation and to provide the rheological processability [Kim, S. 2003].

The drying process is as important as the coating process for a successful production of polymeric thin films because it has a substantial influence on the structure and properties of final coating products [Gutoff 1995]. Also, even a trace amount of solvent can cause final coating products to malfunction [Miltz 1992]. The properties of coating products may also be enhanced by utilizing UV curing at the drying stage or may be deteriorated by applying inappropriate drying conditions [Kim, S. 2003]. Furthermore, the optimization of the drying process is of great importance for a successful commercialization of polymeric thin film products, because the drying process entails huge capital and operating expenditures, and is the main limiting factor in increasing production rate [Kim, S. 1998]. Therefore, it is essential to fully understand the drying process and to optimize drying conditions.

In this section, general background information on the drying process of *non-reactive binary polymer-solvent system on an impermeable substrate* will be covered. First, the transport phenomena that occur during the drying process and their characteristics will be presented in 2.4.1. Then, previous modeling work of film drying will be covered in 2.4.1.

## 2.4.1 Nature of film drying

### 2.4.1.1 Heat and mass transfer phenomena in film drying

Removal of solvents from a coated film is a very complex process involving simultaneous heat and mass transfer phenomena at the interface between the coated film and convection air [Blandin 1987], and with the introduction of other solvents and additives, these transfer phenomena become even more complicated [Waggoner 1989]. The elemental heat and mass transfer phenomena of the film drying process are schematically presented in Figure 2.4-2, and their details are discussed below.

- Convective heat transfer at the exposed surface: Since evaporation is a typical endothermic process, the latent heat necessary for solvent evaporation must be supplied to the coated solution. Convection, radiation, conduction, or any

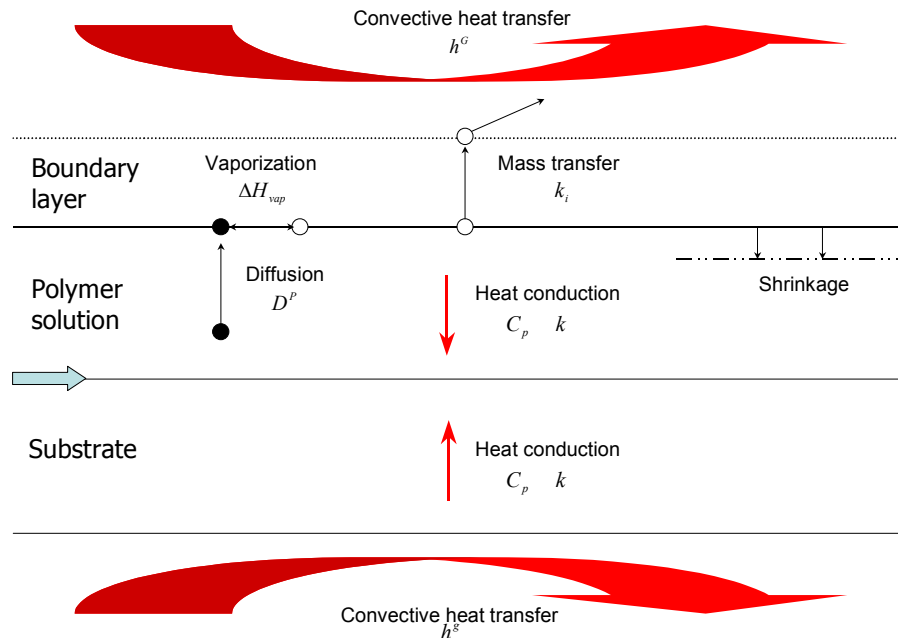


Figure 2.4-2. Elemental heat and mass transfer phenomena of the drying process of coated films.

combination of these methods may be used [Cohen 1992]. However, convective heating is the most commonly used primary method because it not only supplies energy to the coated film, but also facilitates the mass transfer of solvent vapor away from the surface of the coated film [Cussler 1997]. Radiative and conductive heating are also commonly used as ancillary heating methods.

- Vaporization of solvent at the exposed surface: Solvent is evaporated into air adjacent to the exposed surface of the coated solution.
- Diffusive mass transfer of solvent in the adjacent air: Diffusion of solvent vapor into the stagnant air layer over the coated film is a relatively slow process, and thus is a rate-limiting step. Frequently, forced convection over the exposed surface considerably enhances the diffusion rate of solvent vapor [Cussler 1997]. For this reason, convective heating is most commonly employed as a basic heating method.
- Diffusive mass transfer of solvent through the coated film: As the evaporation of solvent proceeds, the concentration of solvent at the exposed surface decreases. Accordingly, a concentration gradient develops in the direction of the film thickness. In proportion to the concentration gradient, the diffusive mass transfer of solvent occurs through the coated film from the substrate side to the exposed surface.
- Evaporative cooling and conductive heat transfer through the coated film and the substrate: As long as the exposed surface is fully wetted with solvent, the energy provided by the convective heating is preferentially utilized for the evaporation of solvent [Cohen 1992], and the temperature of the exposed film surface rarely increases because of the evaporative cooling effect. When the surface is no longer fully wetted, the energy is used to increase the temperature of the coated solution.

However, the convective heat supplied by the air on the substrate side is entirely used to increase the temperature of the substrate and is not affected by the evaporative cooling effect.

- Shrinkage of the coated film: As the evaporation of the solvent proceeds, the volume of the coated film gradually decreases, and, finally, only a thin polymeric film remains on the substrate.

#### 2.4.1.2 Drying regimes and their characteristics

According to the characteristic temperature behavior and drying rate of the coated film, the drying process can be divided into two different periods: constant drying rate period (CDRP) and falling drying rate period (FDRP) [Cohen 1992]. Observation of the temperature behavior and drying rate of the coated film gives insight into the nature of these periods. A graph of the characteristic temperature behavior and drying rate of polymer solutions plotted versus drying time is given in Figure 2.4-3. During the initial

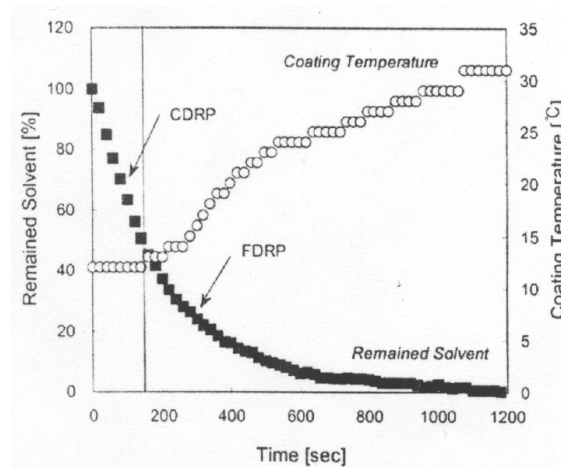


Figure 2.4-3. Characteristic drying curves of the coated polymer solution films: changes of film temperature and drying rate as a function of the drying time [Kim, S. 2001] (Illustrated under “Fair Use” copyright guidelines).

stage of the drying process, the coated film has a high solvent concentration. Thus, the exposed surface of the coated film is completely wetted with the solvent, and the solvent can move freely to the exposed surface. Because the coated film enters the dryer at low temperatures, the coated film experiences a short transitional period and then reaches a steady state where the drying rate is constant. This period is usually called the constant drying rate period (CDRP). The CDRP lasts as long as the rate of the solvent diffusion through the coated film is comparable with the rate of solvent evaporation at the surface of the coated film. As the film drying proceeds, the concentration of polymer in the coated film increases and the diffusive transfer of solvent molecules is limited by polymer molecules. In the CDRP, all of the energy supplied to the coated film is used to evaporate the solvent, and the rate of evaporative cooling is equal to the rate of heating so that the temperature of the exposed surface remains constant. Therefore, the external mass transfer rate is a limiting factor to the drying of the coated films, and the film drying rate increases proportionally with the temperature and velocity of convection air.

As the drying of the coated film proceeds, the concentration of solvent in the coated film decreases, and polymer molecules retard the movement of solvent to the exposed surface by diffusion [Kim, S. 1998]. This means that the rate-controlling step changes from convective to diffusive mass transfer in the coated film. Finally, the vapor pressure of solvent at the exposed surface falls and so does the drying rate of solvent. This period is called the falling drying rate period. Meanwhile, the temperature of the coated film increases with the same heat input. In order to understand and improve the drying process during FDRP, it is necessary to understand the diffusive transfer of

solvent in coated films. According to the free volume theory, two conditions are necessary to enable the diffusive transfer of the molecules: (1) formation of a free volume with sufficient size adjacent to a molecule and (2) the possession of sufficient energy by the molecule [Vrentas 1977]. Based on this free volume theory, Vrentas and Duda [1985 a, b] formulated the following equations to predict the binary diffusion coefficient:

$$D^p = D_1(1 - \phi_1)^2(1 - 2\chi\phi_1) \quad (\text{Eq. 2.4-1})$$

$$D_1 = D_0 \exp\left(-\frac{E}{RT}\right) \exp\left[\frac{-(\omega_1 \hat{V}_1^* + \omega_2 \xi \hat{V}_2^*)}{\omega_1 \left(\frac{K_{11}}{\gamma}\right)(K_{21} - T_{g1} + T) + \omega_2 \left(\frac{K_{12}}{\gamma}\right)(K_{22} - T_{g2} + T)}\right] \quad (\text{Eq. 2.4-2})$$

The definitions of the model parameters are listed in Table 2.4-1. Figure 2.4-4 shows the binary diffusion coefficient of toluene as a function of concentration and temperature in the polystyrene-toluene solution predicted by Vrentas et al. [1985]. The diffusion

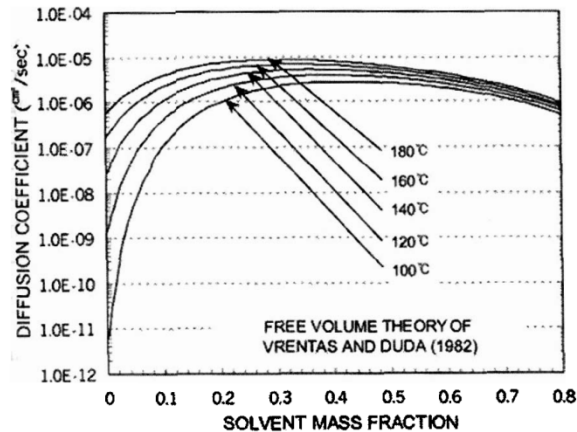


Figure 2.4-4. Binary diffusion coefficient of toluene in the polystyrene-toluene solution as a function of concentration and temperature by Vrentas et al [1982] (Illustrated under “Fair Use” copyright guidelines).

Table 2.4-1. Model parameters of free volume theory by Vrentas-Dada's.

Symbol	Definition
$D^P$	Polymer/solvent binary mutual diffusion coefficient
$D_1$	Solvent self-diffusion coefficient
$\hat{V}_i^*$	Specific critical hole free volume of component i
$\omega_i$	Mass fraction of component i
$T_{gi}$	Glass transition temperature of component i
$\phi_1$	Solvent volume fraction
$\chi$	Polymer-solvent interaction parameter
$D_0$	Constant pre-exponential factor
$E$	Molar energy required for a molecule to overcome attractive forces
$\gamma$	Overlap factor; the same free volume is available to more than one molecule
$K_{11}$ and $K_{21}$	Free-volume parameters for the solvent
$K_{12}$ and $K_{22}$	Free-volume parameters for the polymer
$\xi$	The ratio of molar volumes for the solvent and polymer jumping units

coefficient decreases by several orders of magnitudes as the solvent concentration decreases and increases as the temperature increases. Another important fact is that the concentration dependency of the diffusion coefficient at low solvent concentrations considerably weakens at higher temperatures. This means that high temperature is required to facilitate the removal of residual solvent in the FDRP. However, the maximum temperature is also restricted by the onset of high-temperature defects and the thermal properties of coated materials such as melting temperature [Kim, S. 2001].

#### 2.4.2 Modeling of film drying

It has been a long-time goal in industry to monitor the amount of residual solvent in coated wet films at known drying conditions and, thus, to decide the drying time and dryer length [Kim 1998]. However, in most cases, in-situ measurement of the amount of residual solvent in the dryer is not feasible because the line speed and dimensions of

industrial production scale dryers do not allow real-time measurement and equipment installation. Thus, the ability to predict the amount of residual solvent in coated wet films is of practical interest for the optimum design of new dryers and the optimum operation of existing dryers [Alsoy 1998]. Also, because the drying process may either improve or degrade the properties of final films, it is significant to understand the fundamental nature of the heat and mass transfer phenomena and their mechanisms during the film drying process. This is much more significant, in the case where significant chemical reactions are accompanied with the film drying [Cairncross 1992]. Therefore, there have been many theoretical and experimental studies on film drying in order to correctly predict the concentration and temperature of the coated wet films and their profiles as a function of drying time (or dryer length) and film depth.

In this section, previous studies on modeling of film drying will be covered first. Then, the most advanced model of film drying and its limitations will be presented in detail. Lastly, current research efforts in modeling of film drying will be briefly mentioned.

In order for a model to correctly predict the behaviors of film drying, most of all, all the phenomena associated with film drying should be considered and reflected in the model in an appropriate way. As described in 2.4.1, the film drying model should include convective heat transfer at the exposed surface, vaporization of solvent at the exposed surface, diffusive mass transfer of solvent into the adjacent air, diffusive mass transfer of solvent through the coated film, conductive heat transfer through the coated film and the substrate, and shrinkage of the coated film (time-dependence of the position of the interface). A list of characteristics, notable achievements, and details of previous studies

on the modeling of film drying is given in Table 2.4-2. In earlier studies by Blandin et al. [1987] and Waggoner et al. [1989], the film drying process was described as unsteady state diffusion, and the heat transfer effects and shrinkage of coated films were neglected. In addition, they used experimental or literature values as mass transfer boundary conditions for the external film surface instead of directly calculating them using their model. Also, temperature dependency of the diffusion coefficient was not considered in the study of Blandin et al. [1987].

However, more comprehensive models that integrate the unsteady state heat and mass transfer as well as film shrinkage and diffusion-induced convection have been suggested. Okazaki et al. [1974] modeled the drying of polyvinylalcohol aqueous solutions by considering the diffusive and convective mass transfer, heat transfer, and time-dependence of the interface position. They also incorporated the effects of unequal component densities into the model. More recently, Yapel [1988] developed a more general model for the drying of a coated film that can contain any number of components. This model enabled the determination of the concentration and temperature profile within the coating and substrate by solving the unsteady state heat and mass transfer equations. The numerical simulation results showed that a very steep concentration gradient developed in the film near the interface between the convective air and coated film. The temperature gradient in the coated film and substrate was negligible because the resistance to heat transfer in the gas phase was even greater than that in both coated film and substrate. Accordingly, the variation of the physical properties of the polymer and solvent in the coated film caused by temperature gradients was negligible. This has not

Table 2.4-2. Summary of previous modeling works of drying of non-reactive polymer-solvent system on an impermeable substrate.

Year	Author	Model			
		Basic characteristics	Mass transfer analysis based on	Temp. gradient neglected?	Film shrinkage considered?
1974	Okazaki et al.	Incorporation of heat and mass transfer	Mass avg. vel.	Yes	Yes
1987	Blandin et al.	Mass transfer, no heat transfer considered	Mass avg. vel.	-	No
1988	Yapel <sup>1)</sup>	Incorporation of heat and mass transfer	Mass avg. vel.	No	Yes
1989	Waggoner and Blum	Mass transfer, no heat transfer considered	Mass avg. vel.	-	No
1992	Cairncross et al.	Incorporation of heat and mass transfer	Vol. avg. vel.	Yes	Yes
1992	Sano	Incorporation of heat and mass transfer	Mass avg. vel.	Yes	Yes
1994	Vrentas and Vrentas	Incorporation of heat and mass transfer	Vol. avg. vel.	Yes	Yes
1994	Kim et al.	Incorporation of heat and mass transfer w/ no diffusion considered	-	Yes	Yes
1998	Alsoy and Duda	Incorporation of heat and mass transfer	Vol. avg. vel.	Yes	Yes
1999	Alsoy and Duda <sup>1)</sup>	Extension of Alsoy and Duda's model (1998) to multi-component system	Vol. avg. vel.	Yes	Yes
2004	Wong et al. <sup>1)</sup>	Incorporation of heat and mass transfer	Vol. avg. vel.	Yes	Yes

<sup>1)</sup> Expandable to multi-component system

Table 2.4-2. Continued.

Author	Experiment system <sup>2)</sup>	Performances <sup>3)</sup>	Diffusion coefficient		
			Method	Temp.-dependency	Conc.-dependency
Okazaki et al.	PVA/water	Characteristic drying curve 1, 2, and 3	3 different experiments	Yes	Yes
Blandin et al.	Fire retardant coating	Characteristic drying curve 1, concentration profile	“Short test”	No	Yes
Yapel <sup>1)</sup>	PVA/methanol	Validation of “negligence of temp. gradient” assumption	Free-volume theory	Yes	Yes
Waggoner and Blum	PS/Tol	Characteristic drying curve 1, concentration profile	PGFE NMR <sup>4)</sup>	Yes	Yes
Cairncross et al.	PS/Tol	Effect of $k_i^j$ , $h^j$ , $D^p$ ( $\rho$ , $T$ ), and $\Delta H_{\text{vap}}$ on drying rate	Free-volume theory	Yes	Yes
Sano	PI/p-CP	Characteristic drying curve 1, 2, and 3	Empirical relation	Yes	Yes
Vrentas and Vrentas	PS/Tol, THF	Most advanced equations of transfer phenomena	Free-volume theory	Yes	Yes
Kim et al.	Pigment, binder/Tol, MEK, CYC	Characteristic drying curve 1	-	-	-
Alsoy and Duda	PVAc/Tol PS/Tol	Characteristic drying curve 1, 2, and 3, effect of convection air temp. and speed, process paths	Free-volume theory	Yes	Yes
Alsoy and Duda <sup>1)</sup>	PS/Tol, Bz PS/Tol, Ethylbz	Characteristic drying curve 1, 2, and 3, advantage of multi-zone oven	Free-volume theory	Yes	Yes
Wong et al. <sup>1)</sup>	PVA/water, methanol	Characteristic drying curve 1, 2, and 3, effect of $T^G$ , $X(0)$ , and $\rho$ on drying rate	Free-volume theory	Yes	Yes

<sup>2)</sup> Abbreviations: PVA; Poly vinyl alcohol, PS; Poly styrene, Tol; Toluene, PI; Poly imide, p-CP; para-Chlorophenol, THF; Tetra Hydro Furan, MEK; Methyl ethyl ketone, CYC; Cyclohexanone, PVAc; Poly vinyl acetate, Bz; Benzene (pliolite, TiO<sub>2</sub>, retardant agent / xylene, benzene)

<sup>3)</sup> Characteristic drying curve 1; Remaining solvent amount vs. time, 2; Film temperature vs. time, 3; Film thickness vs. time.

<sup>4)</sup> Pulsed-gradient, spin-echo nuclear magnetic resonance.

<sup>5)</sup> Not available in the reference.

been experimentally confirmed yet because of the limitations of current science and technology. However, this assumption was frequently used in the following studies by Alsoy et al. [1998 & 1999] and Wong et al. [2004] because it allowed a significant reduction in the computational work required to simulate the complex film drying process. The computational capability of a UNIX-based workstation or even a personal computer is good enough for the simulation of film drying process under this assumption. Nowadays this assumption is accepted as an axiom because many previous studies obtained fairly good agreements between their theoretical calculations and experimental results. Also, the Yapel [1988] model utilized the free volume theory of Vrentas & Duda [1985 a,b]'s in order to calculate the diffusivity of solvents in polymer films as a function of both concentration and temperature. Another advantageous feature of the Yapel [1988] model is that the equation formulation of the mass transfer process was based on the volume average velocity in the species continuity equation instead of the mass average velocity. This significantly reduces the complexity in the description of the film drying process in which the film components have different densities [Alsoy 1998].

The most sophisticated equations for the description of the film drying process were introduced by Vrentas et al. [1994]. They utilized jump balances in the formulation of boundary conditions at the interfaces and also introduced a solution scheme for solving the coupled non-linear equations. In this review, the assumptions and final equations will be briefly introduced without detailed information pertaining to their derivation because of their lengthiness. A schematic of the drying geometry with the resultant equations that describe the heat and mass transfer is shown in Figure 2.4-5, and the nomenclature are listed in Table 2.4-2. The model is based on the following assumptions:

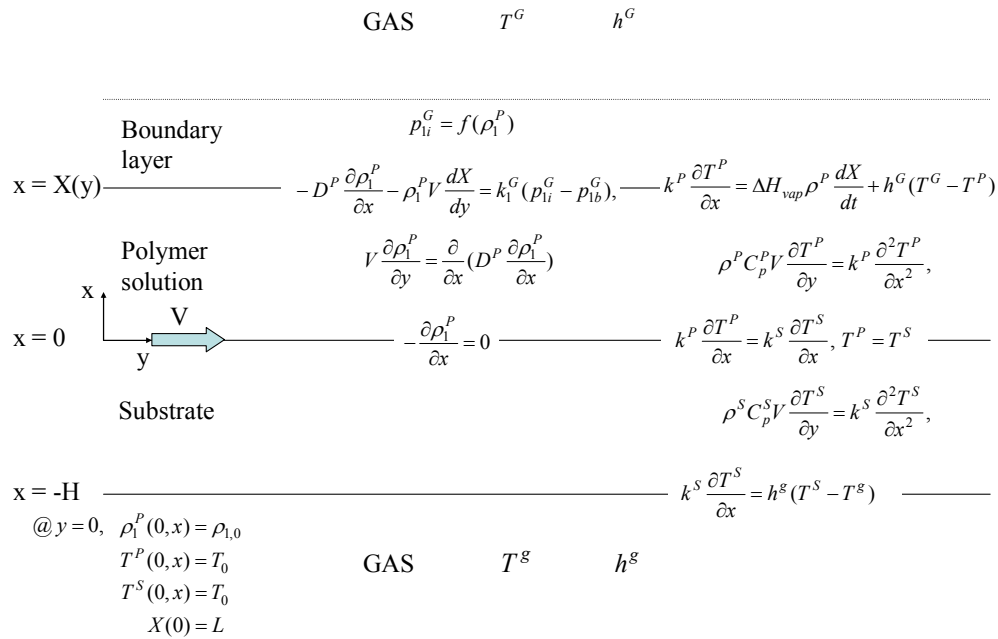


Figure 2.4-5. A schematic of the drying geometry and the model equations by Vrentas et al [1994] .

- Two-dimensional system: no gradients or velocities in the z direction exist because of the relatively much larger dimension of the coated film width in comparison with the film thickness;
- Heat and mass transfer equations are decoupled from the momentum equation;
- There is no volume change on mixing of polymer and solvent;
- Values of the densities, heat capacities, and thermal conductivities of the polymer solution and substrate averaged over the temperature and concentration ranges can be used;

- No temperature gradient exists in the direction of film depth because of the much greater convective resistance to heat transfer in the gas phase in comparison with the conductive resistance to heat transfer in the coated film and substrate;
- The gas phase applies no drag on the coated film;
- Diffusion and conduction in the direction of the substrate movement (y-axis) do not exist;

Table 2.4-3. Summary of model parameters used in the modeling of film drying by Alsoy et al.[1998 & 1999].

(a) Material properties

Symbol	Definition	Determination method
$C_P^j$	Heat capacity	Reference
$\Delta H_{vap}$	Heat of vaporization	Reference
$k_j$	Thermal conductivity	Reference
$D^P$	Diffusion coefficient	Free-volume theory
$p_{li}^G$	Gas partial pressure at the interface	Antoine equation, Flory-Huggins theory
$p_{lb}^G$	Gas partial pressure at the bulk phase	Assumed to be zero
$\rho_j$	Density	Reference

(b) Operation conditions

Symbol	Definition	Determination method
$h^j$	Heat transfer coefficient	Cohen's method
$k_i^j$	Mass transfer coefficient	Chilton-Colburn analogy
$H$	Thickness of substrate	Input variable
$V$	Moving speed	Input variable

(c) Superscripts and subscripts

	Superscript		Subscript
G	Film side	1	Solvent
g	Substrate side	2	Polymer
P	Polymer phase		
S	Substrate phase		

- Radiative heat transfer, viscous dissipation, and gravitation effects are negligible.

Alsoy et al. [1998] accepted the model and equations of Vrentas et al.'s, developed a more simple and advanced solution scheme and validated the model by applying it to polyvinylacetate/toluene and polystyrene/toluene systems. Their manipulation of the equations shown in Figure 2.4-5 yielded the following basic transport equations:

- Heat transfer equation

$$\frac{dT}{dt} = \frac{\Delta H_{vap} \rho^P \frac{dX}{dt} + h^G (T^G - T) - h^S (T - T^S)}{X(t) \rho^P C_p^P + H \rho^S C_p^S} \quad T(0) = T_0 \quad (\text{Eq. 2.4-3})$$

- Continuity equation for the solvent

$$\frac{\partial \rho_1}{\partial t} = \frac{\partial}{\partial x} (D^P \frac{\partial \rho_1}{\partial x}) \quad x=0: \frac{\partial \rho_1^P}{\partial x} = 0 \quad (\text{Eq. 2.4-4})$$

$$x=X(t): -D^P \frac{\partial \rho_1^P}{\partial x} - \rho_1^P \frac{dX}{dt} = k_1^G (p_{li}^G - p_{lb}^G)$$

$$\rho_1^P(0, x) = \rho_{10}^P$$

- Equation for the time-dependence of the interface position

$$\frac{dX}{dt} = \left[ \frac{D^P \hat{V}_1^P}{(1 - \rho_1^P \hat{V}_1^P)} \frac{\partial \rho_1^P}{\partial x} \right]_{x=X(t)} \quad X(0) = L \quad (\text{Eq. 2.4-5})$$

The dimensionless form of the heat transfer equation can be obtained by introducing the dimensionless variables  $T^*$ ,  $X^*$ , and  $t^*$  defined as follows:

$$T^* = \frac{T - T_0}{T^G - T_0} \quad X^* = \frac{X}{L} \quad t^* = \frac{D_0^P t}{L^2} \quad (\text{Eq. 2.4-6})$$

Combination of Eq. 2.4-3 with Eq. 2.4-6 gives the following equation for the dimensionless temperature:

$$\frac{dT^*}{dt^*} = \frac{A[1 - T^*] + E + B \frac{dX^*}{dt^*}}{F + X^*} \quad T^*(0) = 0 \quad (\text{Eq. 2.4-7})$$

where dimensionless parameters  $A$ ,  $B$ ,  $E$ , and  $F$  are defined as follows:

$$A = \frac{L(h^G + h^g)}{D_0^P \rho^P C_p^P} \quad B = \frac{\Delta H_{vap}}{C_p^P (T^G - T_0)}$$

$$E = \frac{h^g (T^g - T^G) L}{D_0^P \rho^P C_p^P (T^G - T_0)} \quad F = \frac{\rho^P C_p^S H}{\rho^P C_p^P L} \quad (\text{Eq. 2.4-8})$$

During the course of film drying, the thickness of coated films reduces with drying time. Thus, in order to make the solvent species continuity equation dimensionless, it is necessary to fix the boundary at the interface between the convective air and coated film. This immobilization can be achieved by using the following transformation:

$$\eta = \frac{x}{X(t)} \quad (\text{Eq. 2.4-9})$$

So, the domain of the coated film is always from  $\eta = 0$  to  $\eta = 1$ . Introduction of a dimensionless mass density of solvent

$$C = \frac{\rho_1^P}{\rho_{1,0}^P} \quad (\text{Eq. 2.4-10})$$

and utilization of Eq. 2.4-6 and Eq. 2.4-10 yield the following dimensionless form of the solvent continuity equation:

$$\frac{\partial C}{\partial t^*} - \frac{\eta}{X^*} \frac{dX^*}{dt^*} \frac{\partial C}{\partial \eta} = \frac{1}{(X^*)^2} \frac{\partial}{\partial \eta} \left( Q \frac{\partial C}{\partial \eta} \right) \quad (\text{Eq. 2.4-11})$$

$$\eta = 0 \quad \frac{\partial C}{\partial \eta} = 0$$

$$\eta = 1 \quad -Q \left( \frac{\partial C}{\partial \eta} \right)_{\eta=1} - C(\eta=1) X^* \frac{dX^*}{dt^*} = S X^*$$

$$C(0, \eta) = 1$$

The dimensionless form of the equation for the time-dependence of the interface position expressed by Eq. 2.4-5 is

$$X^* \frac{dX^*}{dt^*} = [QU \frac{\partial C}{\partial \eta}], \quad X^*(0) = 1 \quad (\text{Eq. 2.4-12})$$

Dimensionless parameters in Eq. 2.4-12 can be defined as follows:

$$Q = \frac{D^P}{D_0^P} \quad S = \frac{k_1^G (p_{1i}^G - p_{1b}^G) L}{D_0^P \rho_{10}^P} \quad U = \frac{\hat{V}_1^P \rho_{10}}{1 - \hat{V}_1^P \rho_{10}} \quad (\text{Eq. 2.4-13})$$

Alsoy et al. [1998] also introduced an advanced numerical scheme for the solution of the above set of coupled non-linear partial differential equations by using a finite difference method and a variable-grid-size technique. As mentioned earlier, a much steeper concentration gradient develops near the interface between the convective air and

coated film. So, they used a mesh with nonuniform grid sizes in the domain: smaller grids in the vicinity of the air-film interface and coarser grids near the substrate. This technique improved the accuracy of the results as well as the efficiency of the numerical calculation.

The film drying model and solution scheme developed by Vrentas et al. [1994] and Alsoy et al. [1998] have been used in several studies because of its accurate prediction, efficient calculation method, etc. Alsoy et al. [1999] expanded the applicability of the model to multi-component systems, and Wong et al. [2004] included the effect of polymer crystallinity on film drying. However, it can be easily recognized that all the previous studies were limited to thermodynamically well-characterized systems such as polystyrene-toluene and polyvinylacetate-toluene. The utilization of Vrentas et al.'s model has been limited because of poor availability of the model parameters, in particular the diffusion coefficients of solvents in polymers as a function of concentration and temperature. Obviously, the application of the model to numerous polymer-solvent systems used in industry and polymer-solvent systems in their development stage seems to be more demanding than can be handled by the current approach. Zielinski et al. [1992] reported the determination methods of all the parameters of Vrentas-Duda's free volume theory. Nevertheless, it also seems to be prohibitively laborious and time-consuming from a practical aspect. Furthermore, because the contribution of ionic components in polymers to the thermodynamics of polymer-solvent systems is much less known than any other solute-solvent system, a complete characterization of the polymer-solvent system to be studied in this thesis work is not achievable.

Kim et al. [Kim, S. 1998] introduced a model of coated film drying based on a lumped parameter system by setting up heat and mass balances at the interfaces, and neglecting the diffusion of solvent inside the coated film. The heat and mass balances are as follows:

$$R_{mass,i} = \rho_i b_c \frac{dz_i}{dt} = k (C_i^{sat} - C_i^\infty) \quad (\text{Eq. 2.4-14})$$

$$(\rho_f b_f C_{pf} + \sum_{i=1}^k \rho_i z_i b_c C_{pi}) \frac{dT}{dt} = h(T - T^\infty) - \sum_{i=1}^k R_{mass,i} (\Delta H_{vap})_i \quad (\text{Eq. 2.4-15})$$

where  $R_{mass,i}$  is the evaporation rate of component  $i$ ,  $z_i$  is the volume fraction of component  $i$ ,  $\rho_i$  is the density of pure component  $i$ ,  $b$  is the thickness,  $C_i^{sat}$  is the saturated solvent concentration of component  $i$ ,  $C_i^\infty$  is the solvent concentration of component  $i$  in the bulk air,  $k$  is the mass transfer coefficient,  $h$  is the heat transfer coefficient,  $T$  is the temperature of coated film,  $T^\infty$  is the temperature of convective air,  $\Delta H_{vap}$  is the heat of vaporization, and  $C_p$  is the heat capacity. Subscript  $f$  and  $C$  mean the substrate and coated film respectively. Kim et al. [Kim, S. 1998] reported that the prediction of this model agreed well with the experimental results only at the constant drying rate period before solvent diffusion became the rate-controlling step of the drying process, as expected. Evidently, negligence of solvent diffusion will result in somewhat inaccurate predictions on the total drying time and dryer length. However, it is believed that this model is adequate to extend film drying modeling to the prediction of the final properties of

copolymer membrane films because most of the morphology formation is completed in CDRP.

So far many previous studies have been dedicated to the film drying process. The elemental heat and mass transfer phenomena have been revealed and a fundamental understanding about the film drying process has been provided. Also, models were developed in order to predict total drying time and total dryer length for the optimization of film drying process. However, no previous studies have been devoted to the prediction of the interrelationship between film drying conditions and the properties of resultant films. In this thesis work, the possibility of the property prediction of resultant films will be explored using Kim et al.'s model based on a lumped parameter system. Even though their model is known to be valid just for constant drying rate period, it should be applicable for the purposes of this study because the rearrangement of polymer molecules is much more vigorous in solutions at low concentrations where most of the membrane film morphology develops [Baker 2004].

## 2.5 References

1. Alberti, G., M. Casciola, and R. Palombari, "Inorgano-organic Proton Conducting Membranes for Fuel Cells and Sensors at Medium Temperatures," *Journal of Membrane Science*, **172**, 233 (2000).
2. Alberti, G., U. Costantino, M. Casciola, S. Ferroni, L. Massinelli, and P. Staiti, "Preparation, Characterization and Proton Conductivity of Titanium Phosphate Sulfophenylphosphonate," *Solid State Ionics*, **145**, 249, (2001).
3. Alsoy, S., and J. L. Duda, "Drying of Solvent Coated Polymer Films," *Drying Technology*, **16**, 15 (1998).
4. Alsoy, S., and J. L. Duda, "Modeling of Multicomponent Drying of Polymer Films," *AIChE Journal*, **45**, 896 (1999).
5. Avrami, M., "Kinetics of Phase Change, 1: General Theory," *Journal of Chemical Physics*, **7**, 1103 (1939).
6. Avrami, M., "Kinetics of Phase Change. 2: Transformation-Time Relations for Random Distribution Nuclei," *Journal of Chemical Physics*, **8**, 212 (1940).
7. Avrami, M., "Granulation, Phase Change, and Microstructure," *Journal of Chemical Physics*, **9**, 177 (1941).
8. Bailly, C. H., L. M. Leung, J. O'Gara, D. J. Williams, F. E. Karasz, and W. J. MacKnight, "In Structure and Properties of Ionomers, Pineri, M. and Eisenberg, A., Eds., NATO ASI Series, Series C: Mathematical and Physical Science 198, Reidel, Dordrecht, 1987.
9. Baker, R. W., *Membrane Technology and Applications*, John Wiley & Sons, New York (2004).
10. Banerjee, S., and Curtin, D. E., Nafion<sup>®</sup> Perfluorinated Membranes in Fuel Cells, *Journal of Fluorine Chemistry*, **125**, 1211 (2004).
11. Bar-On, I., R. Kirchain, and R. Roth, "Technical Cost Analysis for PEM Fuel Cells," *Journal of Power Sources*, **109**, 71 (2002).
12. Bates, F. S., and G. H. Fredrickson, "Block Copolymers – Designer Soft Materials," *Physics Today*, **52**, 32 (1999).
13. Bates, F. S., M. F. Schulz, A. K. Khandpur, S. Förster, and J. H. Rosedale, "Fluctuations, Conformational Asymmetry and Block Copolymer Phase Behaviour," *Faraday Discussions*, **98**, 7 (1994).
14. Bauer, B., D. J. Jones, J. Roziere, L. Tchicaya, G. Alberti, M. Casciola, L. Massinelli, A. Peraio, S. Besse, and E. Ramunni, *Journal of New Materials for Electrochemical Systems*, **3**, 93 (2000).
15. Bébin, P., and H. Galiano, "Processing of PEMFC Membranes by Extrusion: Part 1. Sulfonated Polysulfone in Acid Form," *Advances in Polymer Technology*, **25**, 121 (2006).
16. Bébin, P., and H. Galiano, "Processing of Sulfonated Polysulfone for PEMFC Membrane Applications: Part 2. Polymer in Salt Form," *Advances in Polymer Technology*, **25**, 127 (2006).
17. Blandin, H. P., J. C. David, J. M. Vergnaud, J. P. Illien, and M. Malizewicz, "Modeling the Drying Process of Coating with Various Layers," *Journal of Coatings Technology*, **59**, 27 (1987).

18. Bockstaller, M., R. Kolb, and E. L. Thomas, "Metallo-dielectric Photonic Crystals Based on Diblock Copolymers", *Advanced Materials*, **13**, 1783, (2001).
19. Cairncross, R. A., L. F. Francis, L. E. Scriven, "Competing Drying and Reaction Mechanisms in the Formation of Sol-to-gel Films, Fibers, and Spheres," *Drying Technology*, **10**, 893 (1992).
20. Cotter, R. J., *Engineering Plastics: Handbook of Polyarylethers*, Gordon and Breach Publishers, Basel, Switzerland (1995).
21. Cohen, E. D., "Thin Film Drying", *Coating and Drying Technology*, Cohen, E. D., and Guttoff, E. B. ed., John Wiley & Sons, Inc., New York (1992).
22. Cussler, E. L., *Diffusion Mass Transfer in Fluid Systems*, 2<sup>nd</sup> Ed., Cambridge University Press, Oxford, UK, (1997).
23. Dobrynin, A. V., "Phase Coexistence in Random Copolymers," *Journal of Chemical Physics*, **107**, 9234, (1997).
24. DOE - [http://www1.eere.energy.gov/hydrogenandfuelcells/pdfs/technical\\_targets\\_membr\\_auto.pdf](http://www1.eere.energy.gov/hydrogenandfuelcells/pdfs/technical_targets_membr_auto.pdf)
25. Edens, M. W., *Applications of Polyoxyethylene*, Nace, V. N. Ed., Marcel Dekker, New York, Vol.60, p 185, (1996).
26. Eisenberg, A., and J.-S. Kim, *Introduction to Ionomers*, John Wiley & Sons, Inc., New York (1998).
27. El-Hibri, M. J., and S. A. Weinberg, "Polysulfones," *Encyclopedia of Polymer Science and Technology*, Kroschwitz, J. I., and Mark, H. F. Eds, John Wiley & Sons, Inc., Hoboken, New Jersey, Vol. 4, 1-25, (2003).
28. Floudas, G., S. Vogt, T. Pakula, and E. W. Fischer, "Density and Concentration Fluctuations in Poly(styrene-*b*-phenylmethylsiloxane) Copolymers," *Macromolecules*, **26**, 7210, (1993).
29. Floudas, G., T. Pakula, E. W. Fischer, N. Hadjichristidis, and S. Pispas, "Ordering Kinetics in a Symmetric Diblock Copolymer," *Acta Polymer*, **45**, 176 (1994).
30. Floudas, G., N. Hadjichristidis, H. Iatrou, T. Pakula, and E. W. Fischer, "Microphase Separation in Model 3-Miktoarm+ Star Copolymers (Simple Graft) and Terpolymers. 1. Statics and Kinetics," *Macromolecules*, **27**, 7735, (1994).
31. Förster, S., A. K. Khandpur, J. Zhao, F. S. Bates, I. W. Hamley, A. J. Ryan, and W. Bras, "Complex Phase Behavior of Polyisoprene-Polystyrene Diblock Copolymers Near the Order-Disorder Transition," *Macromolecules*, **27**, 6922 (1994).
32. Fredrickson, G. H., and K. Binder, "Kinetics of Metastable States in Block Copolymer Melts," *Journal of Chemical Physics*, **91**, 7265, (1989).
33. Fredrickson, G. H., and E. Helfand, "Fluctuation Effects in the Theory of Microphase Separation in Block Copolymer," *Journal of Chemical Physics*, **87**, 697 (1987).
34. Fredrickson, G. H., and S. T. Milner, "Thermodynamics of Random Copolymer Melts," *Physical Review Letters*, **67**, 835 (1991).
35. Gehlsen, M. D., and F. S. Bates, "Heterogeneous Catalytic Hydrogenation of Poly(styrene): Thermodynamics of Poly(vinylcyclohexane) Containing Diblock Copolymers," *Macromolecules*, **26**, 4122 (1993).

36. Guttoff, E. and E. Cohen, *Coating and Drying Defects – Troubleshooting Operating Problems*, John Wiley & Sons, Inc., New York, (1995).
37. Hadjichristidis, N., S. Pispas, and G. A. Floudas, *Block Copolymers: Synthetic Strategies, Physical Properties, and Applications*, John Wiley & Sons, Inc., New Jersey (2003).
38. Haile, S. M., “Fuel Cell Materials and Components,” *Acta Materialia*, **51**, 5981 (2003).
39. Hajduk, D. A., P. E. Harper, Sol M. Gruner, C. C. Honeker, G. Kim, E. L. Thomas, and L. J. Fetters, “The Gyroid: A New Equilibrium Morphology in Weakly Segregated Diblock Copolymers,” *Macromolecules*, **27**, 4063 (1994).
40. Hamley, I. W., *The Physics of Block Copolymers*, Oxford University Press, Oxford (1999).
41. Hamley, I. W., “Introduction to Block Copolymer,” Hamley, I. W. Ed., John Wiley & Sons, Ltd., New York (2004).
42. Hamley, I. W., K. A. Koppi, J. H. Rosedale, F. S. Bates, K. Almdal, and K. Mortensen, “Hexagonal Mesophases between Lamellae and Cylinders in a Diblock Copolymer Melt,” *Macromolecules*, **26**, 5959 (1993).
43. Hanley, K. J., and T. P. Lodge, “Phase Behavior of a Block Copolymer in Solvents of Varying Selectivity,” *Macromolecules*, **33**, 5918 (2000).
44. Han, C. D., D. M. Baek, J. K. Kim, T. Ogawa, N. Sakamoto, and T. Hashimoto, “Effect of Volume Fraction on the Order-Disorder Transition in Low Molecular Weight Polystyrene-block-Polyisoprene Copolymer. 1. Order-Disorder Transition Temperature Determined by Rheological Measurements,” *Macromolecules*, **8**, 5043 (1995).
45. Harrison, W. L., F. Wang, J. B. Mecham, V. A. Ghanu, M. Hill, Y. S. Kim, and J. E. McGrath, “Influence of the Bisphenol Structure on the Direct Synthesis of Sulfonated Poly (arylene ether) Copolymers. 1,” *Journal of Polymer Science: Part A: Polymer Chemistry*, **41**, 2264 (2003).
46. Harrison, W. L., M. A. Hickner, Y. S. Kim, and J. E. McGrath, Poly (arylene ether sulfone) Copolymers and Related Systems from Disulfonated Monomer Building Blocks: Synthesis, Characterization, and Performance,” *Fuel Cells*, **5**(2), 201 (2005).
47. Helfand, E., “Block Copolymer Theory. 3. Statistical Mechanics of the Microdomain Structure,” *Macromolecules*, **8**, 552 (1975).
48. Helfand, E., and Z. R. Wasserman, “Block Copolymer Theory. 4. Narrow Interphase Approximation,” *Macromolecules*, **9**, 879-888 (1976).
49. Hickner, M. A., H. Ghassemi, Y. S. Kim, B. R. Einsla, and J. E. McGrath, “Alternative Polymer Systems for Proton Exchange Membranes (PEMs),” *Chemical Reviews*, **104**, 4587 (2004).
50. Hickner, M. A., Y. S. Kim, F. Wang, J. E. McGrath, and T. A. Zawodzinski, “Proton Exchange Membrane Nanocomposites,” *Proceedings of the American Society for Composites, Technical Conference 16<sup>th</sup>*, pp 323, (2001).
51. Hickner, M. A., and B. S. Pivovar, “The Chemical and Structural Nature of Proton Exchange Membrane Fuel Cell Properties,” *Fuel Cells*, **5**(2), 213 (2005).
52. Hickner, M. A., F. Wang, Y. S. Kim, B. S. Pivovar, T. A. Zawodzinski, and J. E. McGrath, 200<sup>th</sup> Meeting of the Electrochemical Society, San Francisco (2001).

53. Huang, J., D. G. Baird, G. Fan, Z. Zhang, A. Badami, S. Takamuku, and J. E. McGrath, "Continuous film casting and evaluation of polymer membranes for fuel cells," 2007 Society of Plastics Engineers Annual Conference, Cincinnati, OH, (2007)
54. Johnson, B., I. Yilgor, C. Tran, M., Iqbal, J. P. Wightman, D. R. Lloyd, and J. E. McGrath, "Synthesis and Characterization of Sulfonated Poly(Arylene Ether Sulfones)," *Journal of Polymer Science: Polymer Chemistry*, **22**, 721 (1984).
55. Kasten, H., and B. Stühn, "Density Discontinuity at the Microphase Separation Transition of a Symmetric Diblock Copolymer," *Macromolecules*, **28**, 4777 (1995).
56. Kato, K., "Osmium Tetraoxide Fixation of Rubber Lattices," *Journal of Electron Microscopy*, **14**, 219 (1965).
57. Kim, S. S., and J. C. Hyun, "Drying of Coated Film," *Handbook of Solvent*, Wypych, G. Ed., ChemTec Publishing, Ontario, Canada (2001).
58. Kim, S. S., and M. H. Kwon, "Measurement and Prediction of the Drying Rate in the Drying Process of Magnetic Coated Film," 9<sup>th</sup> International Coating Science and Technology Symposium, Delaware, USA, May 17-20 (1998).
59. Kim, Y. S., Dong, L., Hickner, M. A., Glass, T. E., Webb, V., and McGrath, J. E., State of water in disulfonated poly (arylene ether sulfone) copolymers and a perfluorosulfonic acid copolymer (Nafion) and its effect on physical and electrochemical properties, *Macromolecules*, **36**(17), 6281, 2003.
60. Kim, Y. S., Dong, L., Hickner, M. A., Pivovar, B. S., and McGrath, J. E., Processing induced morphological development in hydrated sulfonated poly (arylene ether sulfone) copolymer membranes, *Polymer*, **44**, 5729-5736, 2003.
61. Kim, Y. S., Hill, M., Wang, F., Hickner, M., Hong, Y. T., Zawodzinski, T. A., McGrath, J. E., 8<sup>th</sup> International Symposium on Polymer Electrolytes, Santa Fe, 2002.
62. Kim, Y. S., Wang, F., Hickner, M., McCartney, S., Hong, Y. T., Harrison, W., Zawodzinski, T. A., and McGrath, J. E., Effect of acidification treatment and morphological stability of sulfonated poly (arylene ether sulfone) copolymer proton-exchange membranes for fuel-cell use above 100 °C, *Journal of Polymer Science: Part B: Polymer Physics*, **41**, 2816-2828, 2003.
63. Knomkova, E. N., Wessling, M., Krol, J., Strathmann, H., and Berezina, N. P., *Polym Sci, Ser A*, **43**(3), 300, 2001.
64. Kopitzke, R. W., Linkous, C. A., and Nelson, G. L., Thermal stability of high temperature polymers and their sulfonated derivatives under inert and saturated vapor conditions, *Polymer Degradation and Stability*, **67**, 335, 2000.
65. Krausch, G., and Magerle, R., Nanostructured thin films via self-assembly of block copolymers, *Advanced Materials*, **14**(21), 1579-1583, 2002.
66. Kreuer, K. D., On the Development of Proton Conducting Polymer Membranes for Hydrogen and Methanol Fuel Cells, *Journal of Membrane Science*, **185**, 29-39, 2001.
67. Kreuer, K. D., Fuchs, A., Ise, M., Spaeth, M. and Maier, J., Imidazole and pyrazole-based proton conducting polymers and liquids, *Electrochimica Acta*, **43**, 1281-1288, 1998.
68. Larminie, J., and Dicks, A., *Fuel Cell Systems Explained*, 2<sup>nd</sup> Ed., John Wiley & Sons, New York, 2003.

69. Leibler, L., Theory of Microphase Separation in Block Copolymers, *Macromolecules*, 13, 1602-1617, 1980.
70. Li, L., Zhang, J., and Wang, Y., Sulfonated poly ether ether ketone membranes cured with different methods for direct methanol fuel cells, *Journal of Materials Science Letters*, 22, 1595-1597, 2003.
71. Lodge, T. P., Block Copolymers: Past Successes and Future Challenges, *Macromolecular Chemistry and Physics*, 204, 265-273, 2003.
72. Matsen, M. W., and Bates, F. S., Unifying Weak- and Strong-Segregation Block Copolymer Theories, *Macromolecules*, 29, 1091-1099, 1996.
73. Matsen, M. W., and Schick, M., Stable and Unstable Phases of a Diblock Copolymer Melt, *Physical Review Letters*, 72, 2660-2664, 1994.
74. McGrath, J. E., Progress in alternate proton exchange membrane materials for fuel cells, *Preprints of Symposia – American Chemical Society, Division of Fuel Chemistry*, 51(2), 371-372, 2006.
75. Matsuura, H., and Eisenberg, A., Glass transitions of ethyl acrylate-based ionomers, *Journal of Polymer Science: Polymer Physics Ed.*, 14, 1201-1209, 1976.
76. Miltz, J., Passy, N., and Mannheim, C. H., Mass Transfer from and through Packaging Materials, *Packaging Technology and Science*, 5, 49, 1992.
77. Nissan; Personal communication.
78. Noolandi, J., Shi, A.-C., and Linse Per, Theory of Phase Behavior of Poly(oxyethylene)-Poly(oxypropylene)-Poly(oxyethylene) Triblock Copolymers in Aqueous Solutions, *Macromolecules*, 29, 5907-5919, 1996.
79. Noshay, A., and McGrath, J. E., *Block copolymer: Overview and Critical Survey*, Academic Press Inc., New York, 1977.
80. Okazaki, M., Shioda, K., Masuda, K., and Toei, R., Drying Mechanism of Coated Film of Polymer Solution, *Journal of Chemical Engineering of Japan*, 7, 99-105, 1974.
81. Perrin, D. D., and Armarego, W. L. G., *Purification of Laboratory Chemicals*, 3<sup>rd</sup> Ed., Permagon Press, New York, 1988.
82. Pivovar, B. S., Wang, Y., and Cussler, E. L., Pervaporation membranes in direct methanol fuel cells, *Journal of Membrane Science*, 154, 155-162, 1999.
83. Rauwendaal, C., *Polymer extrusion*, 4<sup>th</sup> Ed., Hanser Publishers, Munich; Vienna; New York, 2001.
84. Robertson, G. P., Mikhailenko, S. D., Wang, K., Xing, P., Guiver, M. D., and Kaliaguine, S., Casting solvent interactions with sulfonated poly(ether ether ketone) during proton exchange membrane fabrication, *Journal of Membrane Science*, 219, 113-121, 2003.
85. Robeson, L. M. and Matzner, M., U.S. Patent 4,380,598, Flame retardant polyarylate compositions, 1983.
86. Sankir, M., Bhanu, V. A., Ghassemi, H., Wiles, K. B., Hill, M. L., Harrison, W., Sumner, M. J., Glass, T. E., Riffle, J. S., McGrath, J. E., Systematic study of the synthesis and characterization of 3,3'-sulfonylbis(6-chlorobenzenesulfonic acid) disodium salt monomer for proton conducting polymeric membranes in fuel cell applications, *ACS Polymer Preprints*, 44, 1079-1080, 2003.

87. Semenov, A. N., and Likhtman, A. E., Theory of Secondary Domain Structures in Disordered Multiblock Copolymers, *Macromolecules*, 31, 9058-9071, 1998.
88. Solvay Advanced Polymers, L.L.C., Alpharetta, GA, Design Guide for RADEL<sup>®</sup> A – Polyethersulfone and RADEL<sup>®</sup> R – Polyphenylsulfone.
89. Sopian, K., and Daud, W. R. W., Challenges and future developments in proton exchange membrane fuel cells, *Renewable Energy*, 31, 719-727, 2006.
90. Sfatos, C. D., Gutin, A. M., Shakhnovich, E. I., Critical Compositions in the Microphase Separation Transition of Random Copolymers, *Physical Review E*, 51, 4727-4734, 1995.
91. Stadler, R., Auschra, C., Bechmann, J., Krapper, U., Voigt-Martin, I., and Leibler, L., Morphology and Thermodynamics of Symmetric Poly(A-block-B-block-C) Triblock Copolymers, *Macromolecules*, 28, 3080-3097, 1995.
92. Svensson, M., Alexandridis, P., and Linse, P., Phase Behavior and Microstructure in Binary Block Copolymer/Selective Solvent Systems: Experiments and Theory, *Macromolecules*, 32, 637-645, 1999.
93. Tuzar, Z., Adsorption of Block Copolymers at Solid-Liquid Interfaces, in *Solvents and Self-Organization of Polymers*, Webber S. E., Tuzar Z., Munk, P. (Eds) Kluwer Academic Publishers, The Netherlands, p. 1.
94. Ueda, M., Toyota, M., Ochi, T., Sugiyama, J., Yonetake, K., Masuko, T., and Teramoto, T., Synthesis and Characterization of Aromatic Poly (ether sulfone)s Containing Pendant Sodium Sulfonate Groups, *Journal of Polymer Science: Part A. Polymer Chemistry*, 31, 853-858, 1993.
95. van Vlimmeren, B. A. C., Maurits, N. M., Zvelindovsky, A. V., Sevink, G. J. A., Fraaije, J. G. E., Simulation of 3D Mesoscale Structure Formation in Concentrated Aqueous Solution of the Triblock Polymer Surfactants (Ehtylene Oxide)<sub>13</sub>(Propylene Oxide)<sub>30</sub>(Ethylene Oxide)<sub>13</sub> and (Propylene Oxide)<sub>19</sub>(Ethylene Oxid)<sub>33</sub>(Propylene Oxide)<sub>19</sub> Application of Dynamic Mean-Field Density Functional Theory, *Macromolecules*, 32, 646-656, 1999.
96. Vigild, M. E., Almdal, K., Mortensen, K., Hamley, I. W., Fairclough, J. P. A., and Ryan, A. J., Transformation to and from the Gyroid Phase in a Diblock Copolymer, *Macromolecules*, 31, 5702-5716, 1998.
97. Vrentas, J. S., and Duda, J. L., Diffusion in Polymer-Solvent systems: II. A predictive Theory for the Dependence of Diffusion Coefficients on Temperature, Concentration, and Molecular Weight, *Journal of Polymer Science: Part B: Polymer Physics*, 15, 417-429, 1977
98. Vrentas, J. S., Duda, J. L., and Ling, H.-C., Free-Volume Theories for Self-Diffusion in Polymer-Solvent Systems. I. Conceptual Differences in Theories, *Journal of Polymer Science: Polymer Physics Ed.*, 23, 275-288, 1985.
99. Vrentas, J. S., Duda, J. L., Ling, H.-C., and Hou, A.-C, Free-Volume Theories for Self-Diffusion in Polymer-Solvent Systems. II. Predictive Capabilities, *Journal of Polymer Science: Polymer Physics Ed.*, 23, 289-304, 1985.
100. Vrentas, J. S. and Vrentas, C. M., Drying of Solvent Coated Polymer Films, *Journal of Polymer Science: Part B: Polymer Physics*, 32, 187-194, 1994.
101. Waggoner, R. A., and Blum F. D., Solvent Diffusion and Drying of Coatings, *Journal of Coatings Technology*, 61, 51-56, 1989.

102. Wakizoe, M., and Watanabe, A., Study of Asahi Aciplex membrane for highly durable PEMFCs, 2000 Fuel Cell Seminar, Oct. 30-Nov. 2, 2000, Portland, Oregon; 2000, p.p. 23-26.
103. Wang, F., Hickner, M., Kim, Y. S., Zawodzinski, T. A., and McGrath, J. E., Direct Polymerization of Sulfonated Poly (arylene ether sulfone) Random (statistical) Copolymers: Candidates for New Proton Exchange Membranes, *Journal of Membrane Science*, 197, 231-242, 2002.
104. Wanka, G., Hoffmann, H., and Ulbricht, W., Phase Diagrams and Aggregation Behavior of Poly(oxyethylene)-Poly(oxypropylene)-Poly(oxyethylene) Triblock Copolymers in Aqueous Solutions, *Macromolecules*, 27, 4145-4159, 1994.
105. Winey, K. I., Gobran, D. S., Xu, Z., Getters, L. J., Thomas, E. L., Compositional Dependence of the Order-Disorder Transition in Diblock Copolymers, *Macromolecules*, 27, 2392-2397, 1994.
106. Wong, S.-S., Altinkaya, S. A., and Mallapragada, S. K., Drying of Semicrystalline Polymers: Mathematical modeling and Experimental Characterization of Poly(vinyl alcohol) Films, *Polymer*, 45, 5151-5161, 2004.
107. Yang, Y., and Holdcroft, S., Synthetic strategies for controlling the morphology of proton conducting polymer membranes, *Fuel Cell*, 5(2), 171-186, 2005.
108. Yapel, R. A., The Physical Model of Drying of Coated Films, M.S. Thesis, University of Minnesota, Minneapolis, U.S.A., 1988.
109. Zawodzinski, T. A., Neeman, M., Sillerud, L. O., and Gottesfeld, S., Determination of water diffusion coefficients in perfluorosulfonate ionomeric membranes, *Journal of Physical Chemistry*, 95, 6040-6044, 1991.
110. Zawodzinski, T. A., Springer, T. E., Davey, J., Jestel, R., Lopez, C., Valerio, J., and Gottesfeld, S., A comparative study of water uptake by and transport through ionomeric fuel cell membranes, *Journal of Electrochemical Society*, 140(7), 1993.
111. Zheng, W., and Wang, Z. -G., Morphology of ABC Triblock Copolymers, *Macromolecules*, 28, 7215-7223, 1995.
112. Zielinski, J. M., and Duda, J. L., Predicting Polymer/solvent Diffusion Coefficients Using Free-volume Theory, *AIChE Journal*, 38, 405-415, 1992.

## CHAPTER 3

### EFFECTS OF SOLUTION-CASTING CONDITIONS ON THE FINAL MORPHOLOGY AND PROPERTIES OF DISULFONATED POLY (ARYLENE ETHER SULFONE) MULTIBLOCK COPOLYMER FILMS FOR PROTON EXCHANGE MEMBRANES

#### 3.0 Abstract

The effects of solvent type and film drying conditions on the final morphology and properties of the disulfonated poly(arylene ether sulfone) multiblock copolymer films for use in proton exchange membranes (PEMs) were investigated from the viewpoint of phase separation of block copolymers. Our results demonstrated that solvent selectivity, drying temperature, and solvent removal rate as well as the block length had considerable effects on the final morphology and properties. The proton conductivity and water uptake could be significantly increased by simply utilizing a selective solvent, dimethylacetamide (DMAC), which is good and marginal for the sulfonated and unsulfonated blocks, respectively, rather than N-methyl-2-pyrrolidone (NMP), a neutral solvent for both blocks. Drying temperature and solvent removal rate were observed to have considerable effects on the water uptake and swelling behavior, being coupled with solvent selectivity. Also, it was shown that the multiblock copolymer consisting of longer blocks was more sensitive to the processing conditions. From the morphological study

using transmission electron microscopy and small-angle X-ray scattering, evidences for the above observations were obtained.

### 3.1. Introduction

The proton exchange membrane (PEM) fuel cell (FC) has been proposed as an alternative energy conversion technology due to its high efficiency and environment-friendly nature. However, its widespread commercialization is far from being fulfilled because of a number of technical problems remaining to be solved [Devanathan 2009]. Currently, insufficient performance of PEMs at elevated temperatures and low humidity, platinum catalysts that are susceptible to carbon monoxide, and cost are some of main technical issues. In order for fuel cells to be widely used, significant scientific and technological progress is needed as well as considerable cost reduction. In particular, operation of the fuel cell at elevated temperatures above 120 °C is highly desirable [Roziere 2003]. Elevated temperature operations not only increase the reaction rates at the electrodes but also enable reduction of carbon monoxide poisoning of the platinum catalyst and even potential utilization of more economical catalysts.

Nafion has been a benchmark PEM material for years owing to its outstanding properties such as excellent proton conductivity under some conditions, endurance in the fuel cell environment, mechanical toughness and moderate water uptake [Mauritz 2004]. However, it is generally recognized that perfluorinated Nafion-type membranes are inappropriate for elevated temperature operation. Absorbed water in the membranes lowers the glass transition temperature and  $\alpha$  relaxation of the membranes, which leads to deterioration of mechanical properties and fuel cell performance as well [Kim 2003

Macro, Savadogo 2004]. In addition, high cost and high permeability to methanol are major drawbacks of the Nafion-type membranes.

Over the last decade, researchers have tried to produce PEMs with improved performances by employing promising materials [Sopian 2006]. Numerous materials and their variations based on hydrocarbons such as polyaromatic or polyheterocyclic repeat units have been introduced as alternative PEM materials due to their excellent thermal, oxidative and hydrolytic stability, availability, and good mechanical properties [Roziere 2003]. Partially sulfonated random copolymers based on the hydrocarbon-based candidate materials were obtained via direct copolymerization or post-sulfonation, and their performances and properties for PEM applications were examined [Hickner 2004]. The proton conductivities at fully hydrated conditions and excellent stability indicated that the partially sulfonated random copolymers were promising as PEMs. However, the proton conductivities at low humidity were significantly lower than the Nafion-type membranes.

More recently, extensive efforts are being devoted to improve the performance of the hydrocarbon-based PEMs at low humidity by modifying their molecular architecture. It has been demonstrated that the microstructure of PEMs is crucial for their performance in the operation of fuel cells [Kreuer 2001, Kim 2003 JPS]. As the continuity and ion-richness of the sulfonated hydrophilic domains increase, PEMs show improved performance. In view of the fact that block copolymer systems can develop phase-separated ordered microstructures such as lamellae, gyroid, and cylinders [Hamley 1998], several previous studies hypothesized that block copolymer PEMs consisting of sulfonated and unsulfonated blocks would result in the formation of more continuous and

ion-rich hydrophilic domains and, accordingly, improved performance of PEMs [Lee 2008a, Lee 2008b, Lee 2007, Zhao 2006, Wang 2006, Ghassemi 2004]. Sulfonated block copolymers based on polyaromatic or polyheterocyclic repeat units have been introduced and evaluated as PEMs. Their results demonstrated that the proton conductivities of block copolymer PEMs were noticeably higher than those of the random copolymer PEMs in spite of similar degrees of sulfonation. Lee et al. [2007] also showed that the PEMs consisting of longer blocks of disulfonated PAES and unsulfonated PI produced higher proton conductivity due to more continuous hydrophilic domains based on their morphological study using atomic force microscopy.

For the evaluation of new PEM materials at the early stage of their development, membranes are usually prepared based on a lab-scale batch casting method: dilute polymer solutions are cast onto glass plates through syringe-filters, with the solvent then being removed by means of evaporation using an oven or a heat lamp. The casting process is critical for a successful production of polymeric thin membranes because it has substantial influence on the microstructure and properties [Guttoff 1995]. Thus, it is essential to identify the effects of processing conditions and to utilize an appropriate processing technique.

In several previous studies the importance of PEM processing conditions has been reported. Kim et al. [2003] investigated the effects of thermal treatment on the final morphology and properties of partially sulfonated PAES membranes. Their results indicated that the proton conductivity and water uptake of the membranes acidified at 100 °C were higher than those of the membranes treated at 30 °C. Based on a morphological study using atomic force microscopy, they concluded that membrane treatment at 100 °C

enabled the formation of larger and more continuous hydrophilic domains owing to the plasticizer-like effect of water absorbed by the membranes. More recently, Bébin and Galiano [2006 a, b] examined the possibility of using melt-extrusion for the manufacture of sulfonated PEEK membranes with the help of suitable plasticizers. They observed that the melt-cast PEMs exhibited proton conductivity values that were one half of those of the solution-cast PEMs. Even though these previous studies strongly implied that processing conditions have substantial effects on the final properties of PEMs, the significance of material processing have not gained much attention so far. Large discrepancies in proton conductivity data among PEMs with similar composition presented in previous studies could be due to different processing conditions, as already pointed out by Robertson et al. [2003].

In the case of block copolymer systems for PEMs, processing conditions are anticipated to play a more dominant role in the formation of final morphology and, accordingly, final properties because of the basic principles for microstructure formation of block copolymers. However, the principles have been underestimated in the processing of block copolymer PEMs despite the general recognition of the fact that the aforementioned hydrocarbon-based PEM materials are a typical type of block copolymers consisting of two distinct blocks (e.g. sulfonated and unsulfonated ones). Recently, Huang et al. [2007] reported that the proton conductivity of a block copolymer significantly depended on film drying conditions, possibly such as drying temperature, initial solution concentration, and solvent removal rate, while they were exploring the possibility of manufacturing the PEM films by solvent-casting using a reverse-roll coating technique.

A variety of microstructures of block copolymers can be induced by microphase separation due to the phase behavior of block copolymers [Hamley 1998]. Khandpur et al. [1995] represented the phase behavior of styrene-isoprene (SI) diblock copolymers as a function of two parameters,  $\chi_{AB}N$  and  $f$ . Here,  $\chi_{AB}$  is the Flory-Huggins interaction parameter, which indicates the dissimilarity between different component blocks (A and B).  $N$  is the degree of polymerization, which is the number of statistical segments per chain, and  $f$  is the volume fraction of one component block. According to the diagram, when the product  $\chi_{AB}N$  is larger than a critical value,  $(\chi_{AB}N)_{ODT}$  (ODT = order-disorder transition) for a certain value of  $f$ , phase separation of the block copolymer occurs and a periodically ordered structure such as lamellae, gyroid, etc. develops on a microscale of approximately 5 to 500 nm. That is, once a block copolymer is synthesized,  $N$  and  $f$  are no longer variable, but  $\chi_{AB}$  can still be adjustable during processing because  $\chi_{AB}$  is inversely proportional to temperature, i.e.,  $\chi_{AB} = C_1 + C_2/T$ . Additionally, in a solution, the phase behavior of diblock copolymers is controlled by the interactions between the solvent and the two component blocks ( $\chi_{solv-A} = C_3 + C_4/T$  and  $\chi_{solv-B} = C_5 + C_6/T$ ) as well as the interaction between the two component blocks ( $\chi_{AB}$ ) [Hamley 2004]. These basic principles strongly imply that the processing temperature and solvent selectivity are vital processing conditions of block copolymers used to generate PEMs. Hanley et al. [2000] generated the phase diagrams of a styrene-isoprene (SI) diblock copolymer as a function of temperature and volume fraction in four different solvents with different degrees of selectivity. From the phase diagrams, it can be easily observed that the phase of a block copolymer significantly depended on solvent selectivity and temperature. They also

observed that the SI diblock copolymer in a more selective solvent had a greater tendency to form ordered structures.

Additionally, Huang et al. [2003] showed that the kinetics of phase separation of block copolymers was one of the crucial factors that decided the final morphology of solution-cast styrene-butadiene-styrene triblock and styrene-butadiene diblock copolymer films. Normal equilibrium cylindrical or spherical microstructures with polystyrene cylinders or spheres in polybutadiene matrices were obtained by drying the films for a prolonged time. However, drying of the films in an abridged time resulted in “kinetically frozen-in” inverted cylindrical or spherical microstructures, where polybutadiene cylinders or spheres were embedded in polystyrene matrices, because the polymer molecules had insufficient time to rearrange to the equilibrium microstructures.

Therefore, the primary objective of this study is to initially investigate the effects of solvent selectivity, film drying temperature, and solvent removal rate on the final microstructure and properties of PEMs from the viewpoint of microphase separation of block copolymers. For this study a statistically random PAES copolymer with 35 mol % disulfonation (BPSH35) as a control and three multiblock copolymers consisting of wholly disulfonated and unsulfonated PAES blocks (BPSH100 and BPS0, respectively) with three different lengths (for chemical structures, see Figure 3.1-1), which have proven to be promising PEM materials as reported in previous works, were prepared and utilized [Wang 2002, Lee 2008]. In order to assess the morphology developed during film drying, transmission electron microscopy (TEM) and small angle X-ray scattering (SAXS) were used.

## 3.2 Experimental

### 3.2.1 Synthesis and characterization of copolymers

BPSH35 random copolymer was synthesized by potassium carbonate mediated direct aromatic nucleophilic substitution polycondensation of disodium 3,3'-disulfonate-4,4'-dichlorodiphenylsulfone, 4,4'-dichlorodiphenylsulfone and 4,4'-biphenol as introduced by Wang et al. [2002]. BPSH100-BPS0 multiblock copolymers were prepared by a coupling reaction between phenoxide terminated disulfonated PAES (BPSH100) and decafluorobiphenyl end-capped unsulfonated PAES (BPS0). Details on the synthesis of the oligomers can be found elsewhere [Lee 2008]. Intrinsic viscosities (IV) were determined in NMP containing 0.05 M LiBr at 25 °C using an Ubbelohde viscometer and the ion exchange capacity (IEC) values of the copolymers were determined by titration with a standard NaOH solution. The measured values of IVs and IECs are presented in Table 3.2-1. The IV values of the copolymers were sufficiently high so that tough and ductile membranes could be produced. Compared with the BPSH35 random copolymer, the IEC values of the multiblock copolymers were slightly lower, but they were close to each other, ranging from 1.34 to 1.40 meq/g. The copolymers with similar IEC values were obtained by utilizing the BPSH100 and BPS0 blocks with equal block lengths (5, 10, and 15 kg/mol) with 1:1 stoichiometry.

### 3.2.2 Membrane preparation

The copolymers were dissolved in N-methylpyrrolidone (NMP) or dimethylacetamide (DMAC) by stirring at 60 °C overnight, finally producing to homogeneous 15 w/v % solutions. The solutions were filtered using 5 µm Teflon<sup>®</sup>

syringe filters. Then about 250  $\mu\text{m}$  thick wet films with an area of 3.5 cm  $\times$  8 cm were cast onto clean stainless steel substrates using a hand-casting knife. The wet films were dried using a batch convection drying apparatus constructed in our lab (see Figure 3.2-2). The velocity of the convection air was maintained at 0.2 m/s. The temperature of the convection air was varied between room temperature ( $\sim 20\text{ }^\circ\text{C}$ ) and  $80\text{ }^\circ\text{C}$ . Room temperature was the lowest temperature available without any supplementary equipment and  $80\text{ }^\circ\text{C}$  was the critical temperature, above which bubbling defects significantly occurred because of the high vapor pressure of the solvents. The temperature variation of the convection air above the wet films was below  $\pm 2\text{ }^\circ\text{C}$  during the drying process. The films were additionally dried overnight at  $110\text{ }^\circ\text{C}$  in vacuo to remove the residual solvent. Finally, about 25  $\mu\text{m}$  thick dry films were obtained. The resultant films were acidified by immersing in 0.5 M boiling sulfuric acid aqueous solution for 2 hr. To remove residual sulfuric acid in the films, the acidified films were immersed in boiling DI water for 2 hr.

### 3.2.3 Batch convection drying apparatus

Typically forced convection is used as a primary drying method in industry because of its advantages (e.g., costs, rate of drying) over conduction and radiation [Cohen 1992]. Convection air not only supplies the energy necessary for solvent evaporation but also facilitates the mass transport at the air-liquid interface by sweeping away solvent vapor. Thus, to generate film drying conditions at a semi-industrial level in the laboratory, a batch convection drying apparatus was designed and built by adopting the device used by Romdhane et al [2001]. A schematic of the device is presented in Figure 3.2-2. A flowmeter and two air heaters were employed for the control of air

velocity and temperature, respectively. The convection air passed through a rectangular aluminum duct. A stainless steel substrate was placed on a metal shaft connected to a balance through a passage on the bottom of the duct. A computer connected to the balance through an interface enabled recording the change in the weight of the wet films during the drying process and, consequently, calculation of total drying time and drying rate. A detachable glass window positioned right above the substrate allowed introduction of samples and visual observation during film drying.

#### 3.2.4 Proton conductivity measurement

Proton conductivity of the membrane was measured using a Solatron (1252A + 1287) Impedance/Gain-Phase Analyzer over the frequency range of 10 Hz – 1 MHz. The resistance of the membrane was measured at the frequency that generated the minimum imaginary response. Then proton conductivity of the membrane was determined from the resistance, the dimension of the cell, and thickness of the film [Zawodzinski, 1991]. For measurement of proton conductivity at 30 °C and fully hydrated conditions, membranes were equilibrated in DI water for 24 hr. In order to measure proton conductivity under partially hydrated conditions, membranes were equilibrated for 3 hr before the test in a humidity-temperature oven (ESPEC, SH-240) at relative humidity and temperature in interest.

#### 3.2.5 Water uptake measurement

Water uptake is the ratio of the weight of water absorbed by the membrane to the weight of the dry membrane. Water uptake was determined by measuring the weight of

the sample in dry and wet states ( $W_{dry}$  and  $W_{wet}$ , respectively) and, then, by use of the following equation:

$$Water\ uptake = \frac{W_{wet} - W_{dry}}{W_{dry}} \times 100 (\%) \quad (\text{Eq. 3.2-1})$$

For the measurement of  $W_{wet}$ , the sample was immersed in DI water for 24 hours at room temperature and blotted dry for weighing. Then the sample was dried in an oven at 120 °C for 30 min before weighing.

### 3.2.6 Determination of swelling ratio

The swelling ratios of membranes were determined by measuring the in-plane dimensions (x and y) and through-plane dimension (z) of the dry and wet membranes using a ruler and a thickness gauge with 1  $\mu$  resolution, respectively. The dry and wet membranes were prepared in the same method as for the water uptake measurement.

### 3.2.7 Transmission electron microscopy

The hydrogen ions were replaced with cesium ions by immersing the film samples in an aqueous solution with excessive amount of CsOH, which resulted in appropriate enhancement of electron density contrast. Then samples were embedded in epoxy and ultramicrotomed into about 70 nm thin pieces with a diamond knife. Transmission electron micrographs were attained by operating a Philips EM 420 Transmission Electron Microscope at an accelerating voltage of 100 kV.

### 3.2.8 Synchrotron small angle X-ray scattering

SAXS profiles were acquired at the Brookhaven National Laboratory on the Advanced Polymer Beamline (X27C) at the National Synchrotron Light Source. The wavelength of the X-ray beam was 1.366 Å and the sample-to-detector distance 1904.67 mm. Two-dimensional SAXS images were recorded using a Mar CCD camera with an intensity uncertainty on the order of 2% and analyzed using the POLAR software developed by Stony Brook Technology and Applied Research, Inc. All scattering intensities were corrected for transmission and background scatter due to air and Kapton windows and represented in arbitrary, relative intensity units as a function of the scattering vector,  $q$ , which is a function of the scattering angle through the following relationship,  $q = (4\pi / \lambda) \sin \theta$ , where  $\lambda$  is the wavelength of X-ray beam (1.366 Å) and  $\theta$  is half of the scattering angle ( $2\theta$ ).

## 3.3 Results and discussions

### 3.3.1 Film-casting and –drying

The characteristic drying curves of the BPSH100-BPS0 (15k-15k) multi-block copolymer films are presented as remaining amount of solvent vs. drying time in Figure 3.3-1. The drying curves showed a traditional film drying behavior. Initially, the drying rates remained almost constant as long as the rate of the solvent diffusion through the wet film was comparable with the rate of solvent evaporation at the surface of the wet films [Kim, S. 2001]. As the drying of the wet film proceeded, the concentration of the copolymer in the wet film increased and the diffusive transfer of solvent molecules was

limited by the polymer molecules. Hence, the film drying became controlled by diffusion of the solvent through the polymer film and the drying rate gradually decreased.

As expected, the drying rate and total drying time significantly depended on the solvent type and convection air temperature. The total drying time of the BPSH100-BPS0 (15k-15k) films is summarized in Table 3.3-1. For this estimation, time required to remove the residual solvent using a vacuum oven was not considered. Drying of the films cast with DMAC proceeded faster due to the higher vapor pressure of DMAC. For example, at 60 °C, the vapor pressure of DMAC (11.0 mm Hg) is about three times as high as that of NMP (3.7 mm Hg) [Smallwood 1996]. Thus, drying of the 15k DMAC film could be finished in one-third of the total drying time of the 15k NMP film. Likewise, film drying at higher temperatures considerably accelerated the drying process due to the elevated vapor pressure without regard to solvent type. The total drying time at 20 °C was longer than at 80 °C by more than an order of magnitude.

### 3.3.2 Determination of solvent selectivity

The degrees of solvent selectivity of NMP and DMAC for the component blocks (BPSH100 and BPS0) were determined by measuring the solubility of the wholly sulfonated BPSH100 (15k) and unsulfonated BPS0 (15k) blocks in each solvent. At room temperature (~ 20 °C), more than 30 g of the BPSH100 (15k) was readily dissolved in 100 ml of both NMP and DMAC. However, the solubility of the BPS0 is about 9 g in 100 ml of DMAC, while more than 30 g of the BPS0 was dissolved in NMP. That is, NMP and DMAC are good solvents for the BPSH100 but good and marginal, respectively, for the BPS0 at room temperature ( $\chi_{BPS0-DMAC} > \chi_{BPS0-NMP}$ ). However, at 80 °C, DMAC was

also a good solvent for the BPS0 so that more than 30 g of the BPS0 was dissolved in 100 ml of DMAC.

### 3.3.3 Properties of PEMs

Acronyms for the multiblock copolymer films will be used for convenience, henceforth, where ‘5k-NMP film’ implies the BPSH100-BPS0 (5k-5k) multiblock copolymer film cast with NMP. The resultant films were evaluated as PEMs by measuring the proton conductivity, water uptake, and swelling behavior in order to investigate the effects of solvent selectivity and film drying conditions as well as the block length of the multiblock copolymers.

Figure 3.3-2 presents the proton conductivities of the BPSH100-BPS0 multiblock copolymer films measured at 30 °C and fully hydrated conditions. It is obvious that the block copolymer system was more advantageous for proton conduction over the random copolymer, as already reported elsewhere [Lee 2008]. The proton conductivities of the multiblock copolymer films were comparable or higher than that of the BPSH35 random copolymer film despite the slightly lower IEC values. Also, the proton conductivity increased with increasing block length. The proton conductivities of the 15k films were significantly higher than those of the 5k films, while the 10k films were slightly higher than the 5k films. Solvent selectivity also turned out to be a crucial factor for the proton conductivity of the multiblock copolymer films. The proton conductivities of the multiblock copolymer films were considerably increased by simply using DMAC as a casting solvent, which is selective for the BPSH100 block, instead of NMP, a good solvent for both BPSH100 and BPS0 blocks. In the case of the 15k films, the proton

conductivities of the DMAC films were higher than those of the NMP films by almost 50 %.

Just as observed from the proton conductivity, significant effects of block length and solvent selectivity on the water uptake of the multiblock copolymer films were observed. Figure 3.3-3 represents the water uptake measurement results of the multiblock copolymer films. The water uptake also increased with increasing block length and utilization of DMAC also increased the water uptake of the multiblock copolymer films by the magnitudes comparable to the effects on the proton conductivity. However, it is noteworthy that the drying temperature had substantial effects on the water uptake, although no obvious effects of drying temperature were observed from the proton conductivity. Drying of the multiblock copolymer films at a lower temperature induced higher water uptake. All the DMAC films and 15k NMP films showed this trend, while the water uptake of the 5k and 10k NMP films still did not show obvious dependence on the drying temperature. The effect of drying temperature was most severe for the 15k DMAC films; drying at 20 °C caused more than twice the increase in the water uptake of the film, compared with drying at 80 °C. In general, the proton conductivity increased with increasing water uptake, because both proton conductivity and water uptake depend on the ion contents and degree of aggregation [Wang 2002, Kim 2003]. However, this result is not in agreement with the proton conductivity result, which showed no significant dependence on the drying temperature. The 15k DMAC films dried at 20 °C and 80 °C produced comparable proton conductivities despite the huge difference in their water uptake.

This discrepancy can be explained by investigating the swelling behavior of the multiblock copolymer films. The swelling behavior of the 15k DMAC films, of which water uptake showed the highest degree of dependence on the drying temperature, is presented in Figure 3.3-4. As opposed to the BPSH35 random copolymer films, the 15k DMAC films showed anisotropic swelling behaviors. The through-plane swelling of the 15k DMAC films was much larger than the in-plane swelling. This anisotropic swelling behavior of the 15k DMAC films may be a macroscopic indication of the formation of ordered microstructures of the multiblock copolymer films [Lee 2008]. As well, it is clearly shown that the through-plane swelling of the 15k DMAC films significantly depended on the drying temperature, while the in-plane swelling showed no obvious dependence. Drying of the film at a higher temperature significantly decreased the thorough-plane swelling. The through-plane swelling of the 15k DMAC film dried at 20 °C was larger than that of the 15k DMAC film dried at 80 °C to the extent comparable to the increase in the water uptake. Definitely, this difference in the swelling of the multiblock copolymer films led to the difference in the volume of the films in a wet state and, consequently, in the number of proton-conducting moieties per unit volume of the films. Thus, the IEC values per unit volume of the wet films were estimated. This estimation was conducted for the 4 multiblock copolymers, of which water uptake showed a dependence on the drying temperature (5, 10, and 15k DMAC films and 15k NMP films). For this estimation, it was assumed that the density of the copolymers was 1.29 g/cm<sup>3</sup>, which is the density of a PAES commercially referred to as RADEL-R by Solvay Advanced Polymers [Design Guide 2004]. Figure 3.3-5 displays the estimated the volume-based IEC values of the wet multiblock copolymer films dried at different

temperatures. Generally, the multiblock copolymer films dried at lower temperatures had higher volume-based IEC values. This trend was more obvious for the multiblock copolymer film that showed greater drying-temperature-dependence in the water uptake measurement. This indicates that, as expected, the number of the proton-conducting moieties in unit volume decreased as much as the volume of the multiblock copolymer films increased. Therefore, it can be concluded that the loosened connectivity of the proton-conducting moieties caused by the excessive swelling resulted in comparable proton conductivities of the multiblock copolymer films with higher water uptake.

Figure 3.3-5 also depicts that the block copolymer system is highly desirable for improved proton conduction. The volume-based IEC values of the multiblock copolymers, except the 5k films, were significantly lower than that of the BPSH35 random copolymer, but the multiblock copolymer films produced higher proton conductivities. Furthermore, it can also be confirmed that the multiblock copolymer consisting of longer blocks is more effective for proton conduction. Even with lower or similar volume-based IEC values, the proton conductivities of the 15k films were considerably higher than any other copolymer film.

It can also be concluded that the properties of the multiblock copolymers consisting of longer component blocks are more responsive to the variations in the processing conditions from the following observations. In the first place, the magnitude of the solvent selectivity effects on the proton conductivity and water uptake of the 15k films was greater than that on the 5k and 10k films. For example, the utilization of DMAC increased the proton conductivity of the 15k film by almost 50 %, while only 20 to 25 % increase was observed for the proton conductivities of the 5k and 10k films.

Secondly, the effects of the drying temperature on the water uptake of the 15k DMAC films were significant, but the water uptake of the 5k and 10k DMAC films showed mild dependence on the drying temperature. Lastly, the water uptake of only the 15k NMP films varied with the drying temperature, while the water uptake of the 5k and 10k NMP films showed no dependence on the drying temperature. The BPSH35 random copolymer film showed no variations in the properties because significant differences in its morphology cannot be induced because of the short sequence length of the sulfonated monomers [Noshay 1977]. This result is considered to be supporting for the fact that the properties of the multiblock copolymers consisting of longer component blocks are more responsive to the processing conditions.

#### 3.3.4 Morphology of PEMs

The microstructures of the resultant films were investigated using TEM. The TEM micrographs of the copolymer films cast with NMP and dried at 20 °C are presented in Figure 3.3-6. The unsulfonated BPS0 block domains appear brighter in the micrographs, while the sulfonated BPSH100 block domains appear darker due to the cesium ions replaced with the hydrogen ions to enhance the contrast between the sulfonated and unsulfonated blocks. As shown in Figure 3.3-6 (a), the BPSH35 random copolymer film had no evident phase separation between the sulfonated and unsulfonated blocks. Because of the random sequence of the sulfonated monomers in the backbone, the BPSH35 random copolymer film had the sulfonated monomer scattered over the film instead of developing any noticeable well-defined ionic domains. On the other hand, it can be observed from Figure 3.3-6 (b) ~ (d) that the multiblock copolymer films

developed well-defined ionic domains via the phase separation between the sulfonated and unsulfonated blocks. These TEM micrographs also show the effects of the block length on the microstructure. As the block length increased from 5 to 15 kg/mol, the multiblock copolymer films developed more continuous and wider ionic domains. As discussed earlier, the proton conductivity and water uptake increased with increasing block length. Thus, the effects of block length on the proton conductivity and water uptake can be ascribed to the continuity and size of the ionic domains.

The effects of solvent selectivity and drying temperature on the final microstructures were also investigated using TEM micrographs. The comparison of the micrographs of the 15k NMP and 15k DMAC films (Figure 3.3-7 (a) and (c)) depicts the effects of solvent selectivity. While the 15k NMP film formed a “zebra-like” stripe pattern microstructure, the 15k DMAC film had a totally different microstructure, in which much larger ionic domains were embedded in an unsulfonated block matrix. It is believed that the selective nature of DMAC enabled the formation of much larger ionic domains in the 15k DMAC film ( $\chi_{\text{BPS0-DMAC}} > \chi_{\text{BPS0-NMP}}$ ), resulting in higher water uptake and proton conductivity of the DMAC films.

The effects of drying temperature can be observed from the comparison of the two pairs of micrographs, (a) and (b), & (c) and (d) in Figure 3.3-7. The films dried at 80 °C ((b) and (d)) showed similar morphologies as the equivalent ones dried at 20 °C ((a) and (c)). However, the 15k NMP film dried at 80 °C showed somewhat thinner ionic domains with less continuity and the 15k DMAC film dried at 80 °C had smaller ionic domains embedded in an unsulfonated block matrix. This drying temperature effects can be explained by two possible reasons. First, the changes in the thermodynamic features of

the polymer solution systems might cause the differences in the microstructures of the 15k films. The interaction parameter, which indicates the dissimilarity between the two chemical species, is inversely proportional to temperature (i.e.,  $\chi_{AB} = C_1 + C_2/T$ ). As the temperature increases, the incompatibility between the species diminishes. Thus, the decreased incompatibility at higher temperatures might hinder the phase separation between the sulfonated and unsulfonated blocks. The second possible reason is the kinetics of phase separation. As previously described, the total drying time significantly depended on the temperature of convection air. Drying temperatures of 20 and 80 °C led to a huge difference in the total drying time by more than an order of magnitude. The total drying time at 80 °C might be too short for the multiblock copolymers to complete the phase separation. That is, the microstructures of the films dried at 80 °C might be obtained by kinetic suppression in the middle of the phase separation processes. Because both the 15k NMP and DMAC films dried at 20 °C had microstructures with more continuous and larger ionic domains, their water uptake was higher as compared with the films dried at 80 °C. However, this water uptake increase finally led to the reduction in the volume-based IEC values, offsetting the microstructural advantages for proton conduction.

SAXS is known to be a good tool for investigating the microstructures of block copolymers because small-angle scattering provides the information on the microstructure by probing the entire volume of the sample while TEM gives direct images over a small area of the sample [Hamley 2004]. A morphological study using SAXS was conducted to obtain more information on the microstructures of the BPSH100-BPS0 multiblock copolymers. Figure 3.3-8 presents the scattering profiles of

the BPSH100-BPS0 multiblock copolymer films cast with NMP and dried at 20 °C. The scattering profile of each multiblock copolymer showed one characteristic peak, while no characteristic peak was observed from the scattering profile of the BPSH35 random copolymer. The formation of the peaks can be attributed entirely to the characteristic dimensions within the ionic domains of the multiblock copolymers because the backbone of the BPSH100-BPS0 multiblock copolymer, poly(arylene ether sulfone), is an amorphous polymer. In contrary, Nafion yields two characteristic peaks due to the characteristic dimensions of the ionic domains and the crystallites of the polytetrafluoroethylene-like Nafion backbone [Mauritz 2004]. The SAXS scattering profiles confirmed that a more ordered well-defined morphology was obtained from the multiblock copolymers consisting of longer blocks. As shown in Figure 3.3-8, the characteristic peak systematically shifted to lower  $q$  with increasing block length, becoming sharper. Sharpening of the characteristic peak means that the characteristic dimensions of the ionic domains are distributed in a narrow range, suggesting a well-defined morphology. Another indication of the well-defined morphologies of the 10k and 15k films can be found from the SAXS scattering profiles. In general, the scattering profile of a well-defined morphology has a convex, referred as “2<sup>nd</sup> order peak”, at  $q = 2q_{\max}$  [Spiro 2006, Young 2009]. These 2<sup>nd</sup> order peaks were found at  $q = 2q_{\max}$  on the scattering profiles of the 10k and 15k films.

The SAXS profiles were also utilized to estimate the distance between the ionic domains using Bragg’s law;

$$D_{\text{Bragg}} = \frac{2\pi}{q_{\max}}$$

Here,  $q_{\max}$  is the value of  $q$ , at which the characteristic peak (scattering maximum) is located, and  $D_{\text{Bragg}}$  is Bragg spacing that corresponds to the distance between ionic domains in this study. The estimated values of the interionic distance using Bragg's law are compared in Figure 3.3-9 with the values obtained by analyzing the TEM micrographs (Figure 3.3-6 (b) ~ (d)). The TEM micrograph analysis was conducted by manually measuring the distance between the centers of two parallel ionic domains. The estimated values of the inter-ionic distance for the 5k film was close, but the TEM micrograph analysis yielded somewhat lower values for the 10k and 15k films. However, the two different estimations showed a qualitative agreement, the inter-ionic distance increasing with the block length.

### 3.4 Conclusions

The effects of solvent selectivity, drying temperature, and solvent removal rate on the final microstructures and properties of disulfonated poly(arylene ether sulfone) multiblock copolymer (BPSH100-BPS0) films for PEMs were investigated based on the basic principles of microstructure formation of block copolymers. The variations in the properties and microstructure of the multiblock copolymer films were induced by altering the degree of solvent selectivity. Utilization of a selective solvent, DMAC, yielded the microstructures with larger ionic domains, resulting in higher proton conductivity and water uptake. Drying of the films at lower temperatures resulted in the formation of more continuous and larger ionic domains. However, the formation of larger ionic domains led to the offset of the proton conductivity by the film swelling and subsequent reduction in

the volume-based IEC values. The formation of the smaller ionic domains with less continuity observed in the films dried at higher temperatures might be caused by decreased incompatibility among the chemical species and/or by kinetic suppression of the phase separation process. Additionally, this study reconfirmed the effects of block length by using the volume-based IEC value analysis and SAXS technique. Our results suggest that 10 ~ 15 kg/mol should be the optimal block length and that casting with the selective solvent, DMAC, followed by film drying at the temperature range between 60 and 80 °C should be the optimal processing conditions, which leads to improved proton conductivity, preventing excessive water uptake.

#### \* Acknowledgement

The authors wish to thank the U.S. Department of Energy for their support of this study (Grant No. DE-FG36-06G016038).

#### 3.5 References

- [1] Sopian K, Wan Daud WR, Renewable Energy 2006;31:719.
- [2] Rozière J, Jones DJ, Annual Review of Materials Research 2003; 33:503.
- [3] Mauritz KA, Moore RB, Chemical Reviews 2004;104:4587.
- [4] Kim YS, Dong L, Hickner MA, Glass TE, Webb V, McGrath JE, Macromolecules 2003;36:6281.
- [5] Savadogo O, Journal of Power Sources 2004;127:135.
- [6] Devanathan R, Energy & Environmental Science 2008;1:101.
- [7] Hickner MA, Ghassemi, H, Kim, YS, Einsla, BR, McGrath, J E, Chemical Reviews 2004;104:4587.
- [8] Kim YS, Wang F., Hickner M, McCartney S, Hong YT, Harrison W, Zawodzinski

- TA, McGrath JE, *Journal of Polymer Science: Part B: Polymer Physics* 2003;41:2816.
- [9] Kreuer KD, *Journal of Membrane Science* 2001;185: 29.
- [10] Hamley IW, *The Physics of Block Copolymers*, Oxford; New York: Oxford University Press, 1998.
- [11] Lee HS, Roy A, Lane O, Dunn S, McGrath, JE, *Polymer* 2008;49:715.
- [12] Lee HS, Roy A, Lane O, McGrath JE, *Polymer* 2008;29:5387.
- [13] Lee HS, Badami A, Roy A, McGrath JE, *Journal of Polymer Science, Part B: Polymer Physics* 2007;45:4879.
- [14] Zhao C, Lin H, Shao K, Le X, Ni H, Wang Z, Na H, *Journal of Power Sources* 2006;162:1003.
- [15] Wang H, Badami A, Roy A, McGrath JE, *Journal of Polymer Science, Part A: Polymer Chemistry* 2006;45:284.
- [16] Ghassemi H, Ndip G, McGrath JE, *Polymer* 2004;45:5855.
- [17] E.B. Gutoff and E.D. Cohen, *Coating and Drying Defects – Troubleshooting Operating Problems*, John Wiley & Sons, Inc., New York, 1995.
- [18] Bébin P, Galiano H, *Advances in Polymer Technology* 2006;25:121.
- [19] Bébin P, Galiano H, *Advances in Polymer Technology* 2006;25:127.
- [20] Robertson GP, Mikhailenko SD, Wang K, Xing P, Guiver MD, Kaliaguine S, *Journal of Membrane Science* 2003;219:113.
- [21] Khandpur AK, Förster S, Bates FS, Hamley IW, Ryan AJ, Bras W, Almdal K, Mortensen K, *Macromolecules* 1995;28:8796.
- [22] Hamley, I. W., *Introduction to Block Copolymers*, Edited by Hamley, I. W., *Developments in Block Copolymer Science and Technology*, John Wiley & Sons, Ltd., 2004.
- [23] Hanley KJ, Lodge TP, Huang CI, *Macromolecules* 2000;33:5918.
- [24] Wang F, Hickner M, Kim YS, Zawodzinski TA, McGrath JE, *Journal of Membrane Science* 2002;197: 231.

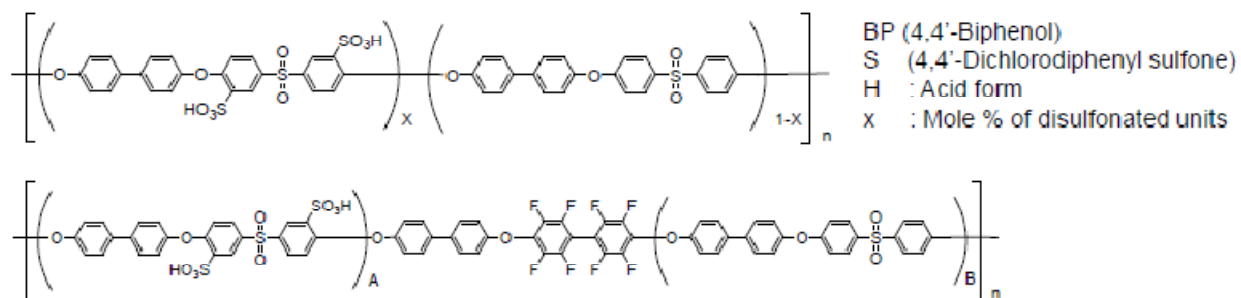


Figure 3.1-1. Chemical structures of BPSH35 random (top) and BPSH100-BPS0 multi-block (bottom) copolymer.

Table 3.2-1. Copolymer characteristics.

Copolymer	IV [dL/g]	IEC [meq/g]
BPSH35	0.74	1.51
BPSH100-BPS0 (5k-5k)	1.01	1.39
BPSH100-BPS0 (10k-10k)	0.89	1.34
BPSH100-BPS0 (15k-15k)	0.94	1.40

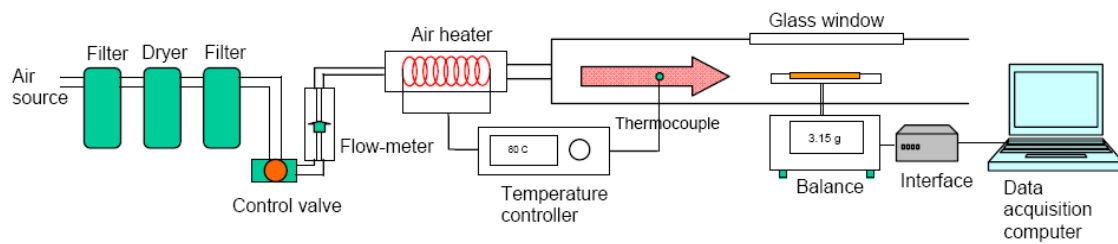
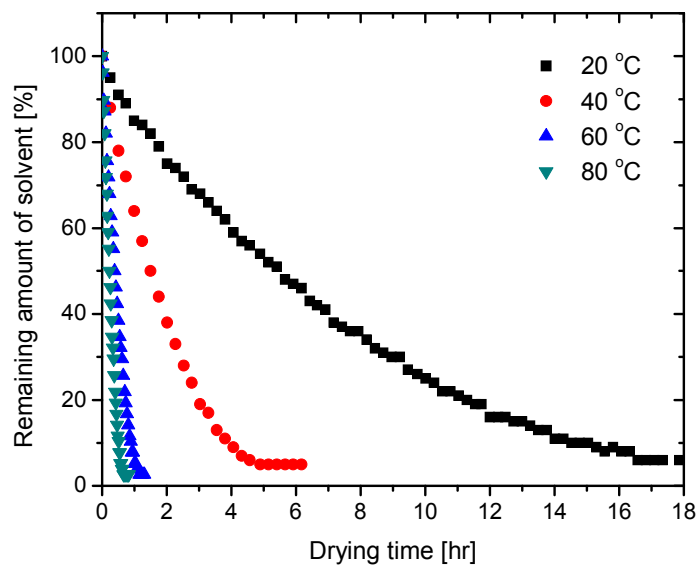


Figure 3.2-2. Schematic of batch convection drying apparatus.

(a) NMP



(b) DMAC

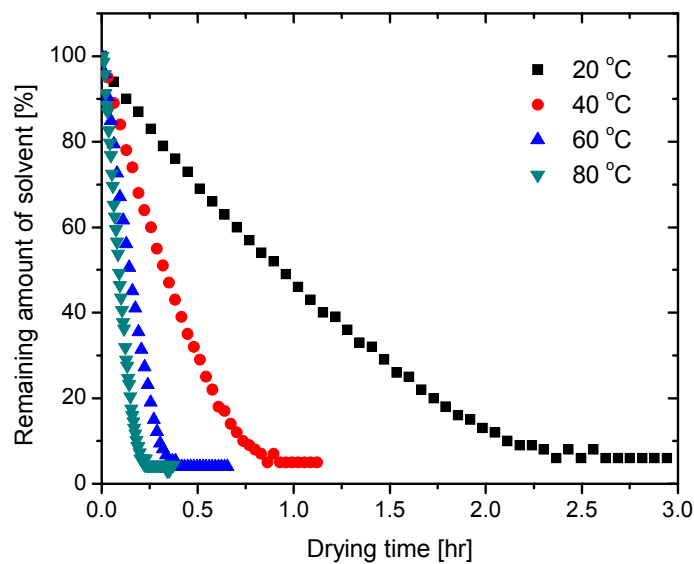


Figure 3.3-1. Characteristic drying curves of the BPSH100-BPS0 (15k-15k) multiblock copolymer films dried by convection air at 0.2 m/s.

Table 3.3-1. Total drying time of the BPSH100-BPS0 (15k-15k) multiblock copolymer films.

Convection air temp. [°C]	Total drying time [hr]	
	NMP	DMAC
20	16.5	2.4
40	4.9	0.9
60	1.2	0.4
80	0.7	0.2

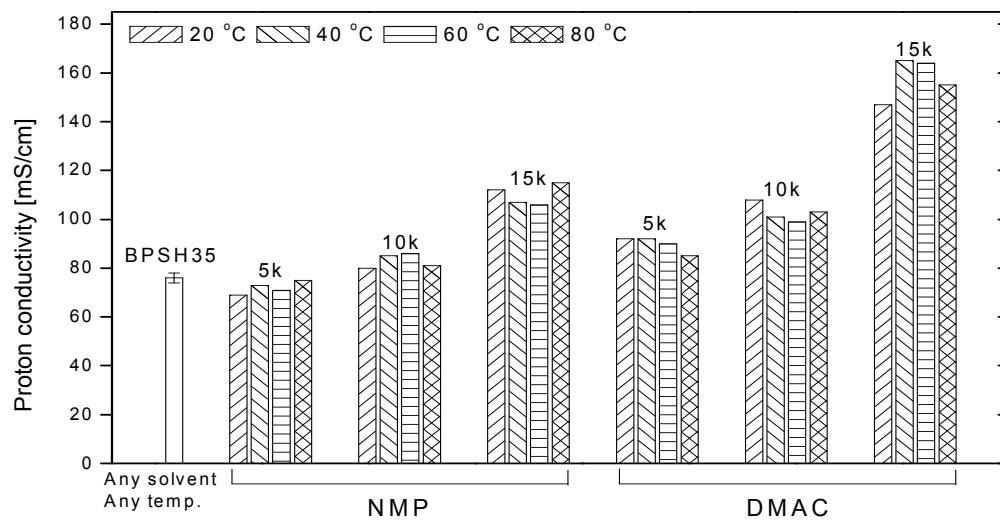


Figure 3.3-2. Effects of block length and solvent type on proton conductivity of the BPSH100-BPS0 multiblock copolymer films (measured at 30 °C and fully hydrated conditions).

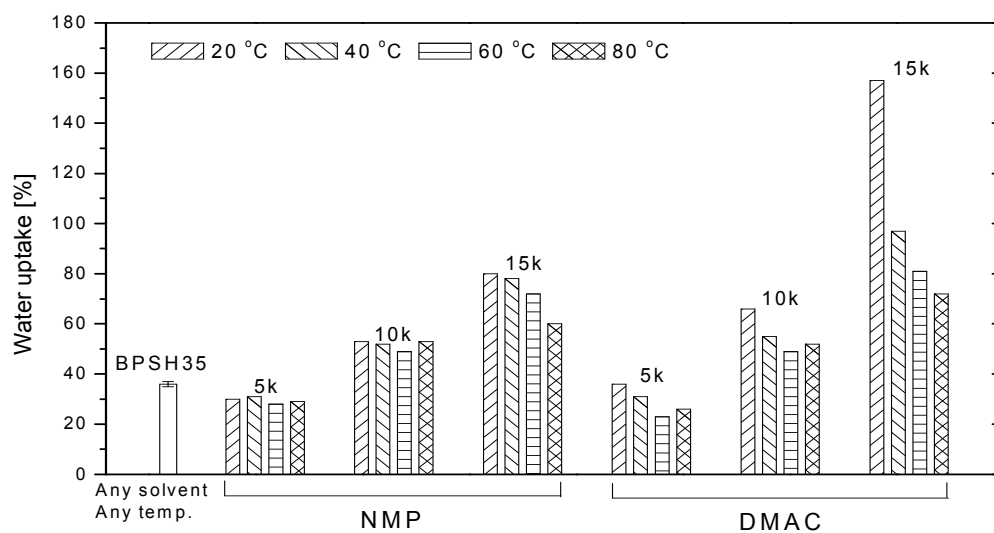


Figure 3.3-3. Effects of block length and casting conditions on water uptake of the BPSH100-BPS0 multiblock copolymer films (measured at 20 °C).

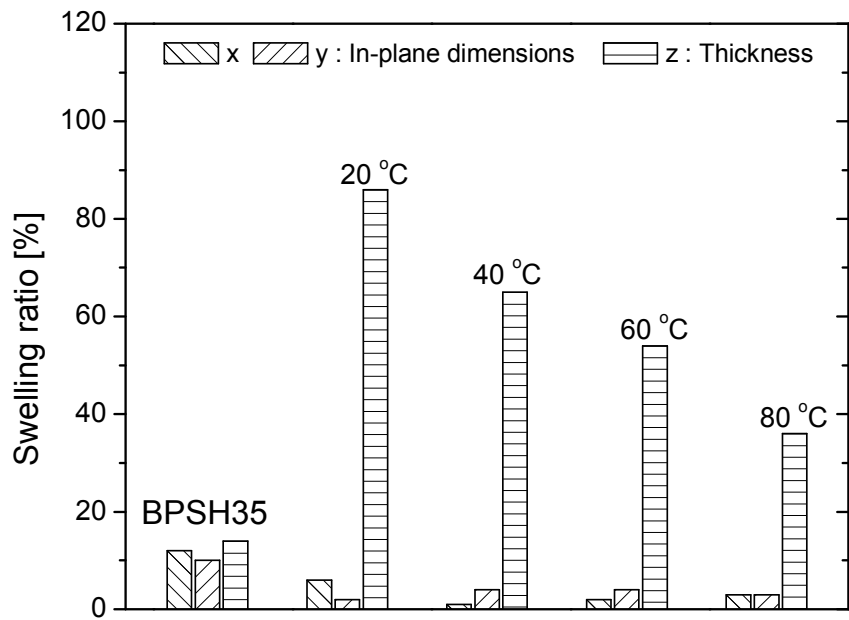


Figure 3.3-4. Swelling behavior of the BPSH100-BPS0 (15k-15k) copolymer films cast with DMAC as a function of drying temperature.

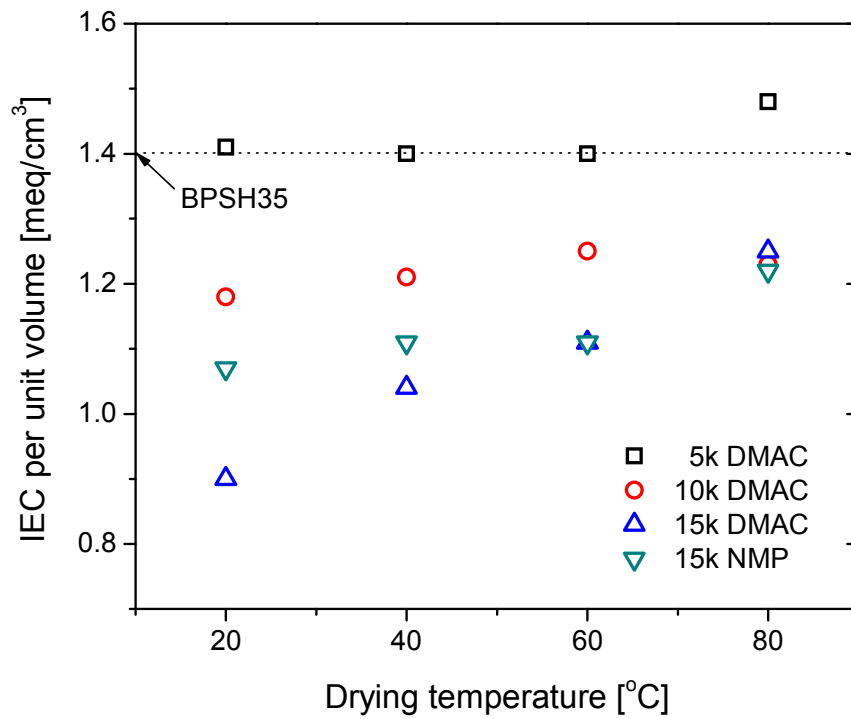
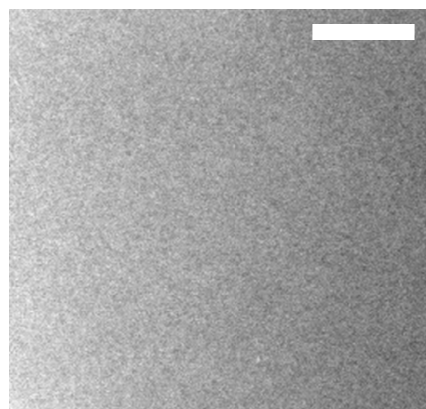
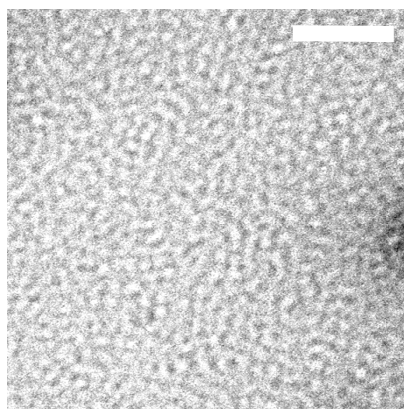


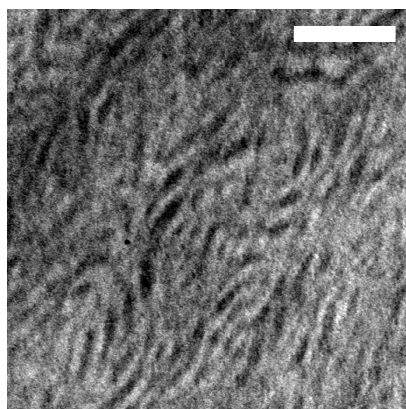
Figure 3.3-5. Estimated volume-based IEC values of the multiblock copolymer films in a wet state.



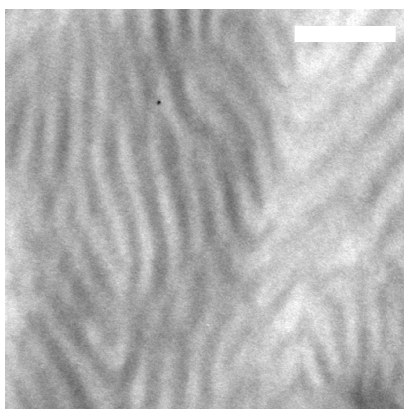
(a) BPSH35



(b) BPSH100-BPSO (5k-5k)



(c) BPSH100-BPSO (10k-10k)



(d) BPSH100-BPSO (15k-15k)

Figure 3.3-6. TEM micrographs of the copolymer films cast with NMP and dried at 20 °C. Length of scale bar = 100 nm.

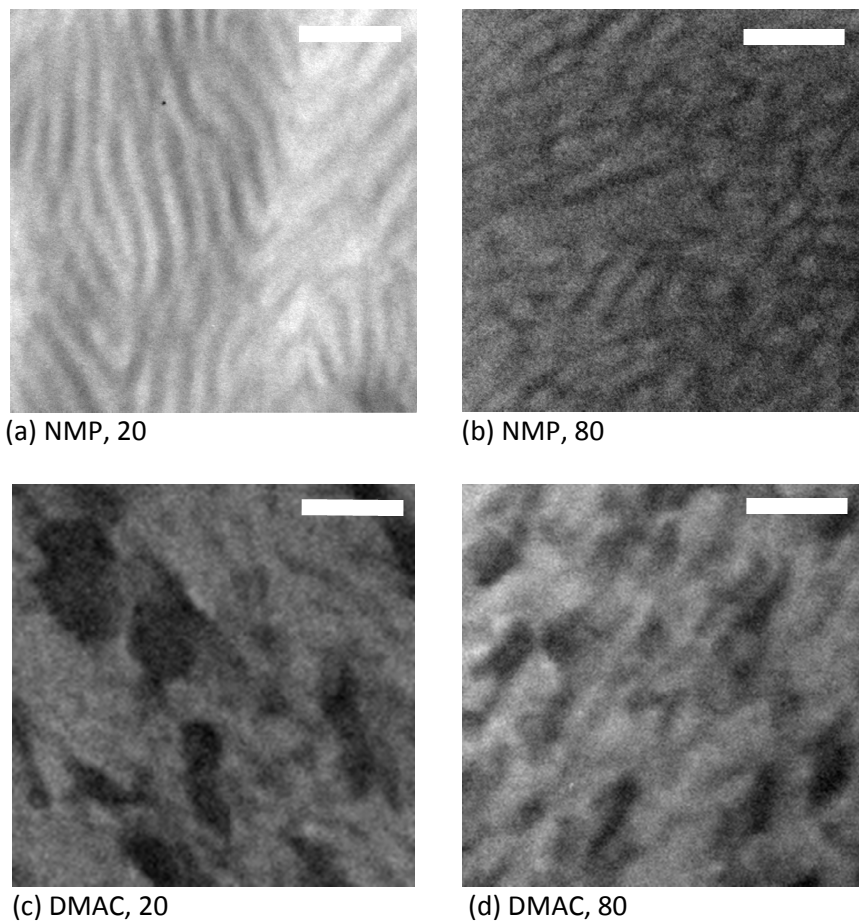


Figure 3.3-7. TEM micrographs of the BPSH100-BPS0 (15k-15k) multiblock copolymer films (solvent type, drying temp. [°C]). Length of scale bar = 100 nm.

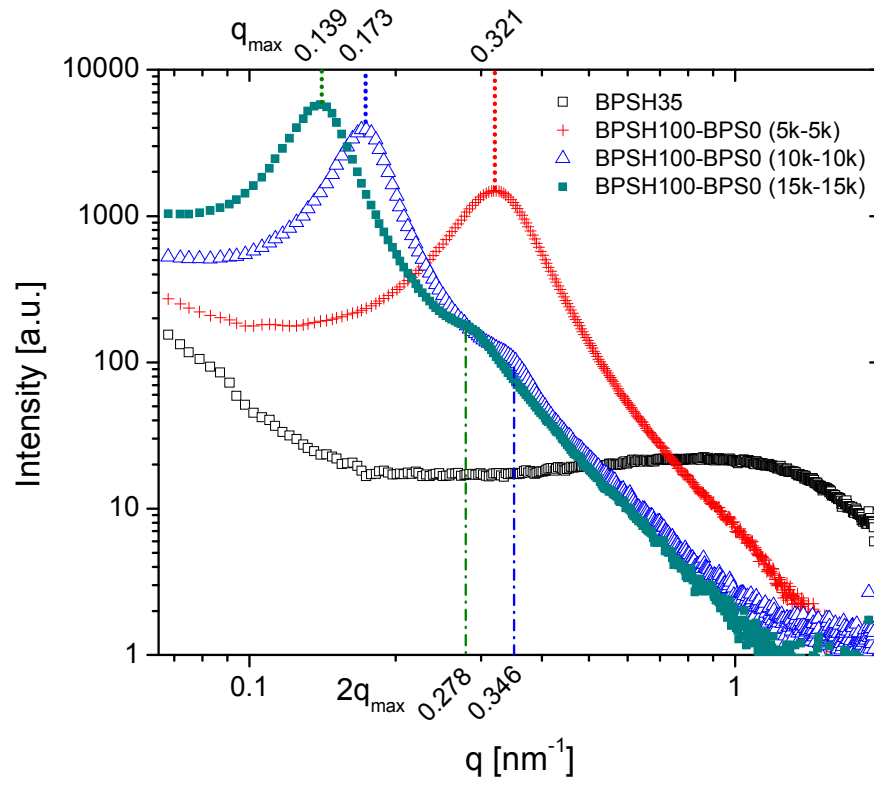


Figure 3.3-8. SAXS profiles of the BPSH100-BPS0 multiblock copolymer films cast with NMP and dried at 20 °C.

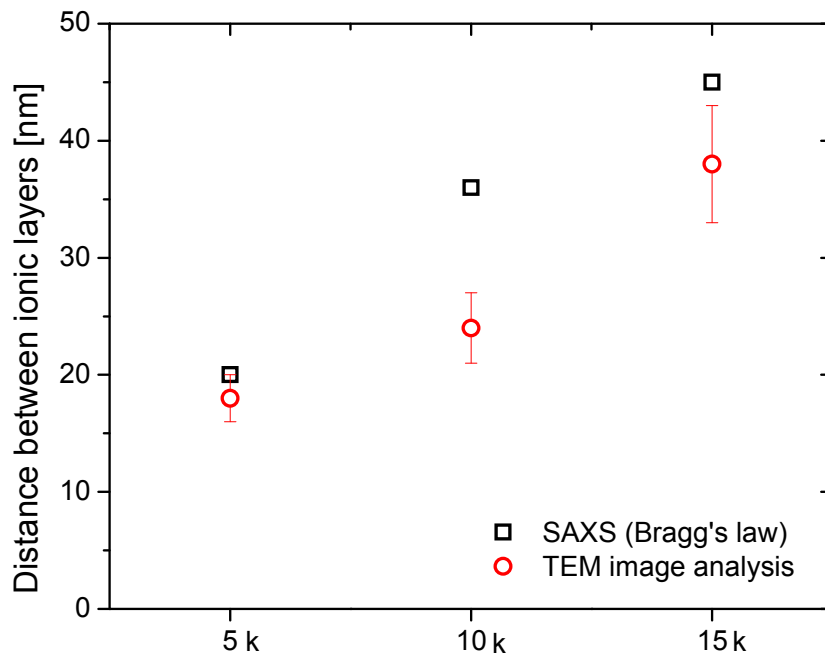


Figure 3.3-9. Comparison of the distance between the ionic domains estimated from the SAXS profiles and TEM images of the BPSH100-BPS0 multiblock copolymer films cast with NMP and dried at 20 °C.

## CHAPTER 4

### STUDY ON THE PHASE TRANSFORMATION AND KINETICS OF BLOCK COPOLYMERS IN SOLUTION-CAST FILMS VIA RHEOLOGICAL PROPERTY MEASUREMENTS

#### 4.1. Introduction

Block copolymers are long-chain molecules consisting of two or more types of monomers that are grouped together in blocks [Hamley 2004]. The different component blocks are usually incompatible with each other and, thus, demix into domains in which a single component block is dominant. The size of the domains cannot exceed a typical block length because the blocks are covalently linked to each other at their ends. Due to this limitation of the domain size, the demixing process and separated region are called *microphase separation* and *microdomain*, respectively [Krausch 2002]. For example, thermoplastic elastomers are block copolymers that contain a rubbery matrix (often polybutadiene or polyisoprene) and glassy hard domains (usually polystyrene). This block copolymer can be molded at high temperatures owing to the presence of the glassy domains, whereas the rubbery matrix provides elasticity at ambient conditions.

Studies on the phase behavior of block copolymers were initially focused on mapping the phase diagram of a diblock copolymer as a function of degree of segregation ( $\chi N$ ) vs. volume fraction of one component block ( $f$ ). Here,  $\chi$  is the Flory-Huggins interaction parameter, which indicates the dissimilarity between different component

blocks.  $N$  is the degree of polymerization, which is the number of statistical segments per chain, and  $f$  is the volume fraction of one component block [Hamley 1999]. When the product  $\chi N$  is larger than a critical value,  $(\chi N)_{ODT}$  (ODT = order-disorder transition) for a certain value of  $f$ , phase separation of the block copolymer occurs and a periodically ordered structure such as lamellae, gyroid, etc. develops in a microscale of approximately 5 to 500 nm. The phase behavior of triblock copolymers and diblock copolymers in solutions is much more complex than diblock copolymers. So far, more than 30 morphologies of triblock copolymers have experimentally been identified with no obvious limit in the number of morphologies. In the case of the phase behavior of block copolymers in solutions, the phase diagrams of only a few block copolymers such as polystyrene-polyisoprene (SI) and polyoxyethylene-polyoxypropylene have been generated. Multiple interaction parameters resulting from the introduction of a distinct third component has thwarted the theoretical prediction of the phase behavior of ternary systems. [Hamley 2004].

Non-equilibrium phase behavior has also gained attention because of its inherent scientific value and numerous potential technological applications [Bockstaller 2001]. The ordering transformation and kinetics of various block copolymers have been widely characterized by observing the evolution of given experimental parameters such as rheological properties and scattering patterns. For example, Floudas et al. [1994a] monitored the evolution of ( $G'$  and  $G''$ ) of styrene-isoprene block copolymers during the structural evolution from the disordered to the ordered phase induced by thermally quenching the copolymer through an order-disorder transition (ODT) temperature. The evolution shape of  $G'$  and  $G''$  was used to analyze the kinetics of structure ordering. Some

typical evolutions of  $G'$  and  $G''$  are presented in Figure 4.1-1. Both  $G'$  and  $G''$  showed a sigmoidal shape with apparent plateaus before and after the upward change. During the course of ordering, the block copolymer was considered to be a composite material consisting of disordered and ordered phases. The proportion of the two phases also changes, inducing the observed changes in the mechanical properties. Floudas et al. [1994a] used the simplest 'series' and 'parallel' mechanical models, which provide the limits for the mechanical response of a two-phase system as a function of the properties of the constituent components and the composition, in order to investigate the time-dependence of the volume fractions of the constituent phases, and finally to analyze the ordering kinetics based on a nucleation and growth mechanism. The series and parallel models are:

$$\frac{1}{G(t)} = \frac{1-\phi(t)}{G_0} + \frac{\phi(t)}{G_\infty} \quad (\text{Eq. 4.1-1})$$

$$G(t) = (1-\phi(t))G_0 + \phi(t)G_\infty \quad (\text{Eq. 4.1-2})$$

, respectively. Here,  $G(t) (= \sqrt{G'^2(t) + G''^2(t)})$  is the absolute value of the complex modulus,  $\phi(t)$  is the fraction of the ordered phase, and  $G_0$  and  $G_\infty$  are the moduli of the completely disordered and ordered phases at the initial and final stages, respectively. Then, the dimensional and kinetics information on the phase transformation was obtained by fitting the  $\phi(t)$  vs. time data into the Avrami equation,

$$\log(-\log(1-\phi(t))) = n \log t + \log z \quad (\text{Eq. 4.1-3})$$

where the Avrami exponent,  $n$ , and the logarithm of the rate constant,  $z$ , are the slope and y-intercept, respectively [Avrami 1939, 1940, 1941].

Recently, the ordering kinetics of block copolymers in solutions was also characterized by the Lodge group [Hanley 2000, Chastek 2004]. Hanley et al. [2000] empirically showed that the phase behavior of a styrene-isoprene (SI) diblock copolymer strongly depended on temperature, solvent selectivity, and solution concentration by generating the phase diagrams of the SI diblock copolymer in four different solvents with different degree of selectivity for each block using small-angle X-ray scattering (SAXS), static birefringence, and dynamic light scattering. They also reported that the SI diblock copolymer had a stronger tendency to form ordered structures in a more selective solvent. Then, the ordering kinetics of the cylinder phase of the SI diblock copolymer in di-n-butyl phthalate induced by thermal quenching was investigated using polarizing optical microscopy (POM) [Chastek 2004]. Not only were dimensional and kinetics information obtained in such a way as Floudas and coworkers [1994a], but also detailed information such as grain growth velocity was obtained.

Additionally, Huang et al. [2003] showed that the kinetics of phase transformation of block copolymers was one of the crucial factors that decided the final morphology of solution-cast styrene-butadiene-styrene triblock and styrene-butadiene diblock copolymer films. Normal equilibrium cylindrical or spherical microstructures with polystyrene cylinders or spheres in polybutadiene matrices were obtained by drying the films for a prolonged time. However, drying of the films in an abridged time resulted in “kinetically

frozen-in” inverted cylindrical or spherical microstructures, where polybutadiene cylinders or spheres were embedded in polystyrene matrices.

It has also been presented that the phase transformation and kinetics of block copolymer melts and block copolymers in solutions have been steadily investigated using a variety of techniques such as rheology, scattering, POM, etc. On the other hand, to the knowledge of the author, studies on the phase transformation and kinetics of block copolymers in solution in processing such as film drying are very rare. Because the number of practical applications of block copolymer products manufactured by solvent-casting has considerably increased, the study of the phase transformation and kinetics of block copolymers in solution is of practical interest for the design and operation of the solvent removal process. It is expected that rheology will be better at probing phase transformations of block copolymers in solution than scattering techniques because the change in the viscoelasticity of block copolymers during phase transformation is usually more observable than that of the intensity peak in scattering profiles [Hadjichristidis 2003]. Moreover, the accessibility of the scattering equipment, of which intensity is high enough for real-time detection of phase transformation of block copolymer, is very limited. Thus, in this study, a measurement scheme of rheological properties ( $G'$  and  $G''$ ) of solution-cast films was developed and the possibility of using the rheological technique for monitoring the phase transformation and kinetics of block copolymer in solution-cast films was explored.

## 4.2 Materials and experiment

### 4.2.1. Materials

Styrene-block-butadiene-block-styrene (SBS triblock) copolymer and toluene were purchased from Sigma-Aldrich, Inc. and used as received. The detailed information about the block copolymer is summarized in Table 4.2-1 and the physical properties of toluene pertaining to this study are given in Table 4.2-2.

### 4.2.2 Experiments

In this thesis work, a Rheometrics Mechanical Spectrometer (RMS-800) (Rheometrics, Inc., Piscataway, New Jersey) was used for the rheological measurements of the test materials. Details on the components and operation principles of the RMS-800 are presented in the user manual [Manual]. In this section, a brief discussion pertinent to this study is represented, with a focus on the modified parallel-plate rheometry and the overall experimental scheme developed for this study.

#### 4.2.2.1 Design of the modified parallel-plate rheometry

Solvent evaporation is a potential issue for rheological property measurements of polymer solutions. This is especially true when volatile solvents are used, because the concentrations and, subsequently, properties of test samples may drastically vary during the course of sample loading and/or testing due to solvent evaporation at the measurement conditions. In this thesis work, toluene, of which vapor pressure (21.8 mm Hg) at room temperature (20 °C) is somewhat higher than that of water (17.5 mmHg) [Smallwood 1996], was used as a solvent for the SBS copolymer. Thus, in order to solve

the potential issue of solvent evaporation, a set of modified parallel-plate rheometer fixtures was designed by adapting a solvent-evaporation-prevention accessory design for the AR Series Rheometers (TA Instruments, New Castle, DE). The design of the fixtures is in Figure 4.2-1. The bottom plate is equipped with a small lip around the rim to allow the polymer solutions to be poured onto the plates and to contain the polymer solutions during the measurements. The sleeve with a solvent trough can be installed around a mounting adapter or a 25 mm regular top plate. The use of the mounting adapter and detachable plates allows rheological measurements with a variety of plate fixtures with different diameters smaller than 44 mm. Two pieces of the covering part are assembled on the bottom plate using four screws after setting the gap. As shown in Figure 4.2-1 (b), the combination of the fixtures can provide an airtight environment for the test samples.

#### 4.2.2.2 Gap-setting procedure with the modified parallel-plate device

The traditional gap-setting procedure established by the manufacturer for the RMS-800 requires that the **gap indicator** should be fixed at a certain suitable position, allowing the exact monitoring of the position change of the top rheometer plate and, eventually, the precise measurement of the gap between the top and bottom plates. However, the position fixation of the **gap indicator** cannot be guaranteed during the course of film drying because each RMS-800 user uses different rheometer plates with different vertical dimensions during the course of film drying, which ranges from several hours up to a couple of days. Therefore, new gap-zeroing and –setting procedures were proposed and have been validated for this study. The details of the two overall protocols

are represented below. Refer to Figure 4.2-2 to distinguish the parts of the RMS-800 written in bold.

**Gap-zeroing procedure** (See Figure 4.2-3)

- Step 1.** Screw down the **stop screw** and **stop nut** all the way with the **dial indicator actuator** off the **stop screw**.
- Step 2.** Lower the **quill** so that the **gap indicator** indicates “0”, which means that the **quill** has been lowered by 66 microns after the **dial indicator actuator** first touches the **stop screw**.
- Step 3.** Raise the **quill** by 1 cm and raise the **stop screw** by 1 cm.
- Step 4.** Repeat **Step 3** once more and screw the **stop nut** all the way down firmly.
- Step 5.** Raise the quill so that the modified rheometer plates can be installed. Then, install the rheometer plates.
- Step 6.** Lower the quill till the gap between the top and bottom plates becomes zero and measure the total displacement of the quill from the point where the **dial indicator actuator** touches the stop screw to the gap-zero point.

It was found by repeating Step 1 through 6 that the gap-zeroing can reproducibly be performed with an acceptable variation using the newly proposed procedure described above. The displacement of the quill from the point where the **dial indicator actuator** touches the **stop screw** to the gap-zeroing point was 5304  $\mu$  and its variation, expressed as a standard deviation, is  $\pm 2 \mu$ . This result implies that the maximum error of gap-setting is less than 0.5 % even though the smallest gap (500  $\mu$ ) is used. Thus, the gap

between the top and bottom plate can reliably be controlled using the new gap-zeroing procedure.

### **Gap-setting procedure**

- Step 1.** Follow Step 1 ~ 4 described in Gap-zeroing procedure.
- Step 2.** Raise the **quill** so that the modified rheometer plates can be installed. Then, install the rheometer plates with a solution-cast film on the bottom plate.
- Step 3.** Lower the **quill** till the top plate touches the sample and measure the total displacement of the **quill** from the point where the **dial indicator actuator** touches the **stop screw** to the point where the top plate touches the sample.
- Step 4.** Calculate the gap between top and bottom plates by subtracting the displacement measured at Step 3 from 5304  $\mu$ , which is the gap-zeroing distance.

#### 4.2.2.3 Overall experimental procedure

10 vol % SBS triblock copolymer solutions in toluene were prepared by vigorously stirring at room temperature for several hours. The volume-based concentration was determined from the weight and density of the copolymer and solvent under the assumption that there was no volume change of mixing. Films were cast by simply pouring the solution of a known amount directly onto the cup-shaped rheometer bottom plate, and the bottom plate was placed in a fume hood at room temperature ( $22 \pm 1$  °C). Then, the change in the weight of the film was monitored for the determination of film concentrations during the drying process. The average drying rate was approximately  $0.07 \text{ g/cm}^2\cdot\text{hr}$  and the total drying time was about 8 hr. As soon as the film

reached a designated concentration, the bottom plate was immediately moved and fitted to the RMS-800 for the rheological property measurement. Then the gap between the top and bottom plates was set according to the procedure represented in Section 4.1.2.2. The time interval between the weight measurement and test start was always kept constant at 2.5 min. Then the time evolution of  $G'$  and  $G''$  was continuously monitored at a frequency of 1 *rad/sec* and the strain amplitude was fixed low at 2 % to minimize the nonlinear effects [Fluodas 1994].

### 4.3 Results and discussions

#### 4.3.1 Validation of the modified parallel-plate rheometry

It is necessary to test the measuring capabilities of the modified parallel plate rheometry fixtures, even though they were accurately designed and machined. Moreover, the solvent in the trough may exert extra torque on the cover parts and, eventually, on the torque transducer during measurements, although the viscoelasticity of the pure solvent, toluene in this study, is expected to be negligible compared with that of the polymer solutions in question.

To validate the accuracy of the rheological measurements in the modified parallel plate rheometry, a PDMS (Polydimethylsiloxane, Rhodorsil Fluid 47 V 300,000, Rhodia Silicones, New Jersey) and a Brookfield Viscosity Standard Material 92,000 cP (Brookfield Engineering Laboratories, inc. Stoughton, MA, U.S.A) were used as reference materials. The steady shear viscosities of the reference materials were first measured with the modified parallel plates because a standard reference material for  $G'$  and  $G''$  was not available. In Figure 4.3-1, the values of steady shear viscosity of the two

reference materials measured with the modified 40 mm parallel plates are compared to the manufacturer's quoted values. In the range of shear rate between 1 and 100  $\text{sec}^{-1}$ , the measured values agreed fairly well with the certified values. Additionally, the values of  $G'$ ,  $G''$ , and  $\eta^*$  of the PDMS measured using the standard 25 mm parallel plates and the modified 40 mm parallel plates are compared in Figure 4.3-2. The values measured with the modified parallel plates also agreed well with those measured with the standard 25 mm parallel plates for  $\omega$  between 0.63 and 100 rad/sec. Therefore, it was concluded that the modified parallel plates correctly impose amplitude oscillatory shear flow of the designated conditions on the samples and can be used for the measurement of  $G'$  and  $G''$ .

It is still necessary to test the solvent-evaporation-prevention ability of the modified parallel-plate fixtures, although the fixtures can keep the air in the fixtures saturated with the solvent by providing an air-tight environment to the test samples. The ability to prevent solvent evaporation was tested by conducting the intermittent steady shear test of a 36 vol % polystyrene/toluene solution, alternating between one-minute shearing and one-minute rest. Figure 4.3-3 presents the results obtained with standard 25 mm parallel plates and the modified 40 mm parallel plates at the shear rate of 2.0  $\text{sec}^{-1}$ . It is obvious that the viscosity measured with the normal plates gradually increased. Moreover, after each shearing cessation, the viscosity jumped considerably and then decreased. It was visually observed that significant solidification of the test sample caused by the solvent evaporation at the air/sample interface along the edge of the standard plates resulted in the jumps in the viscosity after each rest period. However, the viscosity measured with the modified plates remained constant, showing no abrupt upward change. This result indicates that the modified plates are effective for suppressing

the solvent evaporation and can be reliably used for prolonged measurements of rheological properties of polymer solutions.

#### 4.3.2 Evolution of $G'$ and $G''$ of solution-cast SBS/toluene films

The time evolution of  $G'$  and  $G''$  of the solution-cast SBS/toluene films were monitored for the study of phase transformation and kinetics of the SBS triblock copolymer in solution-cast films. The time evolution of  $G'$  and  $G''$  obtained for six different concentrations (35, 40, 45, 50, 55, and 70 vol %) is shown in Figure 4.3-4. Both  $G'$  and  $G''$  gradually increased in a sigmoidal pattern except at 70 vol %, where no noticeable variations in  $G'$  and  $G''$  were observed. After the gradual increases for about 25 min, both  $G'$  and  $G''$  reached steady states and formed plateaus. It is believed that  $G'$  and  $G''$  increased due to the microstructural transformation of the block copolymers in the solution-cast films.

The time evolution of  $G'$  and  $G''$  was utilized to analyze the microstructural transformation and kinetics of the SBS triblock copolymer in solution-cast films. The initial and plateau values of  $G'$  and  $G''$  were assumed to be the mechanical properties of the initial and final states of the film. While the values of  $G'$  and  $G''$  varied, the film was considered as a composite material of the initial and final phases. That is, the microstructural transformation induced the changes in the proportion of the two phases, resulting in the changes of the mechanical properties. An example analysis based on the  $G'$  and  $G''$  data obtained at 40 vol % is shown in Figure 4.3-5. First, the complex modulus was simply calculated from the relationship (Figure 4.3-5 (b)).

$$G^* = \sqrt{(G')^2 + (G'')^2} \quad (\text{Eq. 4.3-1})$$

Then, using the parallel and series models (Eq. 4.1-1 and 2), the fraction,  $\phi$ , of the final state was obtained as a function of time (Figure 4.3-5 (c)). Here, the initial and final values of  $G^*$  were considered to be  $G_o^*$  and  $G_\infty^*$ . Finally, by fitting the  $\phi(t)$  vs. time data into the logarithmic form of the Avrami equation (Eq. 4.1-3), the dimensional and kinetics information on the phase transformation of the SBS block copolymer in the solution-cast film was obtained (Figure 4.3-5 (d)). The rate constant,  $z$ , and Avrami exponent,  $n$ , were obtained from the slope and y-intercept, respectively.

The measurements of  $G'$  and  $G''$  and data analysis were repeated three times for each concentration. All the raw data and data analyses are presented in the Appendix A. The Avrami parameters obtained as a function of concentration are presented in Figure 4.3-6. The rate constant increased in the range of concentration between 35 and 45 vol %. After the rate constant had a maximum value at 45 vol %, it significantly decreased as the concentration increased. Finally, at 70 vol %, the rate constant became almost 0.

These observations can be explained in terms of the relationship between the solution concentration and the interactions among polymer molecules. As the film drying proceeded, the concentration increased and the polymer molecules were close enough for interaction to each other. For a certain range of concentration (up to 45 vol %), as the concentration increased, the molecular interactions became more intense and microstructural change occurred. However, at higher concentrations (above 45 vol %), the molecular interactions and microstructural change became slower because the mobility of polymer molecules was limited. That is, the polymer molecules did not have

enough space for rearrangement in the solution because of a packed situation at the higher concentration range. In the end, the rate constant started converging to zero and all the polymer molecules were “kinetically frozen-in”.

Unfortunately, the Avrami parameters could not be obtained at low concentrations below 35 vol %. The torque exerted by the solutions at that concentration range was below the sensitivity of the torque transducer of the RMS-800. It can be only conjectured that no discernible variation of  $G'$  and  $G''$  would have been observed at very low concentrations due to no serious molecular interactions and microstructural transformation. At very low concentrations, the polymer molecules are widely dispersed in the solvent so that they cannot interact with each other vigorously.

While the rate constant varied with the concentration, the Avrami exponent did not show significant changes, ranging from 0.90 to 1.15 ( $\approx 1$ ), which physically means that the microstructure formation was governed by one-dimensional growth with a constant rate of nucleation [Avrami 1941].

In order to determine whether rheological measurements, in particular, dynamic mechanical properties ( $G'$  and  $G''$ ) of solution-cast films can be used for monitoring the phase transformation and kinetics of block copolymers in solution-cast films, the Avrami parameters were extracted from the  $G'$  and  $G''$  evolution data. As discussed above with Figure 4.3-6, a meaningful data set was obtained. However, to confirm these observations and interpretation,  $G'$  and  $G''$  evolution data should be obtained at the concentrations below 35 vol %. Furthermore, it is necessary to compare the above data with those obtained from state-of-the-art techniques such as SAXS and/or POM.

#### 4.4 Summary

A modified parallel-plate device and a rheology test scheme were developed for the study of the phase transition and kinetics of block copolymers in solution-cast films. It was shown that rheological properties could accurately be measured with the modified parallel-plate device. Also, the device turns out to be effective for suppressing the solvent evaporation during the rheology tests. The evolution of  $G'$  and  $G''$  of the solution-cast SBS triblock copolymer films was obtained as a function of concentration according the protocol developed in this study. Then, the information on the phase transformation and kinetics of the SBS block copolymer in the solution-cast films was obtained from the  $G'$  and  $G''$  data analysis using the Avrami equation. The Avrami exponent was found to be approximately unity, indicating a one-dimensional growth mechanism. The rate constant showed a strong concentration-dependency, which implies that marginal space for the microstructural change as well as the proximity among polymer molecules may lead to an intense phase transformation. It can additionally be concluded that the solvent removal rate is one of the dominant factors that decide the final microstructures of solution-cast block copolymer films. Further investigation is underway to confirm the above observations and to attain the detailed information on the kinetics of the phase transformation.

#### 4.5 References

- [1] Hamley, I. W., Introduction to Block Copolymer, Hamley, I. W. Ed., John Wiley & Sons, Ltd., New York, 2004.
- [2] Krausch, G., and Magerle, R., Manostuctured thin films via self-assembly of block copolymers, *Advanced Materials*, 14(21), 1579-1583, 2002.
- [3] Hamley, I. W., *The Physics of Block Copolymers*, Oxford University Press, Oxford, 1999.
- [4] Bockstaller, M., Kolb, R., and Thomas, E. L., Metallodielectric Photonic Crystals Based on Diblock Copolymers, 13, 1783-1886, 2001.
- [5] Floudas, G., Pakula, T., Fischer, E. W., Hadjichristidis, N., and Pispas, S., Ordering Kinetics in a Symmetric Diblock Copolymer, *Acta Polymer*, 45, 176-181, 1994.
- [6] Avrami, M., Kinetics of Phase Change, 1: General Theory, *Journal of Chemical Physics*, 7, 1103-1112, 1939.
- [7] Avrami, M., Kinetics of Phase Change. 2: Transformation-Time Relations for Random Distribution Nuclei, *Journal of Chemical Physics*, 8, 212-224, 1940.
- [8] Avrami, M., Granulation, Phase Change, and Microstructure, *Journal of Chemical Physics*, 9, 177-184, 1941.
- [9] Hanley, K. J., and Lodge, T. P., Phase Behavior of a Block Copolymer in Solvents of Varying Selectivity, *Macromolecules*, 33, 5918-5931, 2000.
- [10] Chastek, T. Q. and Lodge, T. P., Grain Shapes and Growth Kinetics of the Cylinder Phase in a Block Copolymer Solution, *Macromolecules*, 37, 4891-4899, 2004.
- [11] Huang, J., Baird, D. G., Fan, G., Zhang, Z., Badami, A., Takamuku, S., and McGrath, J. E., Continuous film casting and evaluation of polymer membranes for fuel cells, *Society of Plastics Engineers Annual Conference*, Cincinnati, OH, 2007.
- [12] Hadjichristidis, N., Pispas, S., and Floudas, G. A., *Block Copolymers: Synthetic Strategies, Physical Properties, and Applications*, John Wiley & Sons, Inc., New Jersey, 2003.
- [13] Sigma-Aldrich, Inc., St. Louis, MO, Certificate of Analysis.
- [14] Rheometrics, Inc. Piscataway, NJ, Rheometrics Mechanical Spectrometer/Dynamic Spectrometer RMS-800/RDSII, Owner's Manual.

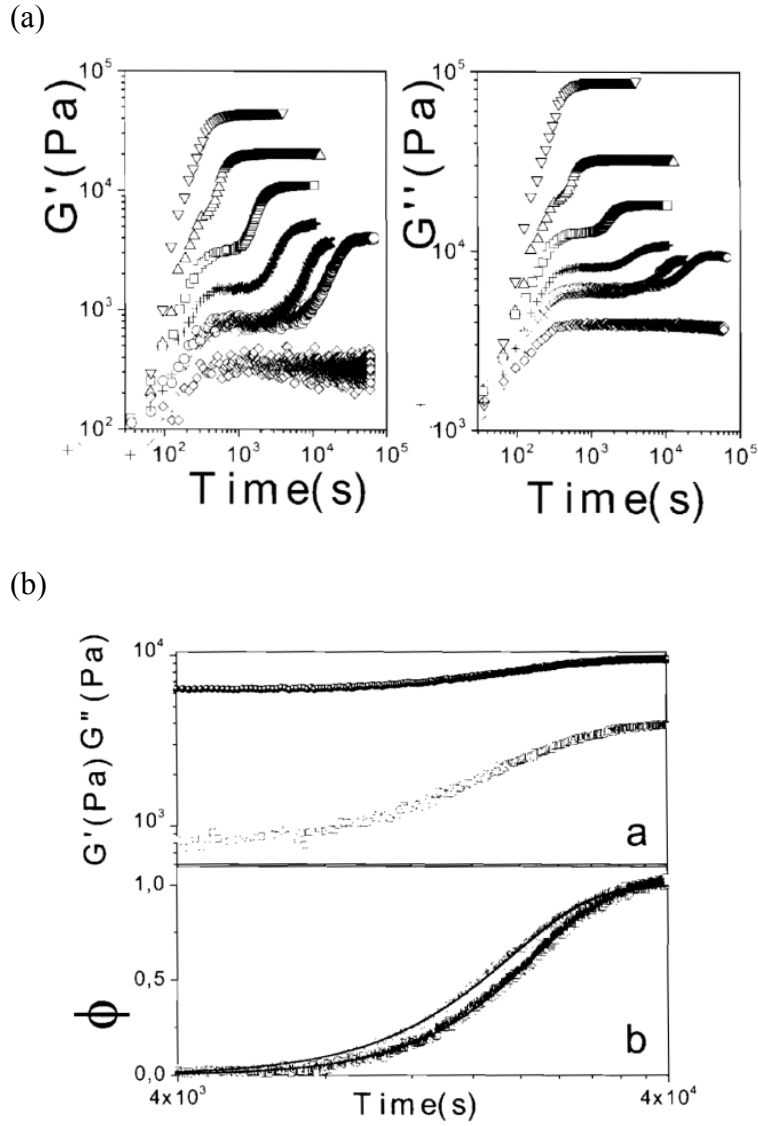


Figure 4.1-1. (a) Time evolution of  $G'$  and  $G''$  for a symmetric poly(styrene-*b*-isoprene) diblock copolymer following quenches from the disordered state to different final temperatures in the ordered phase: rhombus: 359, circles: 358, X: 356.5, +: 356, squares: 355, triangles: 353, and inverted triangles: 347.6 K. (b) a. Time evolution of  $G'$  and  $G''$  at 356.5 K following a quench from 363 K and b. time-dependence of the volume fraction of  $\phi$  of the ordered phase calculated using the 'parallel' (squares) and 'series' (circles) models. Solid lines are fits to the Avrami equation [Floudas 1994].

Table 4.2-1. Characterization of the SBS triblock copolymers used in this study [Certificate].

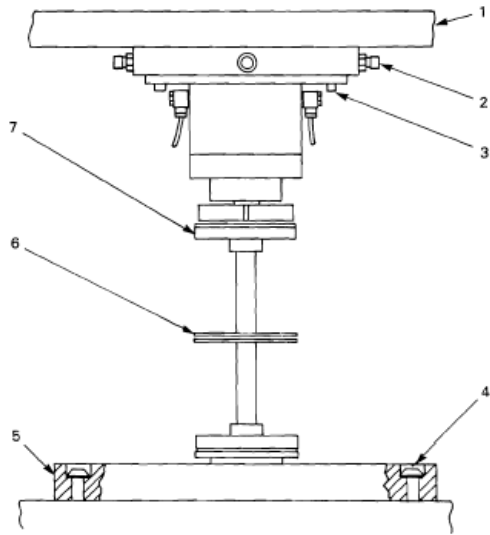
Chemical structure	Density [g/cm <sup>3</sup> ]	Molecular weight [g/mol]	Intrinsic viscosity [dL/g]
(C <sub>8</sub> H <sub>8</sub> ) <sub>x</sub> (C <sub>4</sub> H <sub>6</sub> ) <sub>y</sub> (C <sub>8</sub> H <sub>8</sub> ) <sub>z</sub>	0.94	140,000	1.0

Table 4.2-2. Physical properties of toluene [Smallwood 1996].

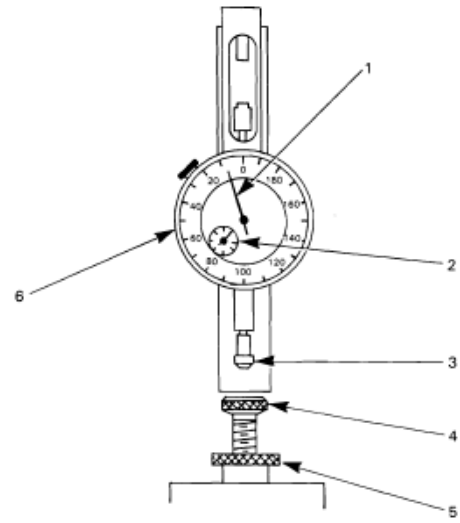
Density	Boiling point	Antoine equation constant <sup>a</sup>			Vapor pressure @ 22 °C
		A	B	C	
0.867 g/cm <sup>3</sup>	110.6 °C	6.95087	1342.31	219.187	24.3 mm Hg

<sup>a</sup> The Antoine equation  $\log p = A - B/(C + T)$  where temperature  $T$  in °C.





1. Quill
2. Flatness adjustment screw
3. Transducer mounting screw
4. Actuator mounting plate screw
5. Actuator mounting plate
6. Test fixture plate
7. Test fixture



1. Needle (graduated in  $\mu$ )
2. Needle (graduated in mm)
3. Dial indicator actuator
4. Stop screw
5. Stop nut
6. Bezel

Figure 4.2-2. Drawings of **test station** and **gap indicator** (Figure 6-25 and -26 in the user manual of the RMS-800 [Manual]).



Step 1



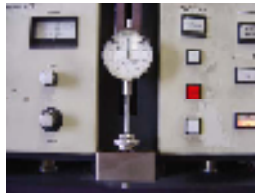
Before Step 2



After Step 2



Step 3



Step 4-1



Step 4-2



Step 6

Figure 4.2-3. Pictures of gap indicator at each step for gap-zeroing procedure.

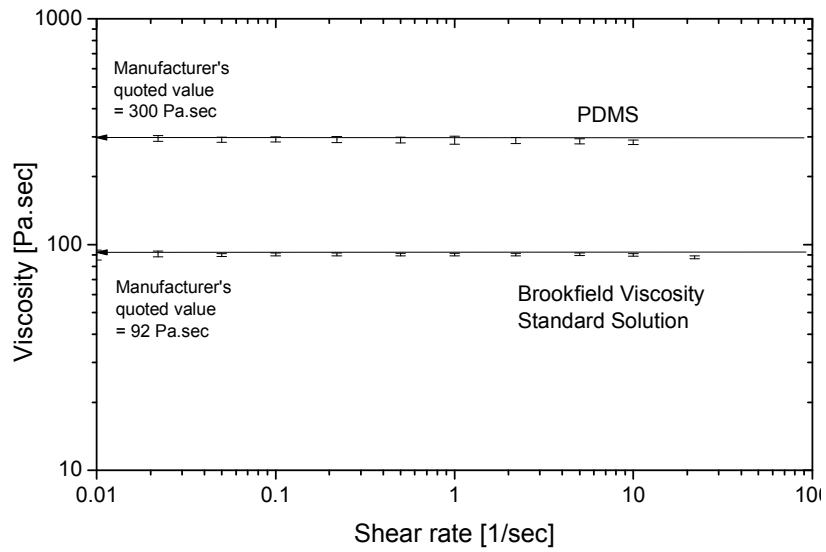


Figure 4.3-1. Evaluation of the viscosity measurement accuracy of the modified parallel plate rheometry fixtures adapted to the RMS-800 by comparing viscosity values of PDMS and Brookfield Viscosity Standard Solution measured at  $22 \pm 1$  °C with the manufacturer's quoted value (300 and 92 Pa•sec).

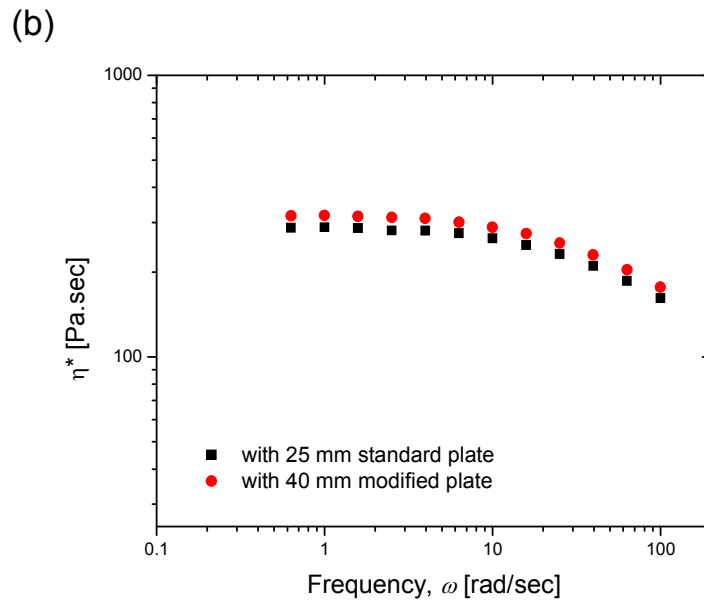
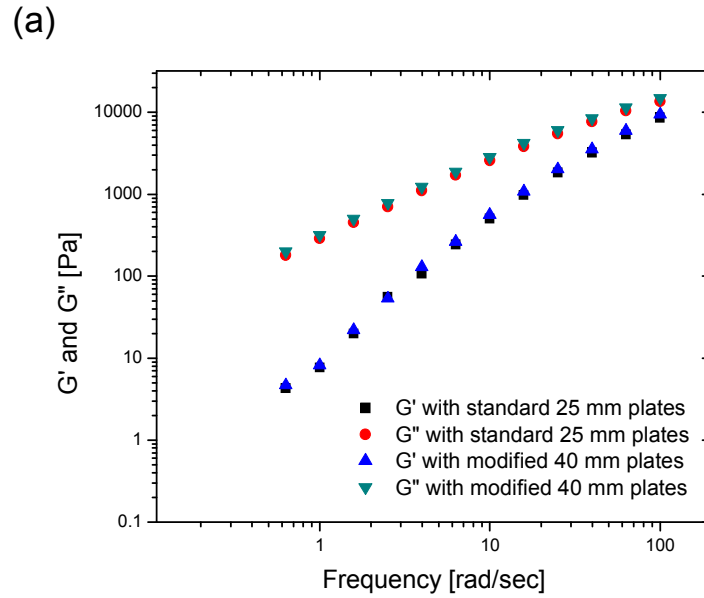


Figure 4.3-2. Evaluation of the  $G'$ ,  $G''$ , and  $\eta^*$  measurement accuracy of the modified parallel plate rheometry fixtures adapted to the RMS-800 by comparing  $G'$ ,  $G''$ , and  $\eta^*$  values of PDMS measured with the modified parallel plate rheometry fixtures at  $22 \pm 1$  °C with those measured with standard 25 mm parallel plates.

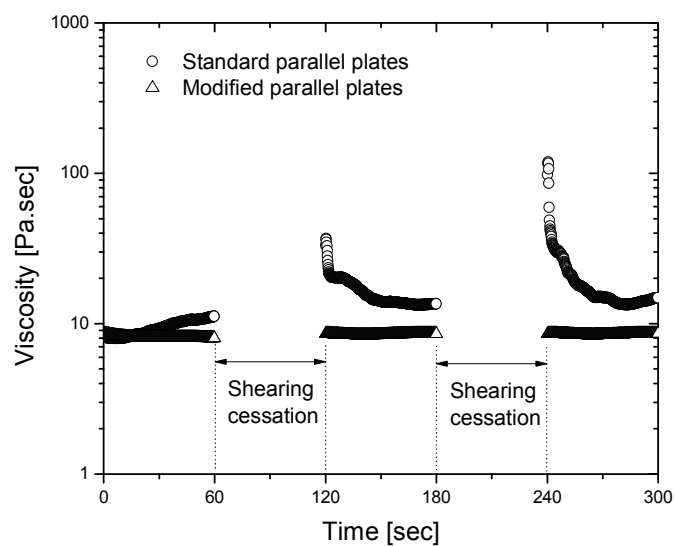


Figure 4.3-3. Test of the ability of prevent solvent evaporation of the modified parallel plate rheometry fixtures adapted to the RMS-800 by comparing the steady shear viscosity values of a 36 vol % polystyrene/toluene solution measured with the modified parallel plates at  $22 \pm 1$  °C with those measured with standard 25 mm parallel plates.

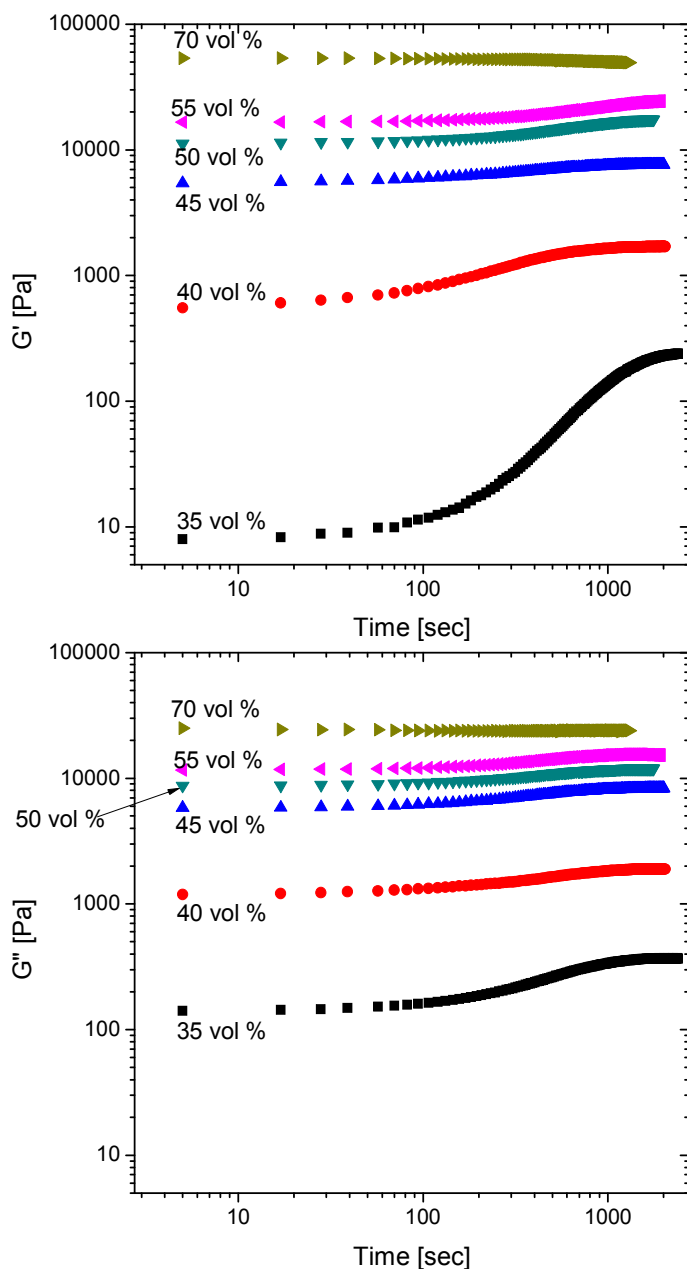


Figure 4.3-4. Time evolution of  $G'$  and  $G''$  of the SBS/toluene films obtained at 6 difference concentrations at  $22 \pm 0.5$  °C.

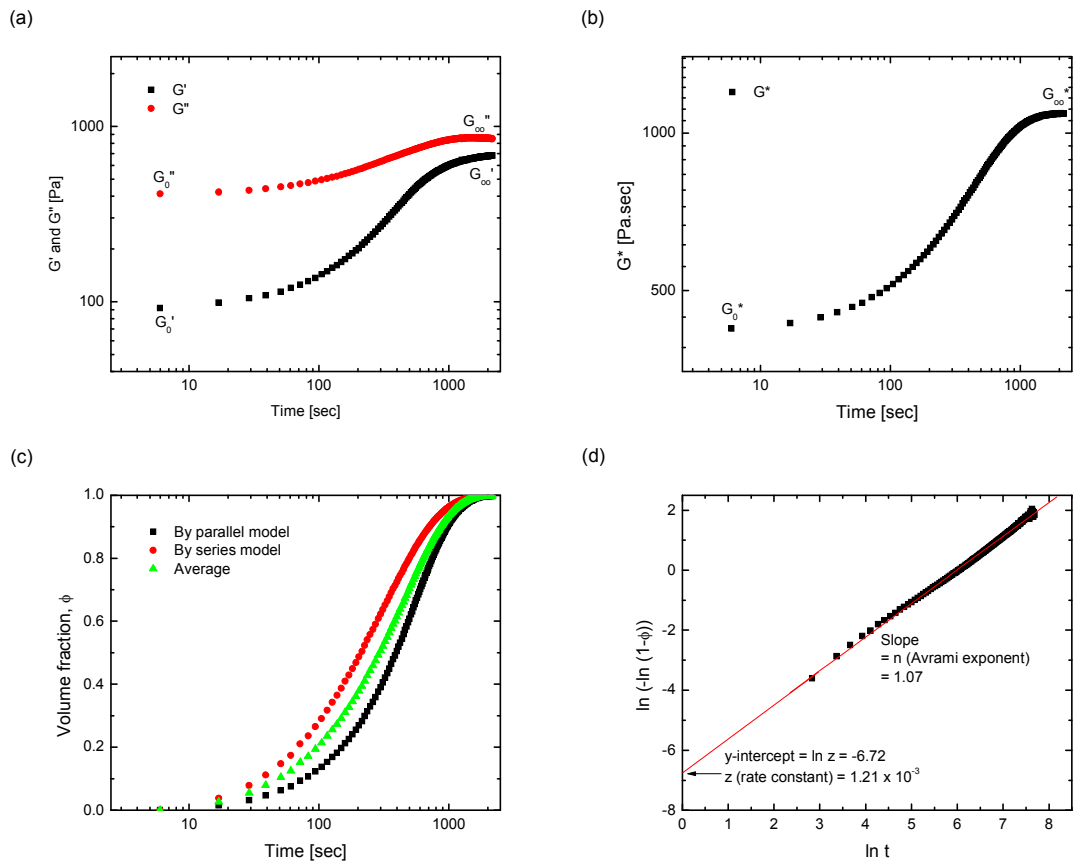


Figure 4.3-5. (a)  $G'$  and  $G''$  measured at 40 vol %. (b) Corresponding complex modulus. (c) Time dependence of the volume fraction,  $\phi$ , of the final phase calculated from the complex modulus using the parallel and series model. (d) Estimation of Avrami parameters by fitting the volume fraction vs. time data into the Avrami equation.

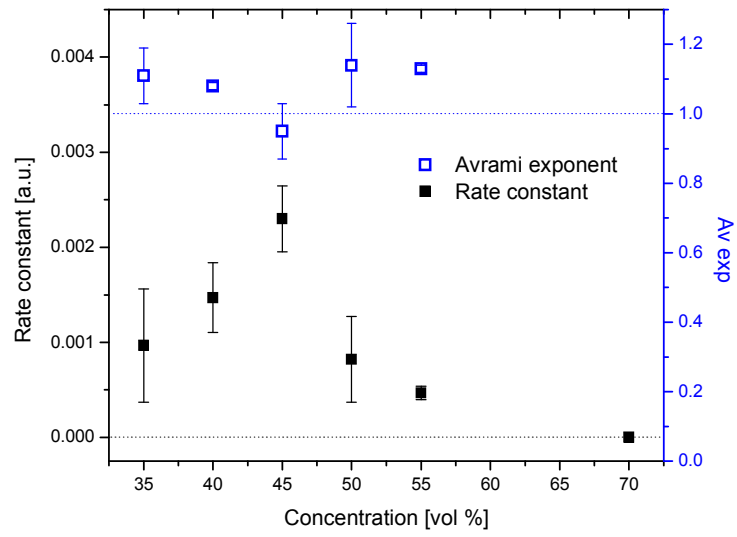


Figure 4.3-6. Avrami parameters estimated by fitting the volume fraction vs. time data to the Avrami equation.

## CHAPTER 5

### RECOMMENDATIONS FOR FUTURE RESEARCH

#### 5.1 Further study on the effects of solution-casting conditions on the final morphology and properties of proton exchange membranes

It was shown that solvent selectivity was one of the crucial factors for the final morphology and properties of the BPSH100-BPS0 multiblock copolymer films for proton exchange membranes. In this study, because of the limited amount of the copolymers, we utilized only two solvents, NMP and DMAC, which are good solvents for the sulfonated BPSH100 blocks but good and marginal, respectively, for the non-sulfonated blocks. However, two more solvents with varying selectivity for the non-sulfonated blocks are available. Dimethylformamide (DMF) and dimethylsulfoxide (DMSO) are good solvents for the sulfonated blocks but marginal and poor, respectively, for the non-sulfonated blocks.

It is recommended to further investigate the effects of solvent selectivity on the final morphology and properties of the multiblock copolymer films using DMF and DMSO. It will provide a clearer understanding of the effects of solvent selectivity. Furthermore, if any distinct microstructures of the multiblock copolymer films other than those induced by using NMP and DMAC are obtained by using DMF and DMSO, it will be helpful for understanding the structure/property relationship of the PEMs. Afterward,

it is also worthwhile to utilize co-solvent systems, because co-solvent can bring about considerable changes in the microstructure of block copolymers in solutions.

It is also generally recognized that the microstructures of block copolymers strongly depend on the volume fraction of the component blocks. However, in this study, the multiblock copolymers consisting of equal block lengths (e.g., 5, 10, and 15 kg/mol) were used. Thus, it is recommended to prepare multiblock copolymers consisting of different block lengths, e.g., BPSH100-BPS0 (10k-5k, 15k-10k, 5k-10k, and 10k-15k), and to investigate the effects of solution-casting conditions on the final morphology and properties. It is believed that this will lead to generation of a variety of morphologies of the multiblock copolymers and, thus, to profound understanding of the structure/property relationship of PEMs.

## 5.2 Study on the phase transformation and kinetics of block copolymers in solution-cast films

A physically meaningful result was obtained while exploring the possibility of using a rheological technique for the study of the phase transformation and kinetics of block copolymers in solution-cast films during the solvent removal process. In order to make a reliable conclusion, it is necessary to validate the results using state-of-the-art techniques. Many studies on the transformation of block copolymer melts and block copolymers in solutions have been conducted using small-angle X-ray and neutron scattering, depolarized light scattering, polarized optical microscopy, and birefringence. However, these techniques have been used only for tracking the phase transformations following a thermal quench through the order-disorder transition temperature by observing the evolution of a given experimental parameter over time. Therefore, it is

recommended to first develop an experimental protocol and, if necessary, experimental devices with one of the state-of-the-art techniques. Then, by comparing the data obtained in this study and from the state-of-the-art technique, the results can be confirmed.

Also, in order to be able to produce PEMs with improved performance by optimizing the solvent removal process, it is necessary to completely understand the phase transformation of the disulfonated multiblock copolymers in the process. Thus, the following are recommended to conduct.

- To generate the phase diagrams of the disulfonated multiblock copolymers in solutions as a function of concentration and temperature.
- To map the trajectories of the solvent removal processes on the diagrams.
- To obtain the detailed information such as the kinetics of the phase transformations at the phase boundaries on the trajectories.

Researchers have been able to generate the phase diagram of diblock copolymers at equilibrium. However, a general phase diagram of ternary systems such as a triblock copolymer and a diblock copolymer in solution has not been able to generate because of the complexities of their physics and thermodynamics. Furthermore, the existence of ions and multiblock architecture of the disulfonated copolymers used in the first part of this study, and non-equilibrium nature of the solvent removal process complicate much more the physics and thermodynamics. Therefore, the completion of the above-mentioned works would be only feasible way to obtain, at least, the empirical relationships between the film drying and phase transformation of the multiblock copolymers with current science and technology. After the relationships between the film drying conditions such as heat and mass transfer coefficients and the parameters that describe the phase

transformation and kinetics of block copolymers are quantitatively clarified, this study can also be extended to a modeling work. This could allow the prediction of the final morphology and properties of the PEMs and, accordingly, the optimization of the drying process of solution-cast block copolymer films.

Currently it takes 2.5 min to start the rheology test after weighing the sample for the estimation of the solution concentration. In this study, film drying was carried out at the drying rate of about  $0.07 \text{ g/cm}^2\cdot\text{hr}$ , which corresponded to the total drying time of 8 hr.

Compared with the total drying time, the 2.5 min time interval is acceptable. However, most of industrial film drying processes are performed at much higher drying rates. So, in order to obtain reasonable data for the film drying carried out at an industrial level, the time interval must considerably be reduced. For this purpose, it is recommended to improve the test devices. The details are as following.

- To install the devices on the rheometer that allow the on-site film drying and the real-time estimation of solution concentration.
- To employ a new quill-moving system that enables the movement of the top plate at the speed of approximately  $1 \text{ cm/sec}$ . The current maximum speed is  $0.25 \text{ cm/sec}$ .
- To set up a temperature control system with an improved accuracy.

## APPENDIX A. RHEOLOGICAL DATA AND ANALYSIS FOR SECTION 4.3

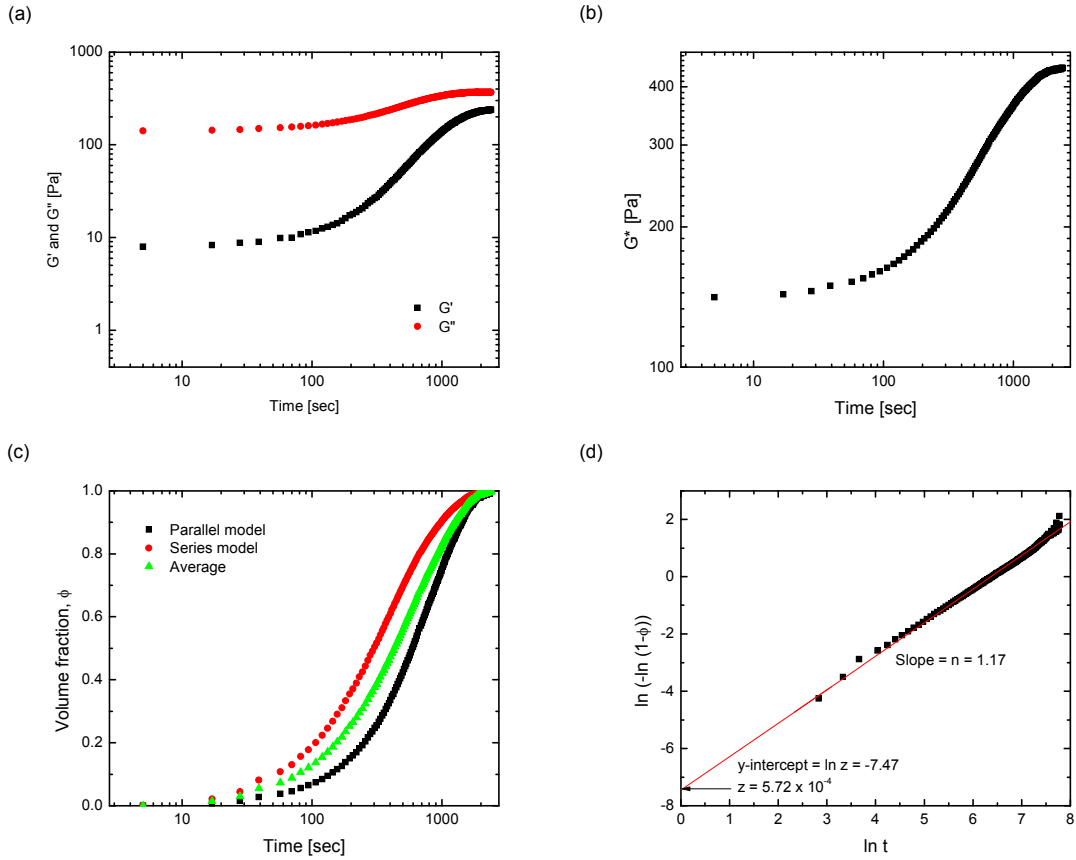


Figure A-1. Time evolution of (a)  $G'$ ,  $G''$ , and (b)  $G^*$  ( $= \{(G')^2 + (G'')^2\}^{1/2}$ ) of the SBS/toluene film (Sample 1-1) at 35 vol %. (c) Time dependence of the volume fraction,  $\phi$ , of the ordered phase calculated from the complex modulus using the parallel and series model. (d) Fitting of the volume fraction vs. time data into the logarithmic form of the Avrami equation.

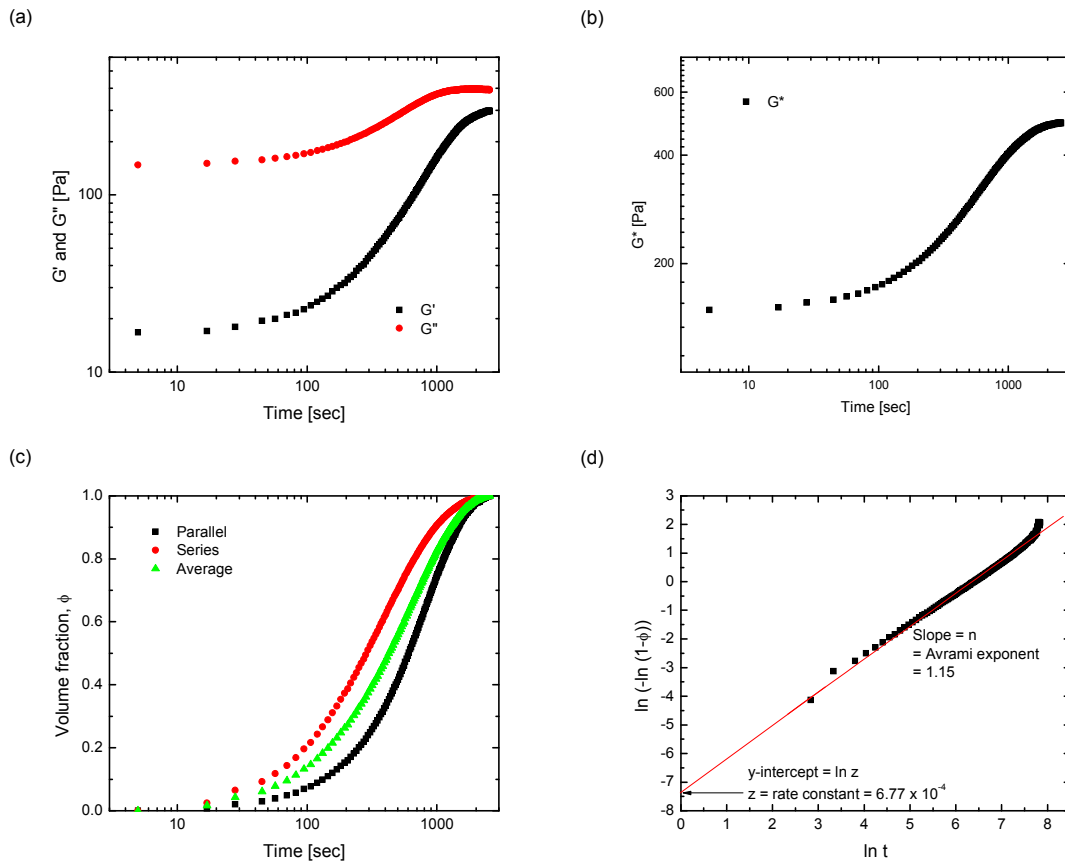


Figure A-2. Time evolution of (a)  $G'$ ,  $G''$ , and (b)  $G^* (= \{(G')^2 + (G'')^2\}^{1/2})$  of the SBS/toluene film (Sample 1-2) at 35 vol %. (c) Time dependence of the volume fraction,  $\phi$ , of the ordered phase calculated from the complex modulus using the parallel and series model. (d) Fitting of the volume fraction vs. time data into the logarithmic form of the Avrami equation.

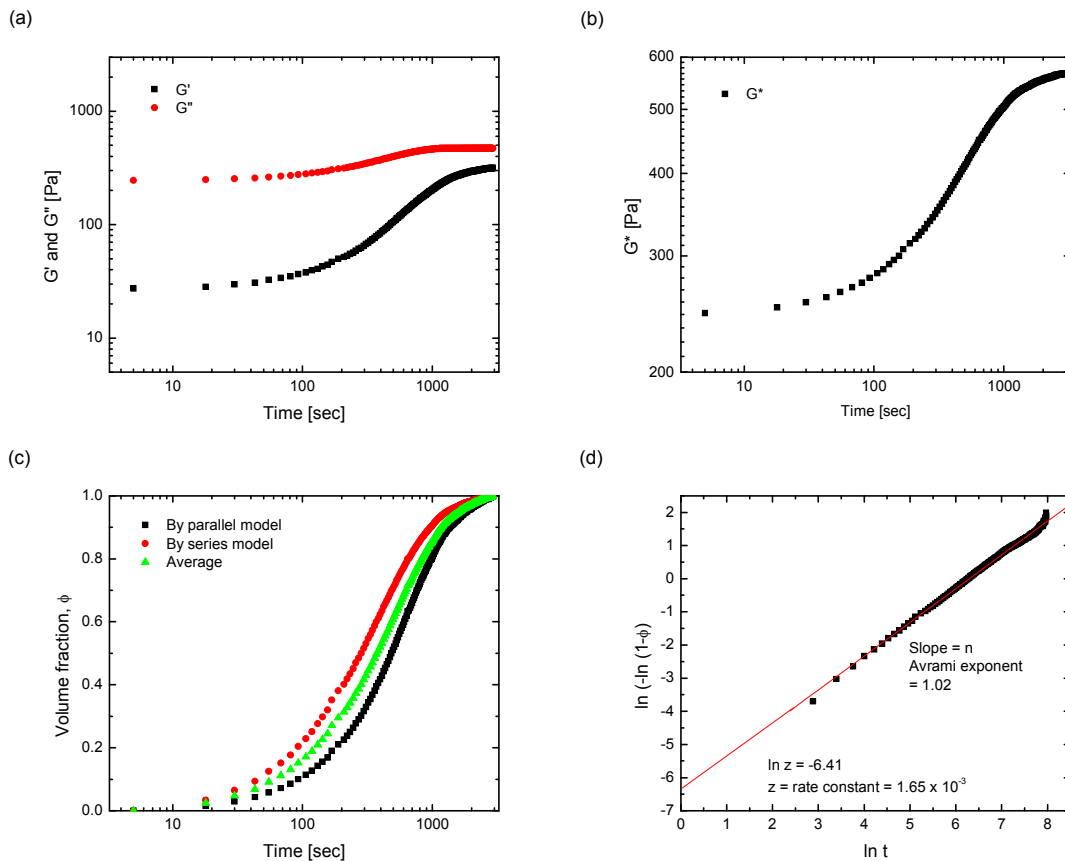


Figure A-3. Time evolution of (a)  $G'$ ,  $G''$ , and (b)  $G^*$  ( $= \{(G')^2 + (G'')^2\}^{1/2}$ ) of the SBS/toluene film (Sample 1-3) at 35 vol %. (c) Time dependence of the volume fraction,  $\phi$ , of the ordered phase calculated from the complex modulus using the parallel and series model. (d) Fitting of the volume fraction vs. time data into the logarithmic form of the Avrami equation.

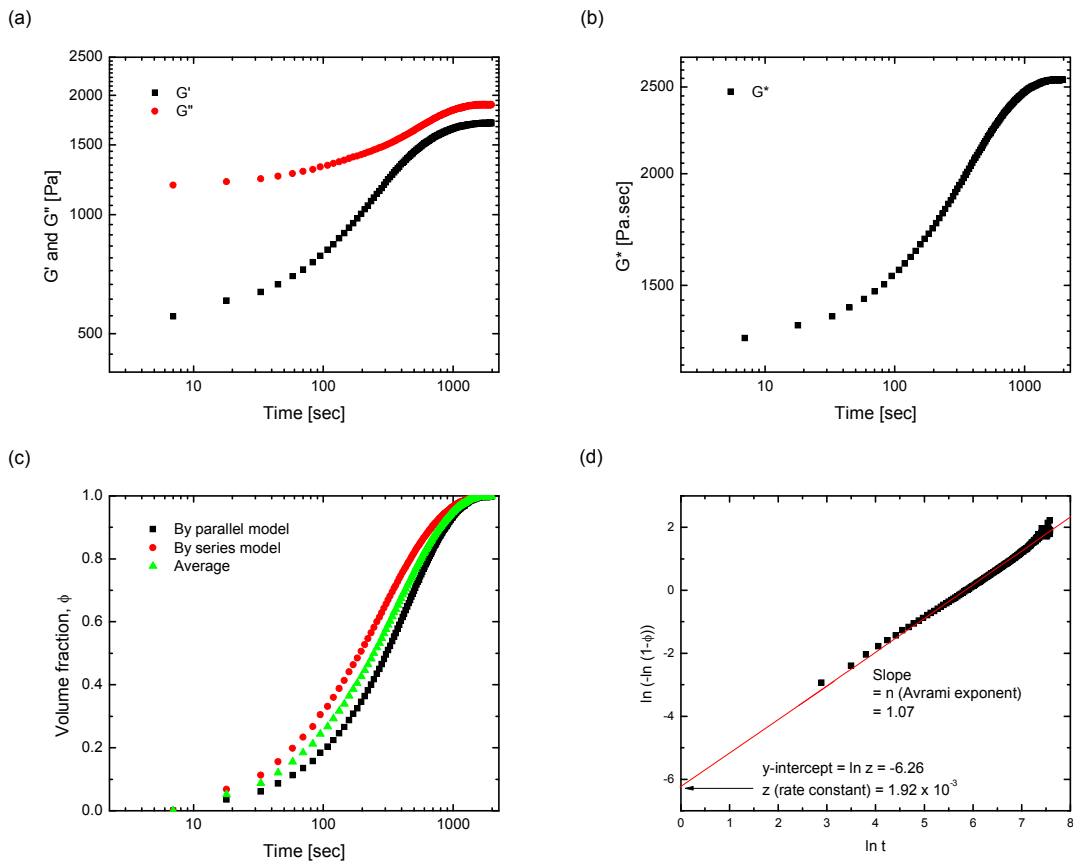


Figure A-4. Time evolution of (a)  $G'$ ,  $G''$ , and (b)  $G^*$  ( $= \{(G')^2 + (G'')^2\}^{1/2}$ ) of the SBS/toluene film (Sample 2-1) at 40 vol %. (c) Time dependence of the volume fraction,  $\phi$ , of the ordered phase calculated from the complex modulus using the parallel and series model. (d) Fitting of the volume fraction vs. time data into the logarithmic form of the Avrami equation.

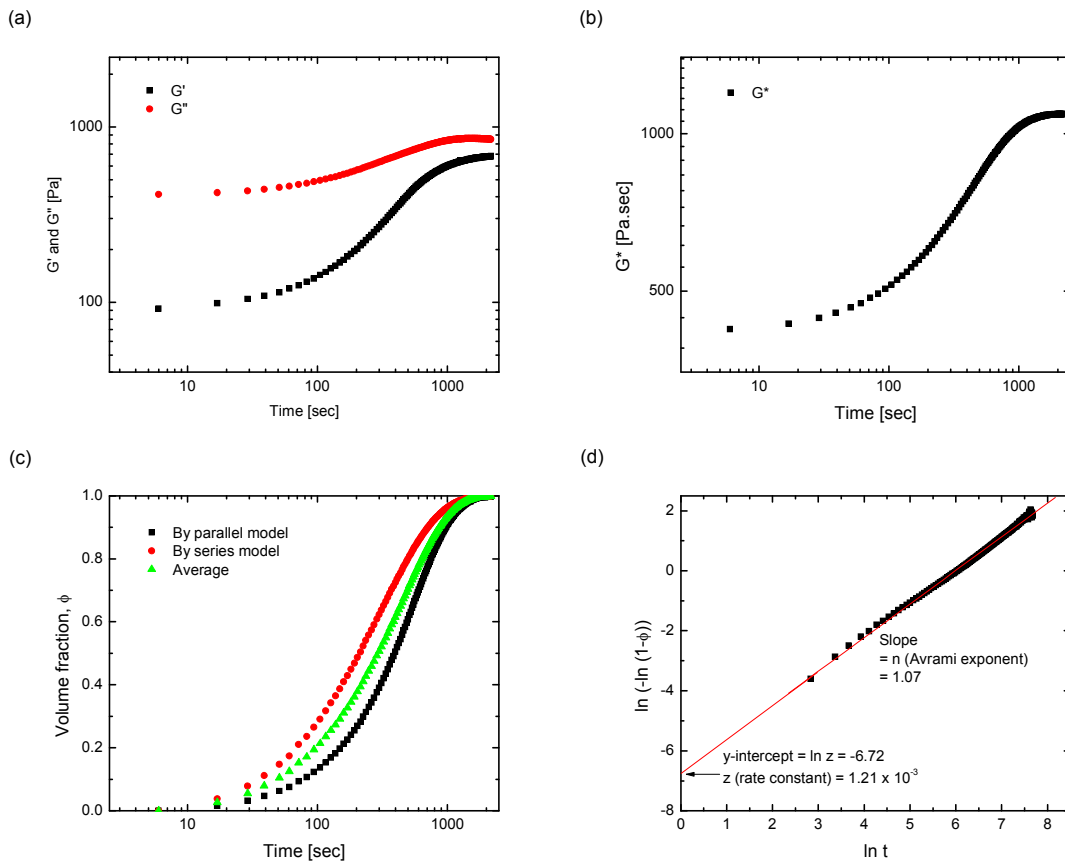


Figure A-5. Time evolution of (a)  $G'$ ,  $G''$ , and (b)  $G^*$  ( $= \{(G')^2 + (G'')^2\}^{1/2}$ ) of the SBS/toluene film (Sample 2-2) at 40 vol %. (c) Time dependence of the volume fraction,  $\phi$ , of the ordered phase calculated from the complex modulus using the parallel and series model. (d) Fitting of the volume fraction vs. time data into the logarithmic form of the Avrami equation.

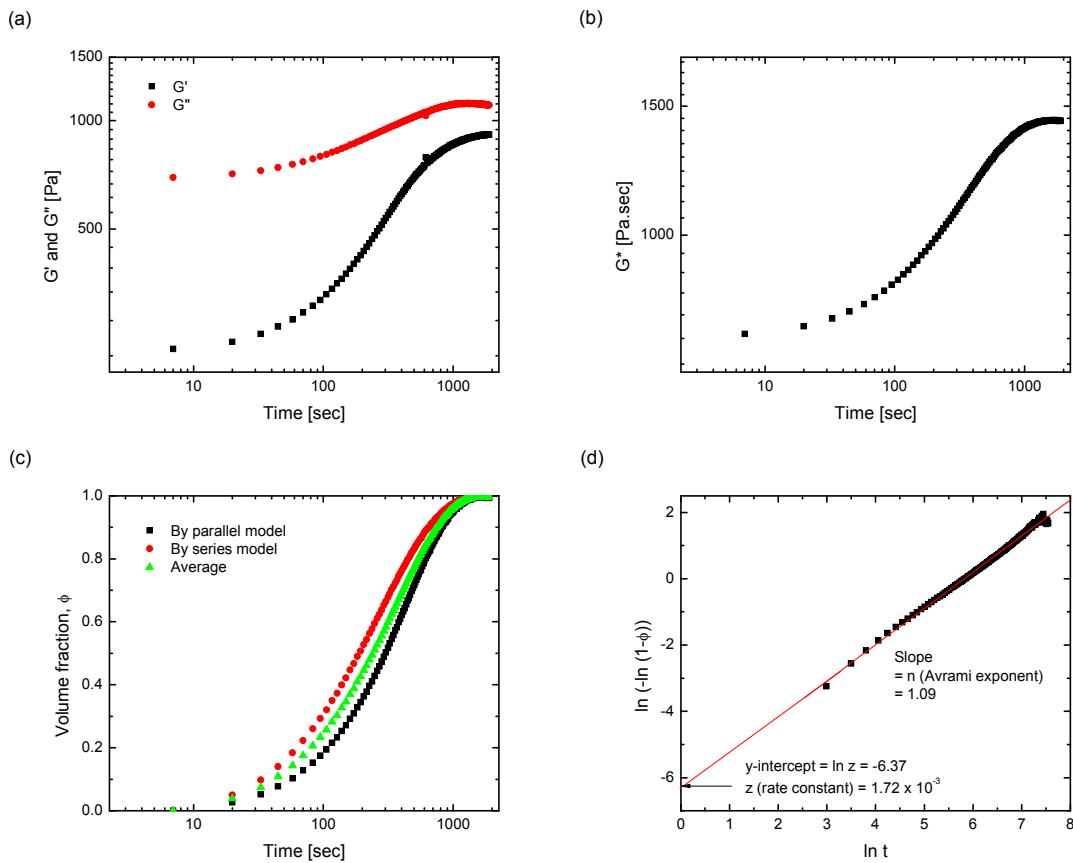


Figure A-6. Time evolution of (a)  $G'$ ,  $G''$ , and (b)  $G^*$  ( $= \{(G')^2 + (G'')^2\}^{1/2}$ ) of the SBS/toluene film (Sample 2-3) at 40 vol %. (c) Time dependence of the volume fraction,  $\phi$ , of the ordered phase calculated from the complex modulus using the parallel and series model. (d) Fitting of the volume fraction vs. time data into the logarithmic form of the Avrami equation.

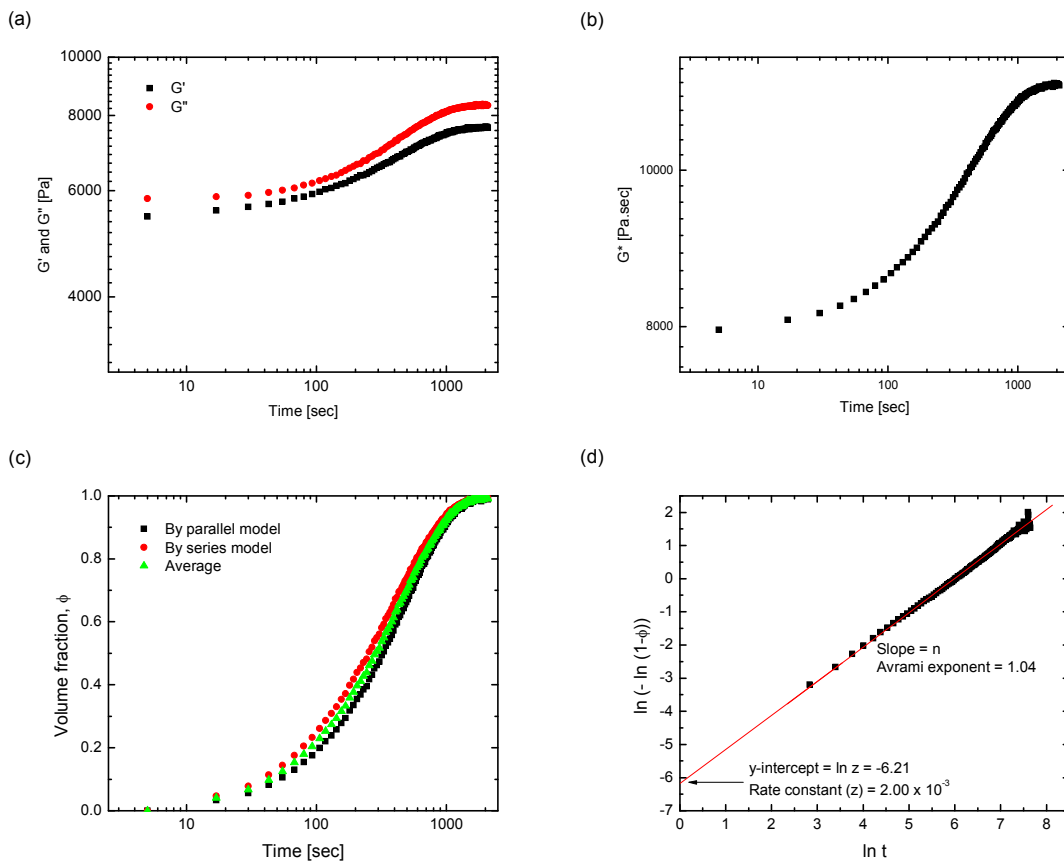


Figure A-7. Time evolution of (a)  $G'$ ,  $G''$ , and (b)  $G^*$  ( $= \{(G')^2 + (G'')^2\}^{1/2}$ ) of the SBS/toluene film (Sample 3-1) at 45 vol %. (c) Time dependence of the volume fraction,  $\phi$ , of the ordered phase calculated from the complex modulus using the parallel and series model. (d) Fitting of the volume fraction vs. time data into the logarithmic form of the Avrami equation.

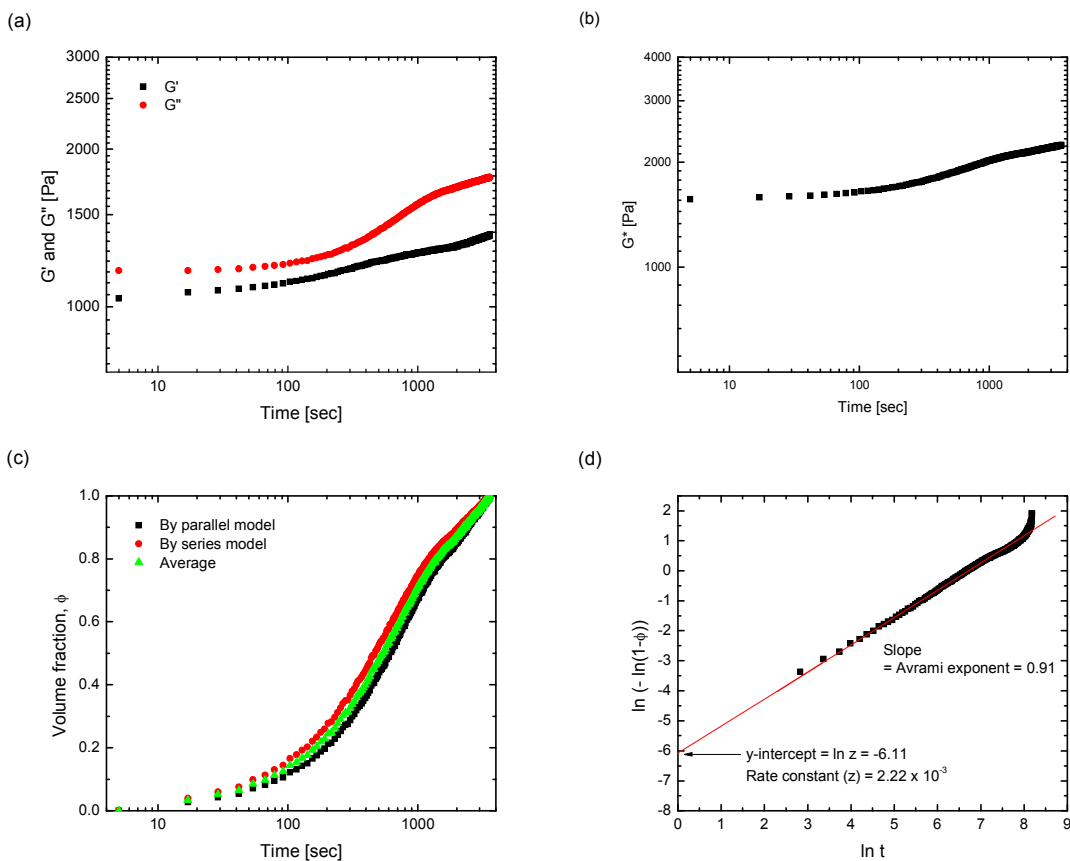


Figure A-8. Time evolution of (a)  $G'$ ,  $G''$ , and (b)  $G^*$  ( $= \{(G')^2 + (G'')^2\}^{1/2}$ ) of the SBS/toluene film (Sample 3-2) at 45 vol %. (c) Time dependence of the volume fraction,  $\phi$ , of the ordered phase calculated from the complex modulus using the parallel and series model. (d) Fitting of the volume fraction vs. time data into the logarithmic form of the Avrami equation.

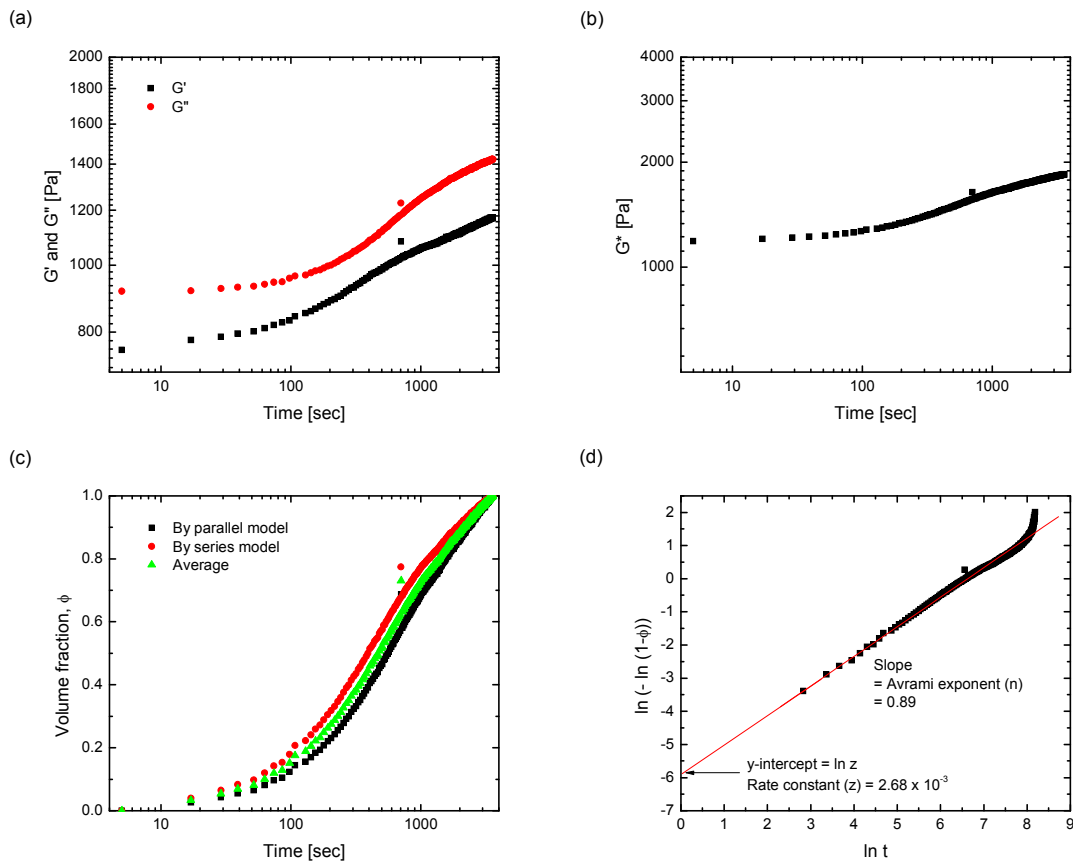


Figure A-9. Time evolution of (a)  $G'$ ,  $G''$ , and (b)  $G^*$  ( $= \{(G')^2 + (G'')^2\}^{1/2}$ ) of the SBS/toluene film (Sample 3-3) at 45 vol %. (c) Time dependence of the volume fraction,  $\phi$ , of the ordered phase calculated from the complex modulus using the parallel and series model. (d) Fitting of the volume fraction vs. time data into the logarithmic form of the Avrami equation.

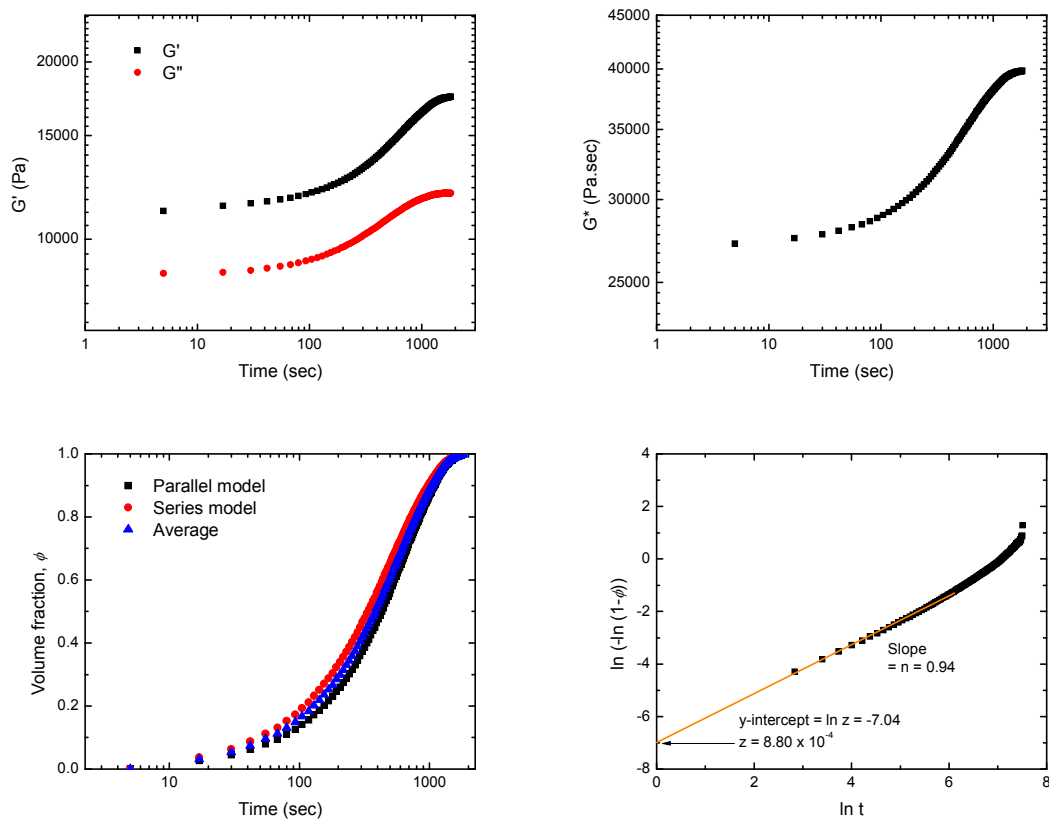


Figure A-10. Time evolution of (a)  $G'$ ,  $G''$ , and (b)  $G^*$  ( $= \{(G')^2 + (G'')^2\}^{1/2}$ ) of the SBS/toluene film (Sample 4-1) at 50 vol %. (c) Time dependence of the volume fraction,  $\phi$ , of the ordered phase calculated from the complex modulus using the parallel and series model. (d) Fitting of the volume fraction vs. time data into the logarithmic form of the Avrami equation.

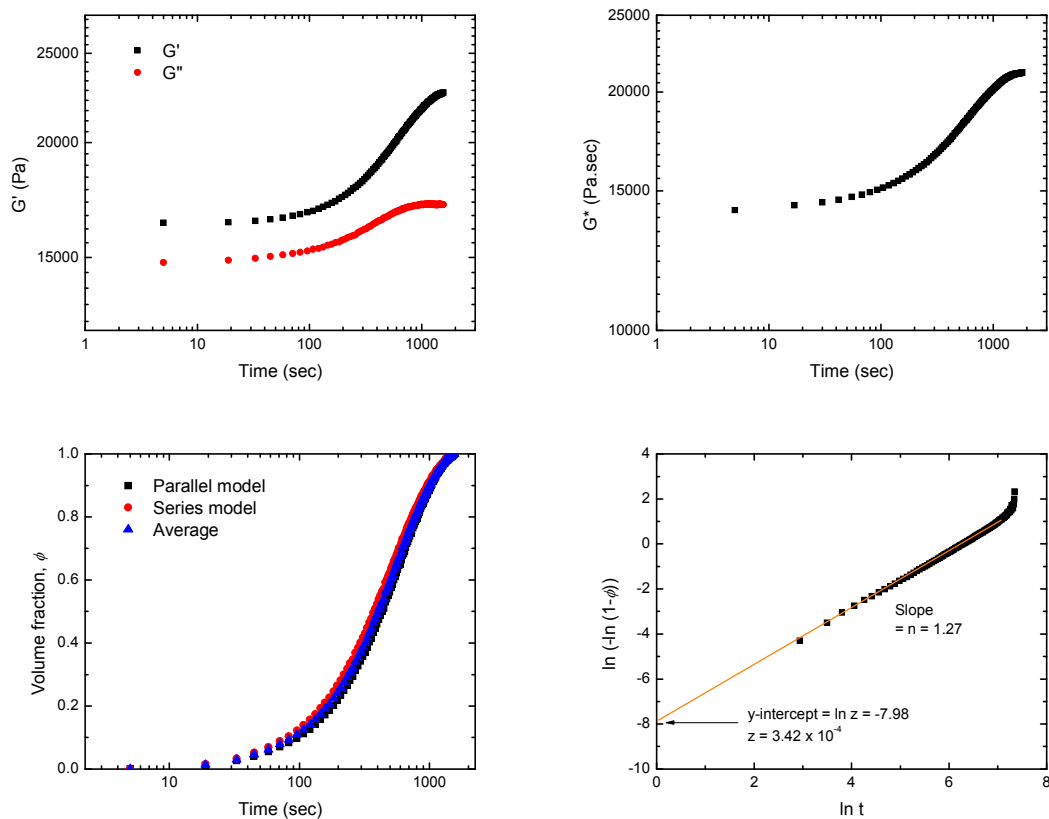


Figure A-11. Time evolution of (a)  $G'$ ,  $G''$ , and (b)  $G^*$  ( $= \{(G')^2 + (G'')^2\}^{1/2}$ ) of the SBS/toluene film (Sample 4-2) at 50 vol %. (c) Time dependence of the volume fraction,  $\phi$ , of the ordered phase calculated from the complex modulus using the parallel and series model. (d) Fitting of the volume fraction vs. time data into the logarithmic form of the Avrami equation.

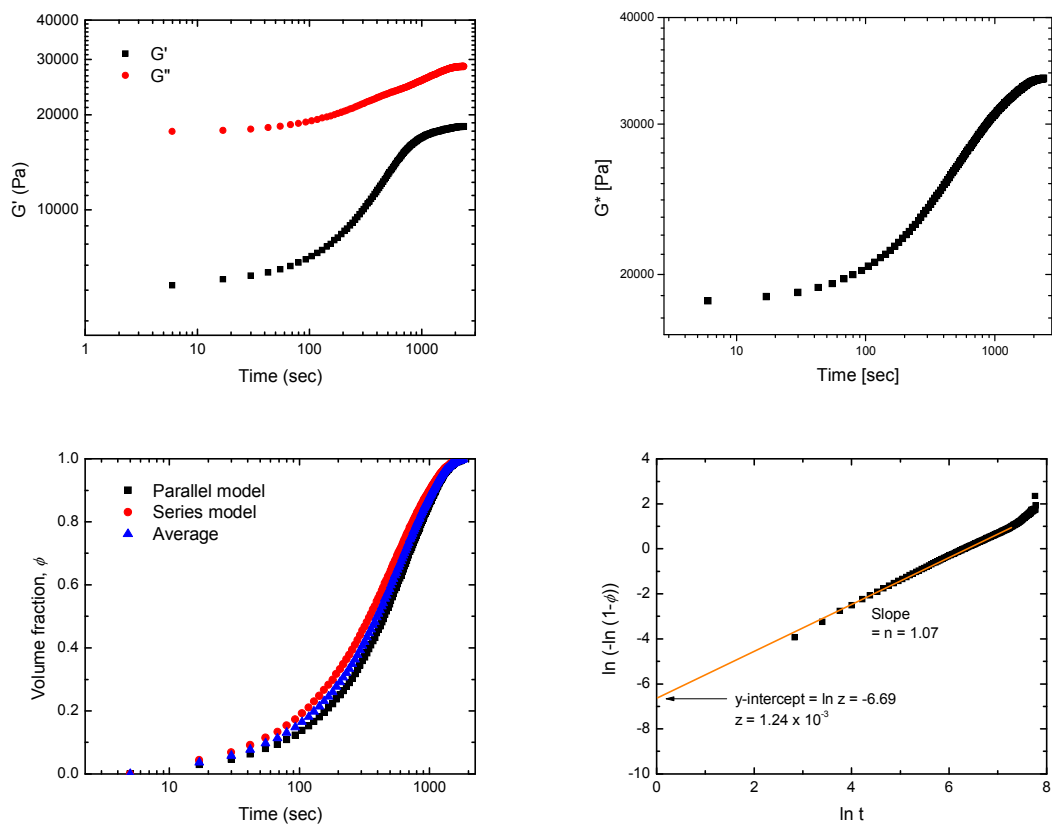


Figure A-12. Time evolution of (a)  $G'$ ,  $G''$ , and (b)  $G^*$  ( $= \{(G')^2 + (G'')^2\}^{1/2}$ ) of the SBS/toluene film (Sample 4-3) at 50 vol %. (c) Time dependence of the volume fraction,  $\phi$ , of the ordered phase calculated from the complex modulus using the parallel and series model. (d) Fitting of the volume fraction vs. time data into the logarithmic form of the Avrami equation.

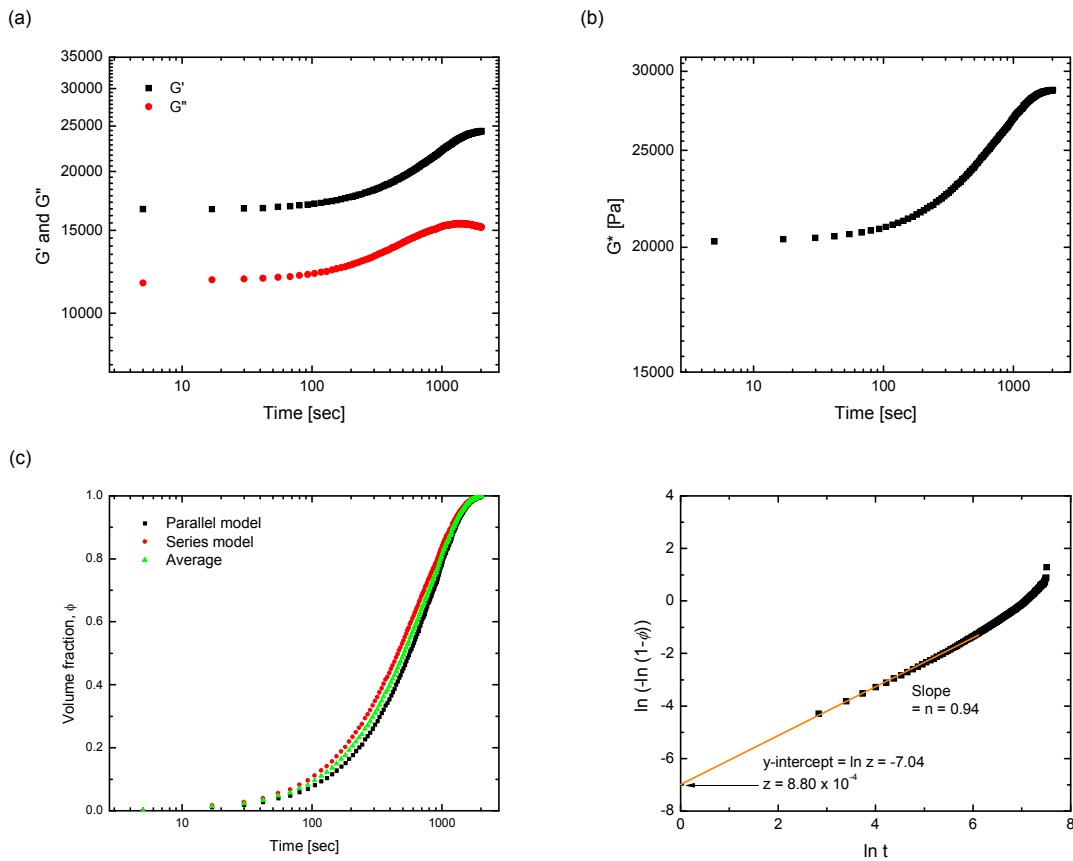


Figure A-13. Time evolution of (a)  $G'$ ,  $G''$ , and (b)  $G^*$  ( $= \{(G')^2 + (G'')^2\}^{1/2}$ ) of the SBS/toluene film (Sample 5-1) at 55 vol %. (c) Time dependence of the volume fraction,  $\phi$ , of the ordered phase calculated from the complex modulus using the parallel and series model. (d) Fitting of the volume fraction vs. time data into the logarithmic form of the Avrami equation.

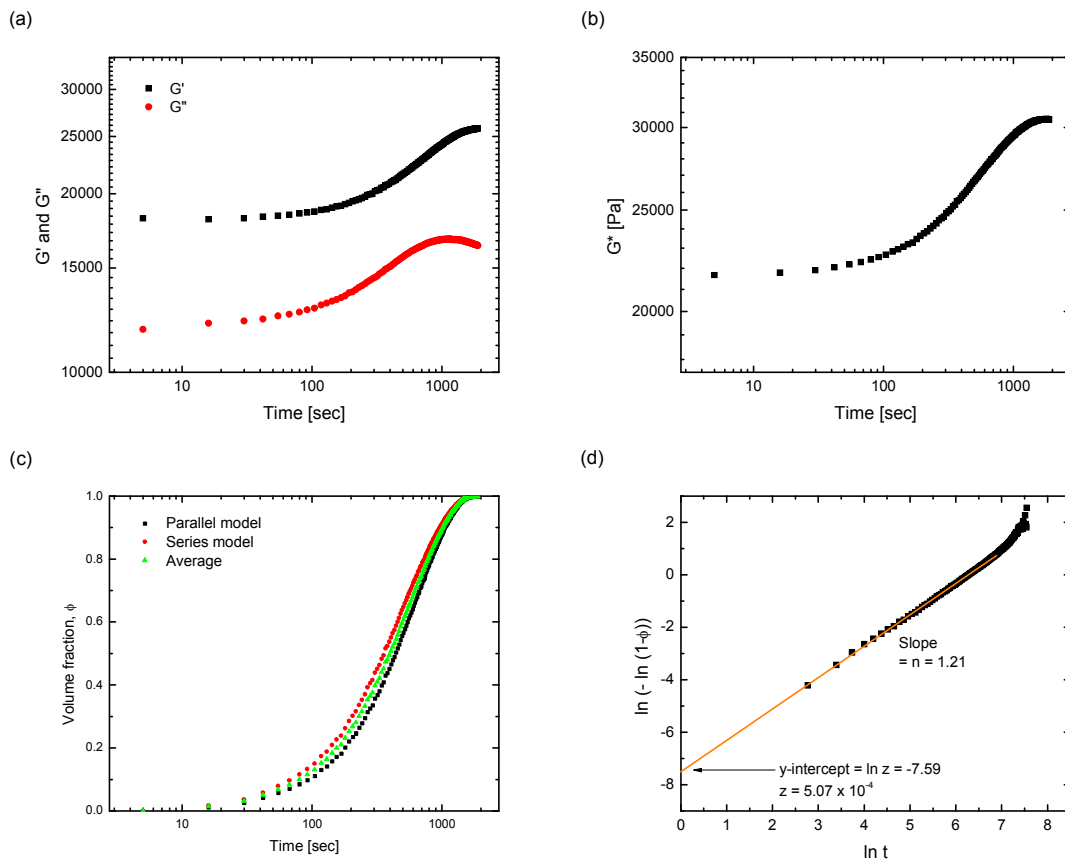


Figure A-14. Time evolution of (a)  $G'$ ,  $G''$ , and (b)  $G^*$  ( $= \{(G')^2 + (G'')^2\}^{1/2}$ ) of the SBS/toluene film (Sample 5-2) at 55 vol %. (c) Time dependence of the volume fraction,  $\phi$ , of the ordered phase calculated from the complex modulus using the parallel and series model. (d) Fitting of the volume fraction vs. time data into the logarithmic form of the Avrami equation.

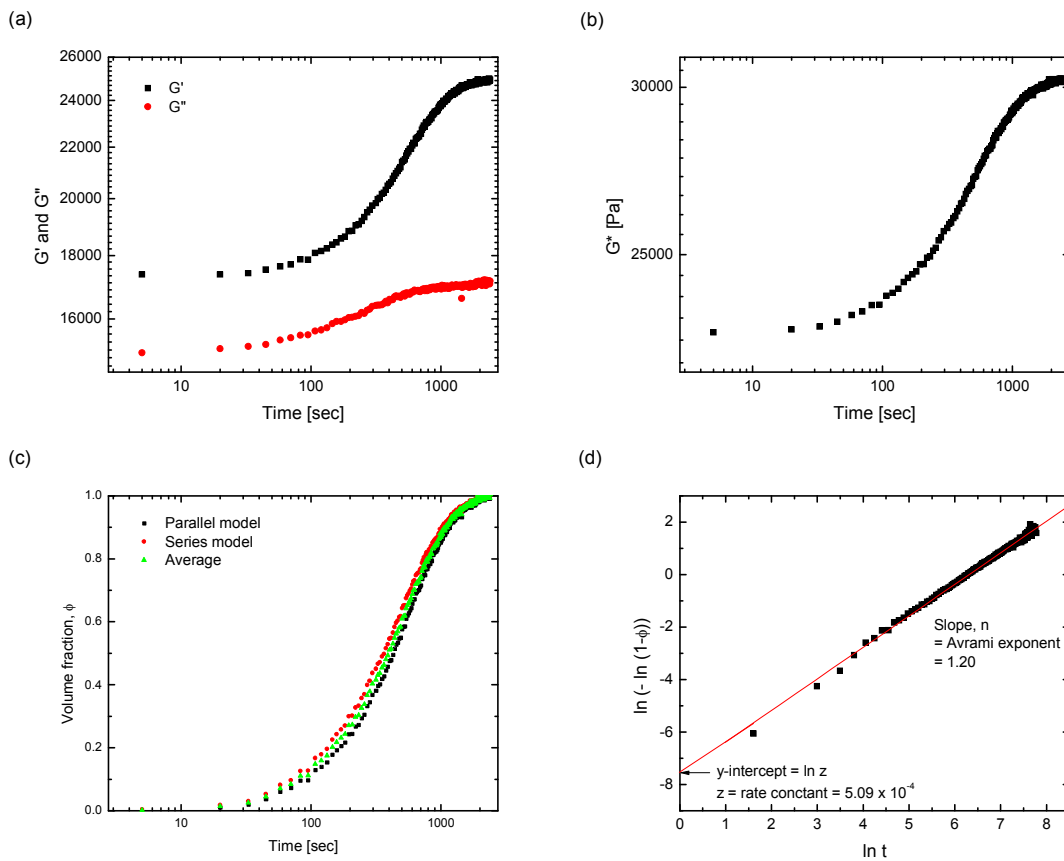


Figure A-15. Time evolution of (a)  $G'$ ,  $G''$ , and (b)  $G^*$  ( $= \{(G')^2 + (G'')^2\}^{1/2}$ ) of the SBS/toluene film (Sample 5-3) at 55 vol %. (c) Time dependence of the volume fraction,  $\phi$ , of the ordered phase calculated from the complex modulus using the parallel and series model. (d) Fitting of the volume fraction vs. time data into the logarithmic form of the Avrami equation.

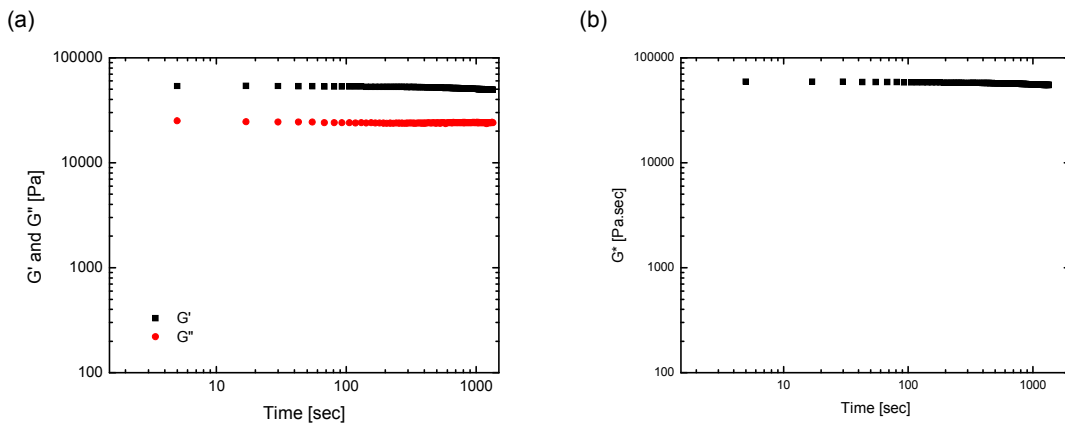


Figure A-16. Time evolution of (a)  $G'$ ,  $G''$ , and (b)  $G^*(= \{(G')^2 + (G'')^2\}^{1/2})$  of the SBS/toluene film (Sample 5-1) at 69.0 vol %.

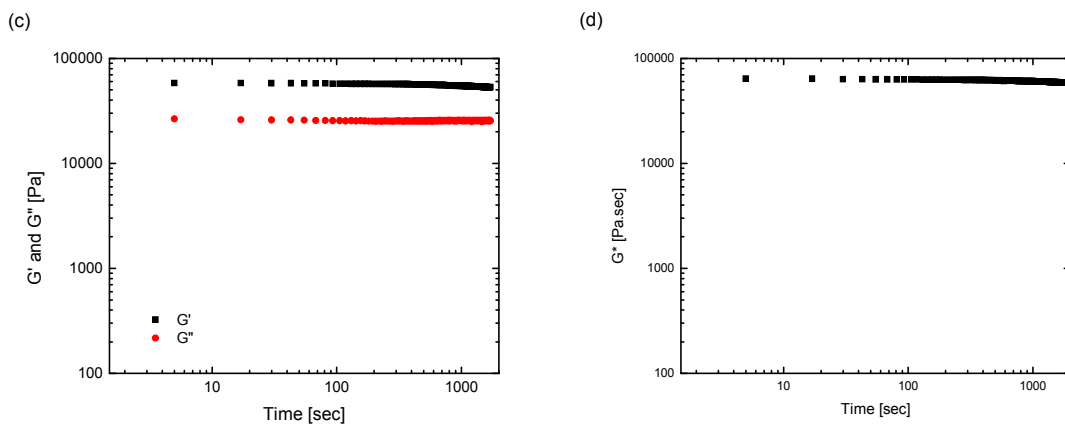


Figure A-17. Time evolution of (a)  $G'$ ,  $G''$ , and (b)  $G^*(= \{(G')^2 + (G'')^2\}^{1/2})$  of the SBS/toluene film (Sample 5-2) at 69.0 vol %.